ALADIN

NEWSLETTER n°31

July-December 2006

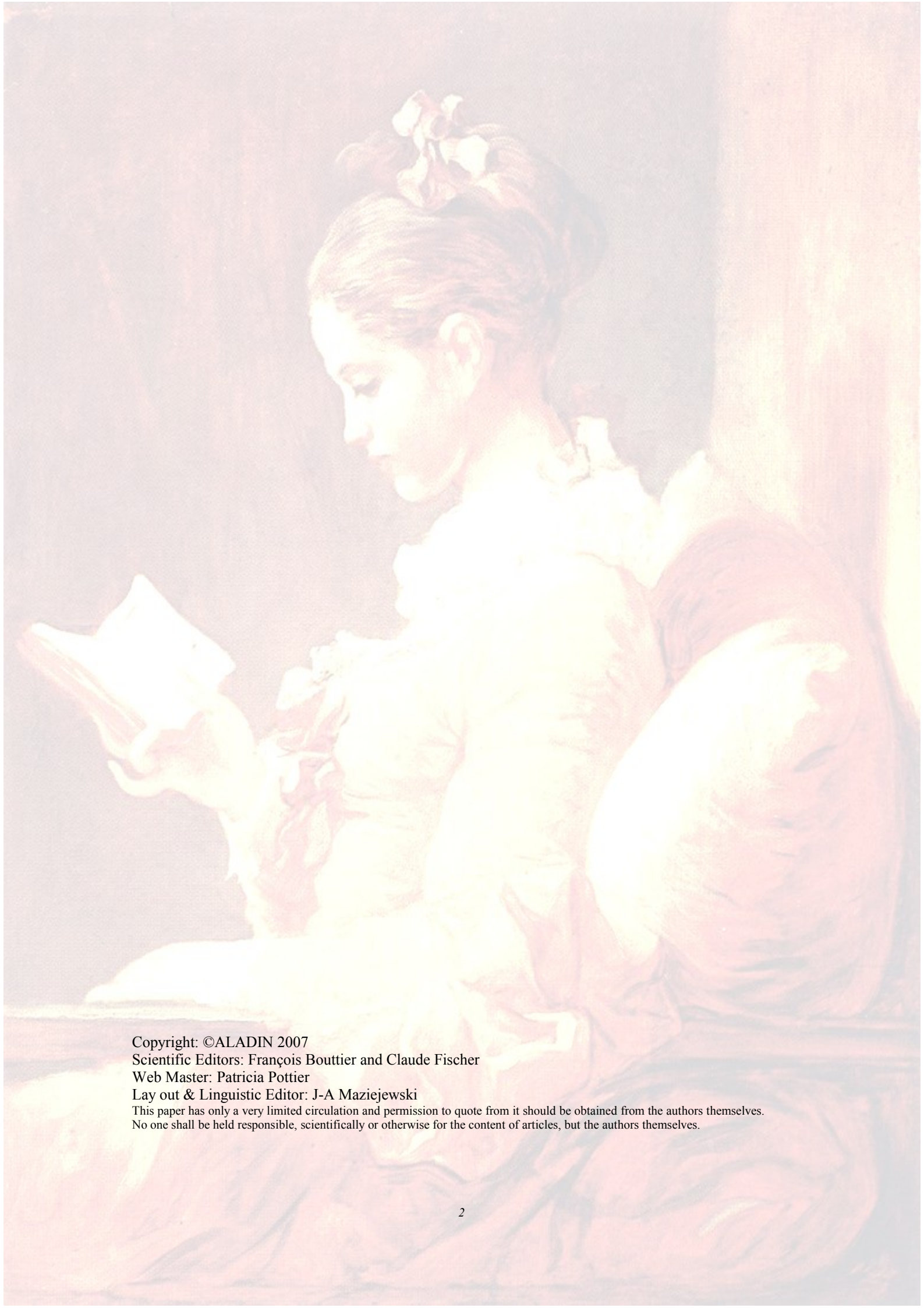

Scientific Editors: François Bouttier and Claude Fischer
Web Master: Patricia Pottier
Lay out & Linguistic Editor: J-A Maziejewski

CONTENT

1. EDITORIAL

Foreword: .

ALADIN/ALARO/AROME: back to the future ?

Big changes are happening in Europe's NWP. Our consortium is getting closer to HIRLAM : after the 2006 ALADIN/HIRLAM Sofia meeting (thanks to our excellent Bulgarian colleagues for the organization), the 2007 ALADIN/HIRLAM Oslo meeting will be another occasion to befriend the HIRLAM scientists. Several other important ALADIN/HIRLAM specialized meetings have taken place: on SURFEX, on data assimilation, etc. so one can appreciate that communication and common planning are becoming a reality. The last, but not the least, step towards full ALADIN/HIRLAM cooperation will be the work on common software - some joint phasing activities have begun in 2006. One can expect a stronger common R&D in 2007, where we start reaping the rewards of an enhanced cooperation. This should be our return on investment in additional meetings and code management efforts.

On a broader scale, attempts are being made to achieve a pan-European cooperation in NWP (with Mediterranean countries included). Some "vision for Europe" talks have been held at the political level. But what does it mean in practice ? Well, it is not obviuos, apart from the very popular SRNWP meetings. In 2007, attempts will be made to start three real development projects: interoperability between NWP software, EurEPS (European Ensemble Prediction System), and verification. They are not going to happen without funding, which will soon be requested from Eumetnet, beside a formal renewal of the SRNWP programme. These efforts address some fundamental questions: do we want a European community of National HydroMeteorological Services (NHMSs), or shall we let one of the bigger institutes become a European Centre for short-range NWP, thereby crushing the competitiveness and independence of the others ? Will the NHMSs spend all their budget on national activity, or will they divert some money towards international cooperation, so that it will be strong enough to be profitable ? Here, one can recognize some of old issues of the ALADIN consortium, or even of the European Union, on a different scale. Eventually, it will determine what kind of R&D we shall be able to do in the future, whether our teams will grow or dwindle, and which people and software we shall work with in a few year's time.

The European Framework Programme 7 is beginning. One topic is of particular interest to us : environmental security. Hopefully, there will be opportunities for some NWP-oriented programs there. Also, note that our ARPEGE/ALADIN/ALARO/AROME software (shall we call it A^4 ?) is becoming increasingly portable on PCs and clusters, making it easily accessible for research labs and universities of ALADIN partner countries. Please note that granting a software licence for research (i.e. non operational, non commercial) purposes in your respective countries is very easy, requiring only minimal authorization in ECMWF member states (it is quite easy to do in other ALADIN states, too).

But let us get back to the ALADIN business. Welcome to the new website of RC-LACE. The event of the year probably is the first operational use of ALARO-0 (less grey-scale convection, at CHMI), after some very brave development carried out in sometimes difficult conditions. Congratulations. It means that our consortium is succeeding in setting up a panel of NWP models to suit all needs, all computers and all resolutions: ALADIN, ALARO and AROME. Of course there have been worries that our consortium was splitting itself. But there has also been large, less visible (they do not have an acronym !) efforts to keep a common software framework. The physics interface and diagnostics have been considerably expanded with considerable effort. Our software maintenance capability has been strained with the plugging in of the HIRLAM, ALARO-0 and

SURFEX physics options. But we keep the faith, and even more staff will be invested into model software in the future, because it is at the heart of our business.

Some important papers have been written in recent months. I would urge you to read the outcome the last ALADIN director's assembly (do not miss the PM's comments about the work plan), of the last Policy Advisory Committee (Lisbon), the SRNWP programme proposals, and the draft of the ten-year ALADIN strategy (soon to be made public). And, please, give your opinion - it does not have to be always the same ones who speak out in ALADIN. Constructive comments are always welcome.

F. Bouttier, Météo-France

1.1. EVENTS

1.1.1.

28th EWGLAM and 13th SRNWP Meetings, 9-12 October 2006, Zurich (Switzerland)
http://srnwp.cscs.ch/Annual_Meetings/2006/entrypage2006.htm

Ze Photo

1.2. ANNOUNCEMENTS

- LACE Steering committee: Ljubljana, Slovenia, 22-23/02/2007.
- Cloudy boundary layer workshop: Toulouse, France,12-14/03/2007

(Please find more details at http://netfam.fmi.fi/CBL07)

- SRNWP Meeting: Norrköping Sweden, 21-23/03/2007.

High resolution data assimilation with emphasis on the use of moisture-related observations – "How to project on a good estimate of the moist attractor before it moves away"

- Alaro training course: Radostovice Czech Republic 26-30/03/2007.
- "6th International Conference on Urban Air Quality" 27-29 March 2007 in Limassol (Cyprus) Information: http://www.urbanairquality.org.

In collaboration with COST-728, a session is dedicated to "Mesoscale Modelling".

- PAC meeting, 3-4 April 2007, Prague.
- 2nd ALADIN-HIRLAM Workshop & 14th SRNWP Meeting: Oslo, Norway, 23-26/04/2007
- Joint NetFAM/COST-728 Workshop on: "Integrated systems of meso-meteorological and chemical transport models" 21-23 May 2007, DMI, Copenhagen.

Workshop web-site: http://netfam.fmi.fi/Integ07/

- ⇨ EWGLAM/SRNWP, 9-12 October 2007, Dubrovnik.
- ⇨ ALADIN GA, end of 2007.

1.3. The User's Guide: Introduction to NEC “tori” machine at Météo-France

J-A. Maziejewski Météo France

1.3.1. Presentation of the computer's architecture.

Introduction

The intensive computing system at Météo-France is composed of 2 NEC systems, each having 16 SX-8R vector nodes, a linux TX7 scalar front-end, a HP-UX batch handler and a GFS file server (also called “NAS head”). These two systems are fully identical. One of these system, called “sumo”, is dedicated to operational tasks while the other one, called “tori” hosts R&D tasks. This latter one is described in this guide.

The configuration can be found on the web site of the IntraDSI under the heading:

DSI/SC -->DSI/SC/CC --> Configuration supercalculateur NEC pour Météo-France.

Acces point open to users

Users can work on the “tori” front-end and the 16 computing vector nodes.

Each of these vector nodes is a symmetrical multi-processor composed of 8 vector processors sharing a 128 Gb memory. The characteristics of a vector node are as follow:

- operating system: Unix system V (Super-UX)
- 8 processors at 35 Gflops theoretical maximum performance each. The R&D theoretical peak performance is therefore of 4,5 Tflops.

The nodes interconnect via a very efficient and high-performance internal crossbar network (IXS) with a maximum transfer rate of 2*8 Gb bidirectional/nodes.

The scalar front-end is the unique access entry point for users. The mainframe characteristics are as follow:

- Linux operating system (Suse)
- 16 cores Intel Itanium2 & 32 Gb memory.

Interactive work is only possible on the scalar front-end.

This front-end shall be used for compiling (cross compiler for SX8), for the submission of tasks on the vector nodes and for file transfer with either “cougar” or other access points of Météo-France's network. Tasks will preferably be launched in batch mode on the front-end (e.g. in the “compile” class). Only short tasks with low resources use will be tolerated in interactive mode (e.g. small editing jobs, library management, small compilation tests, file housekeeping).

Each computer is highly specialized. Computing batch tasks will be executed on the vector nodes, transfers via “ftserv” will be made from the front-end (cf II.4).

Disk configuration

The total user space disk is of 19 Tb. It is shared by all the vector nodes and the scalar front-end through the Global File System (GFS).

A local disk space of 256 Gb is available on each vector node, which can be used as a temporary working space for a "single-node" batch task (/localtmp). In this working space, data from a batch request will be automatically destroyed at the end of the request.

Anyone has access to this disk space, for node-local specific use.

HOMEDIR: user's permanent separate storage area. DSI/SC/CC provides the back up of data stored there. HOMEDIR user's data are saved by the software «Time Navigator». Users are split into 4 different file-systems (/cnrm, /mf, /ch, /ext) see 1.4 for allocation details. Total volume amounts to 6Tb.

TMPDIR: temporary disk space, accessible from every node, which a user can use either during the lifetime of his job or his interactive session. This space is therefore not saved, thus, all data are automatically destroyed at the end of the session (users themselves must transfer files to either their workstations or to O3000/DMF). The explicit path of an TMPDIR is «/utmp». Its total volume amounts to 9Tb.

TMP_LOC: specific to a computing node: temporary disk space specific to a node. Be cautious, this space is unseen by other nodes and to the front-end. It may be of interest to use this space for a single-node job. The I/O efficiency there will be a lot better than on the shared TMPDIR.

FTDIR: buffer zone to be used when transferring through ftserv: see II.4 for advice about its use. This space is monitored by the system (automatic cleaning).

WORKDIR: intermediate (without back up) working space where data is stored as for long as possible. Most of the time, it is a buffer zone: there, users will frequently store retrieved data which is also archived elsewhere (generally on Origin3000/DMF). It is quicker to save files on WORKDIR than to go and retrieve them on «cougar». The oldest files are automatically destroyed as soon as the file system has reached a certain level. The explicit path of an WORKDIR is "/work". Total volume amounts to 4Tb.

Each of these disk space can respectively be reached using the variables $HOME, $TMPDIR or $tmpdir, $TMP_LOC or $tmp_loc, $WORKDIR or $workdir.

Allocation of file system on IMPE

The allocation of the different file systems GFS (visible from all nodes) is as follow:

TMPDIR FTDIR	/utmp	9,5Tb
WORKDIR	/work	4Tb
HOMEDIR	/cnrm /ch /mf /ext	2,5 Tb (CNRM) 2 Tb (operational suite) 1 Tb (Météo-France, non-operational) 1 Tb (non-MF users))

1.3.2. Services

Interactive

The interactive connexion is only allowed on the front-end ("telnet tori").

Only short tasks and resource use will be tolerated in interactive mode (short print and library works, very small compiling tests, file organization, batch job submissions). Big compiling test will have to be submitted in batch on this front-end (qsub -q compile).

Accounts

Login

An account name is made of 7 characters: *sgrpxxx*

- the letter s identifies the partner
- m for Météo
- c for Cerfacs
- s for MERCATOR
- e for outsiders

- grp is made of 3 letters used to identify projects or groups (a group in a unix sense is of the

form *sgrp*).

- *xxx* is a string of 3 digits.

$HOME structure

the $HOME directory name has the structure /group/team/srpg/sgrpxxx with group being:

- cnrm for CNRM
- ch for operational suite
- mf for MF team not on the operational suite and not CNRM (DP, ENM, DIR,...)
- ext for non MF users (Cerfacs, Mercator, NEC, ...) and DSI

and "teams" one of:

- dp for Direction de la Production
- enm for ENM
- dir for all DIRs
- gc for GMGEC
- gc_ext for outside climate labs
- ge for GMME
- gi for GMEI
- gp for GMAP
- mr for MERCATOR
- cf for CERFACS
- dsi for DSI and NEC

Each user will have to transfer its own files from $HOME from "tora" (VPP) to the new NEC system. It was felt that it was not desirable to transfer all files from "tora" as most of them cannot be used on the new system (executables, reallocatable binaries, libraries,...). This will be the opportunity to do a big cleaning! The two systems will jointly operate for 6 months (till the end of June 2007), this period of time will give you the chance to transfer what you think is worth transferring.

Passwords

When creating an account, a temporary password is generated. It must be replaced when logging in for the first time. Then, it must be changed at regular interval within 12 weeks. A password is composed of at least 6 characters with no less than 1 special or numerical character and 2 alphabetic characters.

Batch

All tasks have to be launched in batch. The batch handler is NQSII.

Tasks submission

It is done directly from tori (the front-end).

A batch task (or batch request) can be single-processor, single-node (up to 8 processors) or multi nodes.

The task scheduler being based on real time (or elapsed time), it is absolutely necessary to specify this limit when setting the "qsub" submission options. **Please note that this is new, compared to the VPP procedure**.

For an optimal working of the scheduler, it is very important to describe as precisely as possible, tasks (number of nodes, number of processors per node, CPU time, elapsed time, node memory) and to make sure that options made through "qsub" are consistent with the mpirun command for jobs requiring MPI.

The main standard NQS instructions are as follow:

job submission:

qsub [options] myjob for submitting jobs (myjob = submission script)

ex:

qsub -q vector -b 2 -1 cputim_job=1200, cpunum_job=4, elapstim_req=600, memsz_job=12gb -j o . /test .sh

submits script "myjob" to the "vector" class, on 2 nodes, 4 procs per node, 12Gb memory per node, 1200 sec of CPU time per processor and 10 min total elapsed time.

"man qsub" gives more details about submission options.

Every submission option can be specified either on the « qsub » command line, or in the first lines of script « myjob », in which case they must be prefixed by « #PBS »:

```
#PBS -N JOBNAME                 # Name of the NQSII request
#PBS -q vector                  # NQS class
#PBS -T mpisx                   # type of job (if MPI -T mpisx)
#PBS -b 2                       # number of nodes used
#PBS -1 cpunum_job=2            # number of procs used/node
#PBS -1 cputim_job=00:16:00     # maximum CPU time
#PBS -1  memsz_job=12gb         # maximum memory size by node
#PBS -1 elapstim_req=00:10:00   # elapsed time (real time)
#PBS -j o                       # stdout and stderr on the same JOBNAME.nqsout file name
  ... job commands...
```

The four compulsory options to the scheduler are the following: elaptim_req, cpunum_job, memsz_job and -b. Should you not specify them, the default values will be used and therefore could not be suitable (weak values are set by default).

Job monitoring:

qstat [reqid] or qstat -f [reqid]

To monitor all jobs:

/usr/local/bin/qstat_all

To see the repartition of the reqid job on the different nodes:

qstat -J reqid

To stop/kill a job:

qdel reqid or qsig -9 reqid or qsig -SIGKILL reqid

To suspend/resume a request:

qsig -s STOP reqid and qsig -s CONT reqid

To hold/release a request:

qhold reqid and qrls reqid

Monitoring the output of running jobs:

qcat -o [reqid] for stdout or qcat -e [reqid] for stderr if different

Queue structure

This structure can be modified by the administrators in order to optimize the computer resources. The qstat -Q command gives all the defined queues. The actual queue structure is as follow:

NQSII queue	Executing machine	Number of nodes	Comments
compile	TX7 (tori)		Reserved for compilation jobs
ft	TX7 (tori)		Reserved for transferring files to/from Météo-France's network, especially « cougar ». CPU time is limited to 600 seconds.
vector	SX8	routing towards appropriate queue	Routes towards other queues (mono, express, multi) according to request in the number of procs and CPU time.
express	SX8	2, 3 or4 nodes max 8 procs/node	Multi-node & multiprocessors jobs with number of nodes ≤4 and elapsed time ≤ 3 hours Cannot be addressed directly. To use this queue, submit to « vector ».
mono	SX8	Only 1 node 8 procs maximum (1 proc by default)	Single node multiprocessors tasks Cannot be addressed directly. To use this queue, submit to « vector ».
multi	SX8	5,6,7 or 8 nodes max 8 processors by nodes	higher level multinodes multiprocessor tasks: 4 < number of nodes ≤ 8 Cannot be addressed directly. To use this queue, submit to « vector ».
debug	SX8	Max 2 nodes	Open on request for total view debugging

File transfer software to storage mainframe

The « ftserv » software has been implemented on the front-end only.

The local commands (ftpassword, ftget and ftput) have been implemented in order to regulate and to secure transfers between “cougar” and “tori”. The transfers use the “ftp” protocole, login password on « cougar » is stored in an encrypted form in the config file « .ftuas » in the $HOME of tori.

« ftget » and « ftput » commands must be used from this machine to transfer files between “cougar” and $HOME or $WORKDIR or $FTDIR. The use of FTDIR is recommended should you not wish to keep the files after computing has been done.

These temporarily stored files will be seen from the vector nodes. $FTDIR, contrary to $TMPDIR, will be kept after the retrieval step, therefore stored files will be accessible by the request running on the vector nodes.

Usage:

Update the “ftuas” file using “ftmotpasse -u usercougar -h cougar-tori”

Ex: msys001@tori:/dsi/msys/msys001> ftmotpasse -u msys001 -h cougar-tori

Enter password for the machine: cougar-tori

New password:

Check:

2007/01/08 10:30:17 INFO pid(6371) update OK for the file '/dsi/msys001/.ftuas' for the remoteuser[msys001] on the remotehost[cougar-tori]

« Cougar-tori » is the name of the 10Gbit interface: the fast link between tori and cougar.

Use the “ftget” and the “ftput” commands to transfer from or to cougar. “ftput” command can be used in an asynchronous mode (the job will resume without waiting for the end of the transfer).

Enter “ftmotpasse”, “ftget” or “ftput” for more details about the different options of these commands.

Ex: ftget –h cougar-tori fic_O3000 $FTDIR/fic_GFS

2007/01/08 10:00:31 INFO pid(8189) Debut de la demande: GET msys001@cougar-tori:fic_O3000 /utmp/ftdir/msys001/fic_GFS

2007/01/08 10:00:53 INFO pid(8189) Fin du transfert FT_OK: GET msys001@cougar-tori:fic_O3000 /utmp/ftdir/msys001/fic_GFS : Transfer complete.

During batch jobs, it is of the utmost importance that jobs/tasks should have the following structure (split into 3 NQS secondary jobs)

1. **Preprocessing step** (jobs running on the front-end “tori” in the “ft” class):
   i. file retrieval under GFS on $FTDIR buffer space (ftget)
   ii. qsub -q vector job_calcul
2. **Computing step** (job running on vector nodes):
   i. links of input files from $FTDIR to $TMPDIR
   ii. computation inside $TMPDIR
   iii. move output files (to be transferred to cougar) to $FTDIR
   iv. qsub -q ft post_processing
3. **Postprocessing step** (job running on the “tori” scalar front-end in the “ft” class):
   i. file archiving on cougar or any other local platform (ftput)

Exemple of a job sequence:

1. **Pre-fetch input files necessary for computation on FTDIR and launch the computation step**:

```
#JOB d'acquisition des fichiers
#PBS -N FILEGET
#PBS -j o
#PBS -o myoutput
#PBS -l cputim_l cputim_job=00:05:00
#PBS -l memsz_job=24mb
#PBS -q ft
set -x
cd $TMPDIR
ftget cougar-input $FTDIR/input
ls -l
cd $HOME/JOB
/usr/bin/nqsll/qsub $HOME/JOB/job.compute
```

2. **Computation job and launch of the archiving step:**

```
#PBS -N FILECOMPUTE
#PBS -j o
#PBS -b 1
#PBS -l cpunum_job=1
#PBS -l cputim_job=00:05:00
#PBS -l elapstim_req=00:05:00
#PBS -l memsz_job=240mb
#PBS -q vector
set -x
```

```
F_PROGINF=detail
export F_PROGINF
cd $TMPDIR
ls -l $FTDIR
ln -s $FTDIR/input fort.4
./a.out
mv fort.5 $FTDIR/output1
mv fort.6 $FTDIR/output2
ls -l
cd $HOME/JOB
/usr/bin/nqsll/qsub $HOME/JOB/job.put
```

3.Save output on cougar

```
#PBS -N FILEPUT
#PBS -j o
#PBS -l cputim_job=00:05:00
#PBS -l memsz_job=24mb
#PBS -q ft
set -x
cd $TMPDIR
ftput $FTDIR/output1 dircougar_experiment/output1
ftput $FTDIR/output2 dircougar_experiment/output2
echo "FIN"
```

HOMEDIR Back up

The software « Time Navigator » saves files which are on permanent space ($HOME). Lost files can be restored with the help of a user interface.

To restore a file, command « tina » must be launched on a client machine from the directory « hardy » (titan, forte, andante, adagio,...) and then, through the graphic interface, reach the NEC front-end using the following steps:

- To recover a file belonging to filesystem /ch or :ext:

  sauvegarde -> Systeme -> Connection -> tori

- To recover a file belonging to filesystem » /cnrm or /mf:

  sauvegarde -> Application -> Connection -> tori.fs

  Then a user interface appears asking for your login and password for tori. You will then see your home directory on tori, you can unfold the directory tree and from the left side window, you can go back. Choose the files to be recovered (tick next to the filename) then:

  Sauvegarde -> Restaurer

Application environment

The FORTRAN Compiler

FORTRAN 95 is the norm for the FORTRAN compiler (sxf90). It is a "cross compiler" which generates codes for vector nodes from the front-end "tori".

« sxf90 » enables to get to the cross compiler, either run « man sxf90 » or read the guide to know the different options (see II.7.2) or the full documentation « cookbook ».

The optimization options are the following:

vector and scalar optimisation:

- SXf90 -C **hopt** code.f **highest level (quite risky)**

- SX f90 -C **vopt** code.f **high level (why not!)**
- SXf90 -C **vsafe** code.f **safe vectorization (if you say so...)**

<u>scalar</u> only optimisation:

- SXf90 -C **sopt** code.f
- SXf90 -C **ssafe** code.f
- SXf90 -C **debug** code.f **(last resort...)**

Debugging:

1) -C debug suppresses every optimization and every vectorization.
2) -gv produces a table of symbols for debugging with vectorization info
3) -eC check for out of bounds array indices
4) -eR check the array syntax

<u>Type représentation</u>:

SX8R can compute in 32 bits or 64 bits.

- SXf90 **-dw** code.f90 **computations on 32 bits**
- SXf90 **-ew** code.f90 **or on 64 bits**

	-dw	-ew
INTEGER*2	integer type(2bytes) <*>	integer type(8 bytes)
INTEGER[*4]	integer type(4 bytes)	integer type(8 bytes)
INTEGER(KIND=2)	integer type(2 bytes)<*>	integer type(8 bytes)
INTEGER(KIND=4)	integer type(4 bytes)	integer type(8 bytes)
LOGICAL*1	logical type(1 bytes)<*>	logical type(8 bytes)
LOGICAL[*4]	logical type(4 bytes)	logical type(8 bytes)
LOGICAL(KIND=1)	logical type(1 bytes)<*>	logical type(8 bytes)
LOGICAL(KIND=4)	logical type(4 bytes)	logical type(8 bytes)
REAL[*4]	real type(4 bytes)	real type(8 bytes)
REAL*8	real type(8 bytes)	real type(8 bytes)
REAL*16	real type(16 bytes)	real type(16 bytes)
REAL(KIND=4)	real type(4 bytes)	real type(8 bytes)
REAL(KIND=8)	real type(8 bytes)	real type(8 bytes)
REAL(KIND=16)	real type(16 bytes)	real type(16 bytes)
DOUBLE PRECISION	real type(8 bytes)	real type(8 bytes)
COMPLEX[*8]	a pair of real type(4 bytes)	a pair of real type(8 bytes)
COMPLEX*16	a pair of real type(8 bytes)	a pair of real type(8 bytes)
COMPLEX*32	a pair of real type(16 bytes)	a pair of real type(16 bytes)
COMPLEX(KIND=4)	a pair of real type(4 bytes)	a pair of real type(8 bytes)
COMPLEX(KIND=8)	a pair of real type(8 bytes)	a pair of real type(8 bytes)

	-dw	-ew
COMPLEX(KIND=16)	a pair of real type(16 bytes)	a pair of real type(16 bytes)
1.23E1	real type(4 bytes)	real type(8 bytes)
1.23D1	real type(8 bytes)	real type(8 bytes)
1.23Q1	real type(16 bytes)	real type(16 bytes)
1.23_4	real type(4 bytes)	real type(8 bytes)
1.23_8	real type(8 bytes)	real type(8 bytes)
1.23_16	real type(16 bytes)	real type(16 bytes)
SQRT	real type(4 bytes)	real type(8 bytes)
DSQRT	real type(8 bytes)	real type(8 bytes)
QSQRT	real type(16 bytes)	real type(16 bytes)

<*> the size is 4 bytes when **-eW** is present. If one wants to keep storage on 2 and 1 bytes respectively, to integer (kind=2) and logical (kind=1), option **-d W** must be specified.

If with -dw one wants to transform REAL in REAL*8, it is necessary to add:

SXf90 -dw **-Wf"-A dbl4"** code.f

The association of these different options of compilation provides a very complete representation of numbers.

Dynamic and statistic allocation

Memory map:

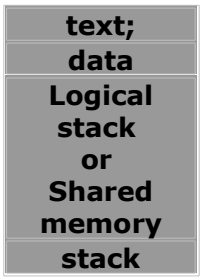

- stack: limited by default to 512 Goctets (or to the maximum of the memory)
- data: static memory zone (keeping local values <-> loss of space memory)

stack and heap can be either set to zero or undefined (NaN, which is useful for debugging) :

SXf90 -P stack **-Wf"-init stack=zero heap=zero"** code.f

Furthermore, common and modules variables (including derived types) can also be initialized at the beginning of the job. Must be specified when editing links:

SXf90 -Wl"-f zero" -o code.x code.o

By default, the static mode is applied and variables are initialized at zero. Almost as in the VPP. It is essential to thoroughly check the code, specially when parallel programs, by ensuring the variables are correctly initialized. This can be done in four steps.

SXf90 -P static -o code.x code.f90

SXf90 -P stack **-Wf"-init stack=zero heap=zero" -Wl"-f zero"** -o code.x code.f90

SXf90 -P stack **-Wf"-init stack=zero heap=zero" -Wl"-f nan"** -o code.x code.f90

SXf90 -P stack **-Wf"-init stack=nan heap=nan" -Wl"-f nan"** -o code.x code.f90

The cost of these initializations can be high. Therefore, once the code has been corrected, one must make sure that the software can run without it.

Compilation options:

syntaxe f90 NEC	Description
f90	compiler
-p	activate profiling mode. place it simply to the link edition
-D*define*	*define* statement for cpp
-U*define*	cancel *define* for cpp
-F	generate the file i.*fichier*.f resulting from pre compilation cpp of *fichier*.f
-P static	local variables created in a static way
-P stack	local variables created in the "stack" space
-P auto	auto tasking
-P multi	parallelization using directives
-Wf'-O nooverlap'	show the compiler that dynamic table (POINTER) do not overlap => vectorisation
-Wf'-pvctl noassume'	interpret a declared "dummy argument" TAB(1) as a vector
-Wf'-pvctl loopcnt=1000000'	set the maximum size of temporary tables
-Wf'-pvctl vwork=stack'	allocate temporary vectors in the "stack" space
-Wf'-ptr word'	the word is the unit for the dynamic allocation of memory
-Wf'-ptr byte'	the octet is the unit for the dynamic allocation of memory
-Wf'-O extendreorder'	optimise the scalar code
-Wf'-init stack=[zero|nan]	initialize the "stack" space to 0 or Not A Number
-Wf'-init heap=[zero|nan]	initialize "heap" space to 0 or Not A Number
-Wf'-Z *n*'	expand the dynamic zone to *n* octets
-Wf'-prob_generate'	create a profile when executing the code
-Wf'-prob_use'	use the previous profile to optimize the code

Main differences with the VPP

- User's work (edit, compiling, linking, library creation…) should be done on the front-end (TX7). The commands to be used are sxf90 (compilation), sxld (link edition) et sxar (SX8 format binary libraries). Then, executables are run on one or several nodes.
- Contrary to the VPP, a MPI parallel executable must be launched with the « mpirun » command.
- Contrary to the VPP, by default, variables are not initialized to zero.
- Equivalence of compilations options between the several systems (source E. Gondet /MERCATOR)

Compaq	IBM SP3	Fujitsu VPP5000	Nec SX	PGI	Sgi O2K	Description
F90	xlf[90][_r]	frt	f90	pgf90	f90	Compiler's name
-c						Sole Compilation
-o *executable*						Creation of an executable
-I *directory*						Directory where to seek "INCLUDE"
-L *directory*						Directory where to seek libraries

Compaq	IBM SP3	Fujitsu VPP5000	Nec SX	PGI	Sgi O2K	Description
F90	xlf[90][_r]	frt	f90	pgf90	f90	Compiler's name
-l *biblio*						link lib*biblio*.a
-version|-what	-#	-v	-v	-V or -flags	-version	Number of the compiler version
-automatic (omp défaut)	-qnosave	-K auto	-Pstack (défaut)	-Mnosave	(défaut)	Mode "stack"= allocation of the local variables in the stack
-noautomatic (défaut)	-qsave	(defaut)	-Pstatic	-Msave	-static	Static mode= allocation of the local variables in the bss
-old_f77|-f77	-qfixed=72 -qsuffix=f=f	-Fixed -X7 (-X7 -> strict F77 norm)	-f0	-Mnofree	-fixedform	Set format, usually by default for file in .f
(default) | -free toto.f	-qfree	-Free -X9	-f4	-Mfree	-freeform (default pour fichier en toto.f90)	Free format and with F90 norm usually by default for file in .f90
-fixed toto.f90	-q fixed=72 -q suffix=f=f90 toto.f90	-Fixed -X9	-f3	-Mnofree toto.f90	-fixedform toto.f90	Set format **but** with F90 norm
(default)	-qmoddir=. (défaut)	-Am	(default)	(default)	(default)	Compilation with F90 modules in the local directory
-qmodule *directory*	-qmoddir = *directory*	-Am – I *directory*	-I *directory*	-module *directory*	-I *directory*	Compilation with F90 modules in another directory

Available libraries

The mathematical libraries optimized by NEC for SX8 are available on tori: /usr/local/SX/lib/MathKeisan/lib. Especially libblas.a, libfft.a, liblapack.a, libparblas.a, libparfft.a, libsblas.a. They must be explicitly specified during the linking.

Local libraries (GRIB, BUFR, NETCDF…) are reached by the command /usr/local/SX/lib.

Environnement variables

$F_PROGINF = [no|yes|detail]	Activates CPU profiling
$F_FILEINF = [no|yes|detail]	Activates I/O profiling
$F_RECLUNIT = [word|byte]	Select direct access for unit RECL
$F_NORCW	Suppresses control words in sequential binary files
$F_SETBUF	Sets I/O buffer size

Miscellaneous

Accounting utilities

To get an idea about the use of the computer resources, set to « detail » the following variable: F_PROGINF , F_FILEINF and MPIPROGINF

WARNING: Be careful, these variables will only evaluate the resources used by a Fortran code but will not evaluate the total resources used by the batch request.

The command « /usr/local/bin/ja » executed at the end of a script, gives an overall picture of the resources used by the request.

It is expected that a more appropriate new command, typically of the form “ja” will be available soon.

Documentation

Two NEC guides can be found on line on intranet under http://intradsi.meteo.fr/:

DSI/SC-->DSI/SC/CC-->Guides utilisateurs de DSI/SC/CC-->documentation NEC
DSI/SC-->DSI/SC/CC--> Guides utilisateurs de DSI/SC/CC-->cookbook

2. OPERATIONS

2.1. INTRODUCTION

2.2. CYCLES

2.3. Transversal informations

2.4. Changes in the Operational Version of ARPEGE

2.4.1. ARPEGE and ALADIN e-suite (implementation postponed till mid 2007)

Evaluation by J. Stein, H. Bénichou, F. Pouponneau and M. Tardy, MF/DPREVI/COMPAS

E-suite description:

A new ARPEGE and ALADIN e-suite based on cycle CY31T1_op1, started on the 14th November 2006. This version includes the following scientific changes:

- The semi-Lagrangian horizontal diffusion called «SLHD » (Vana et al. 2001) was activated on wind, temperature and specific humidity and used jointly with a weaker spectral horizontal diffusion. The scheme has been tuned to the ARPEGE stretched geometry.

- The new parametrization scheme of mountain drag and lift (Catry et al. 2006) is used together with a reduction (50%) of the so-called envelope orography. The total surface drag is increased when the form drag is acting and is diminished in opposite conditions. A new vertical partition of the wave drag deposition is used. The lift effect is introduced to compensate for a missing volume of the resolved orography.

- The shortwave radiation scheme uses 6 new spectral bands instead of 2 in the operational model, to improve the representation of solar absorption in the near infrared spectrum due to clouds and in the ultraviolet due to ozone.

- The amount of ice in convective clouds is increased to improve at the top of the atmosphere, the radiative budget according to CERES satellite climatology and to reduce a cold bias in the upper troposphere in the Tropics.

- The critical relative humidity profile is modified to increase the frequency of low level broken clouds.

- The auto conversion of cloud is called before the radiation computations due to the long time steps used in ARPEGE and ALADIN (respectively 982s and 415s).

- The evaporation formulation of "large scale" precipitation is diminished in case of dry air environment.

- A new sedimentation scheme for precipitation replaces the semi-lagrangian one. The impact is neutral but the new scheme is simpler and less costly in term of CPU.

- The function Fh of Richardson number for heat and moisture in stable conditions is modified to increase vertical mixing.
- The « non linear » balance in the background cost function Jb, already operational in

ARPEGE 4D-Var, is used in ALADIN 3D-Var.

Objective scores for ARPEGE

This e-suite has been compared with the operational model during 3 months separated in three periods. Until the 20 December 2006, a first version of the e-suite has been compared with success with the operational model.

Plotted in figure.1, the scores for the geopotential height, showing the strong stratospheric improvement brought by this e-suite.

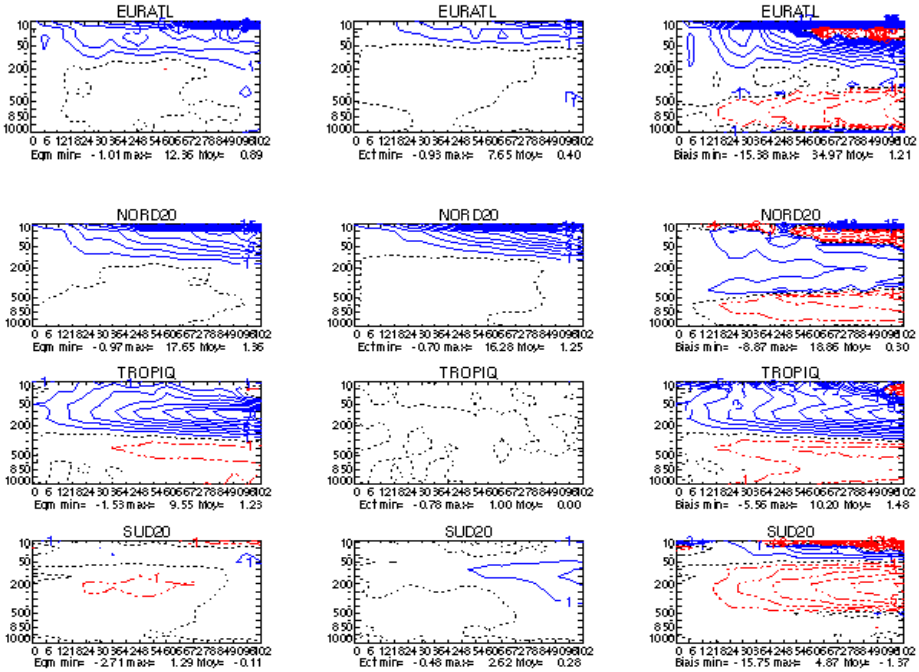

Figure 1: Difference of the scores between the operational and e-suite versions of ARPEGE. The reference is provided by the ECMWF analysis. The considered field is the geopotential height and the different plotted errors are : the RMS (left), the standard deviation (center) and the bias (right). The isolines of error are plotted every meter against the output time along the horizontal and against the pressure along the vertical. These results are temporarily averaged from 14 November 2006 to the 20 December 2006. Blue isolines show better performances for the e-suite and red isoline the contrary.

The winds are also strongly improved, especially above East of Asia and the maximum reaches 2 m/s at 10 hPa after 2 days of simulation. A weaker influence is found over the whole NORTH20 domain in its upper layers.

The second period corresponds to July 2006. The geopotential scores are presented in Figure 2. The stratospheric improvement is removed from the EURATL and NORTH20 domains but now appears in the SOUTH20 more clearly indicating that the physical modifications of the radiation and microphysical schemes are more active in winter conditions.

The third period corresponds to the activation of the increase of the mixing in stable condition in order to compensate the decrease of the low-level wind due to the modification of the parameterization of the subgrid orographic effects. It has been checked, that the same scores are recovered for the first period if we replace the version 1 of the e-suite by its version 2. It should be noted that the summer period has also been performed by the version 2 of the e-suite. The results for the January period are plotted in figure 3.

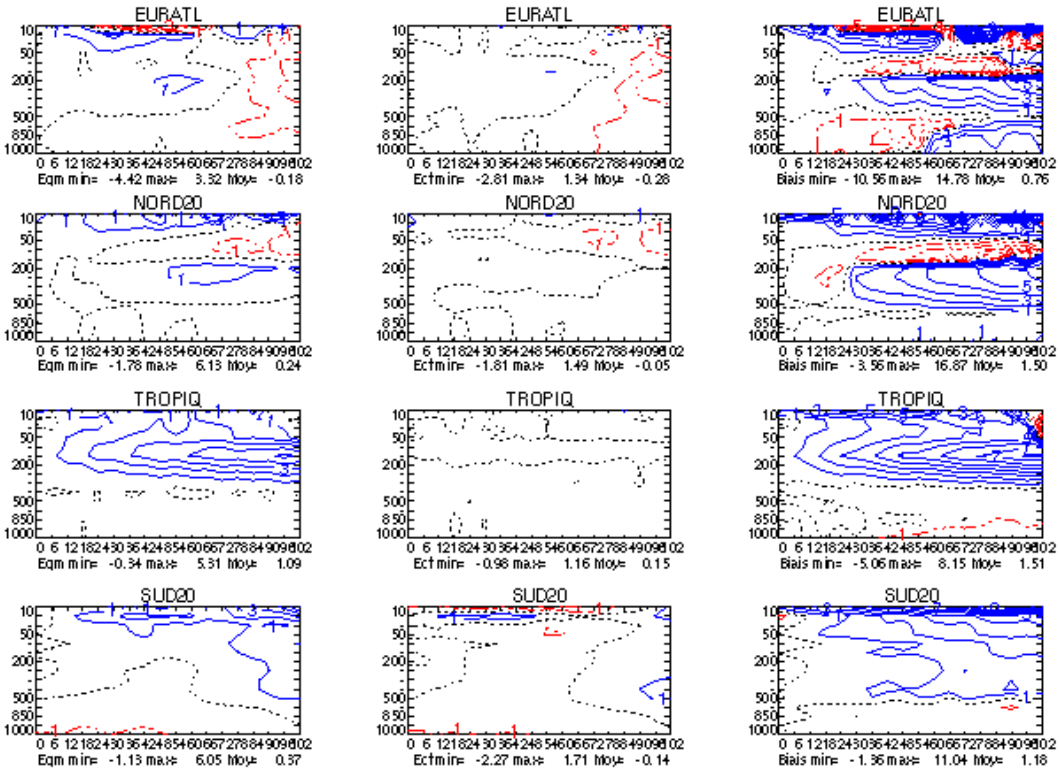

Figure 2: same legend as Figure 1 but from 08 July 2006 to 02 August 2006

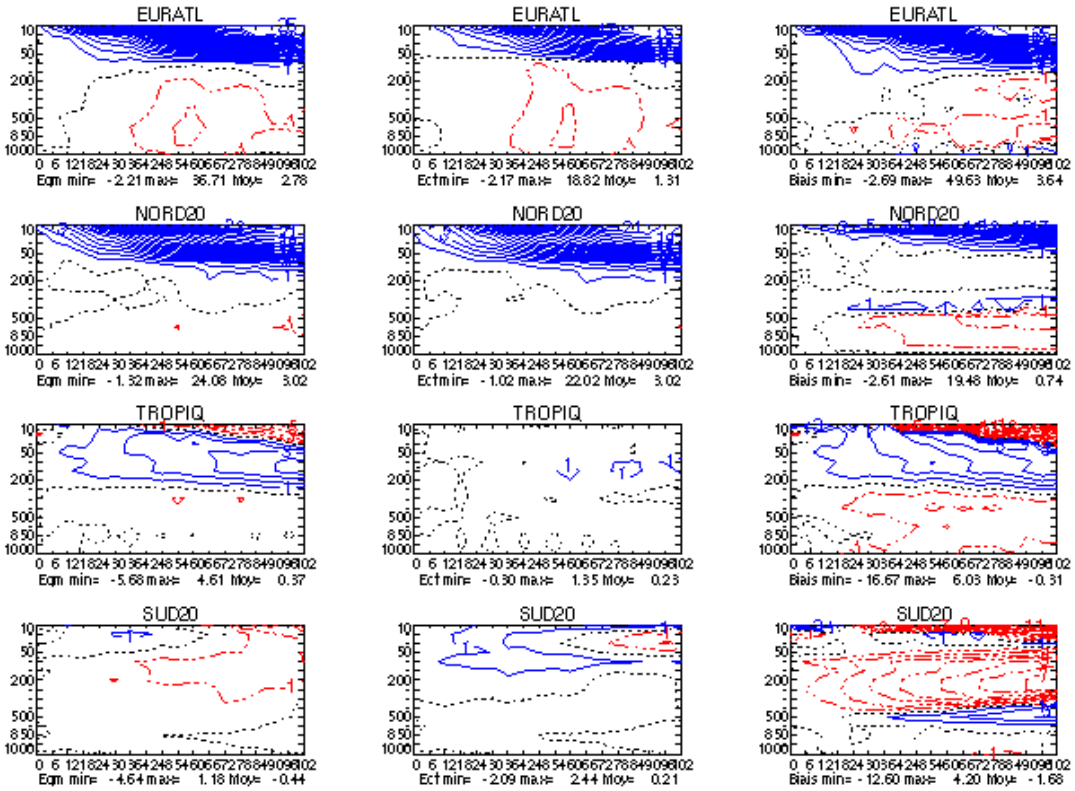

Figure 3: same legend as Figure 1 but from 22 December 2006 to 23 January 2007

It is clear that the stratospheric improvement is conserved but there is a deterioration of the results in the troposphere, especially over Europe and the North-Atlantic Ocean. This is due to a set of very bad forecasts of very rapid zonal fluxes which were present during a whole week. Among them, we find some very important case like the “Baltic case” which happened the 18-19 January

2007 and which caused damages and made victims in the whole of Europe. The e-suite strongly reduces the amplitude of this storm (figure 4) which was not the case of the operational version. Some sensitivity studies pointed out that the SLHD diffusion was too active in this case.

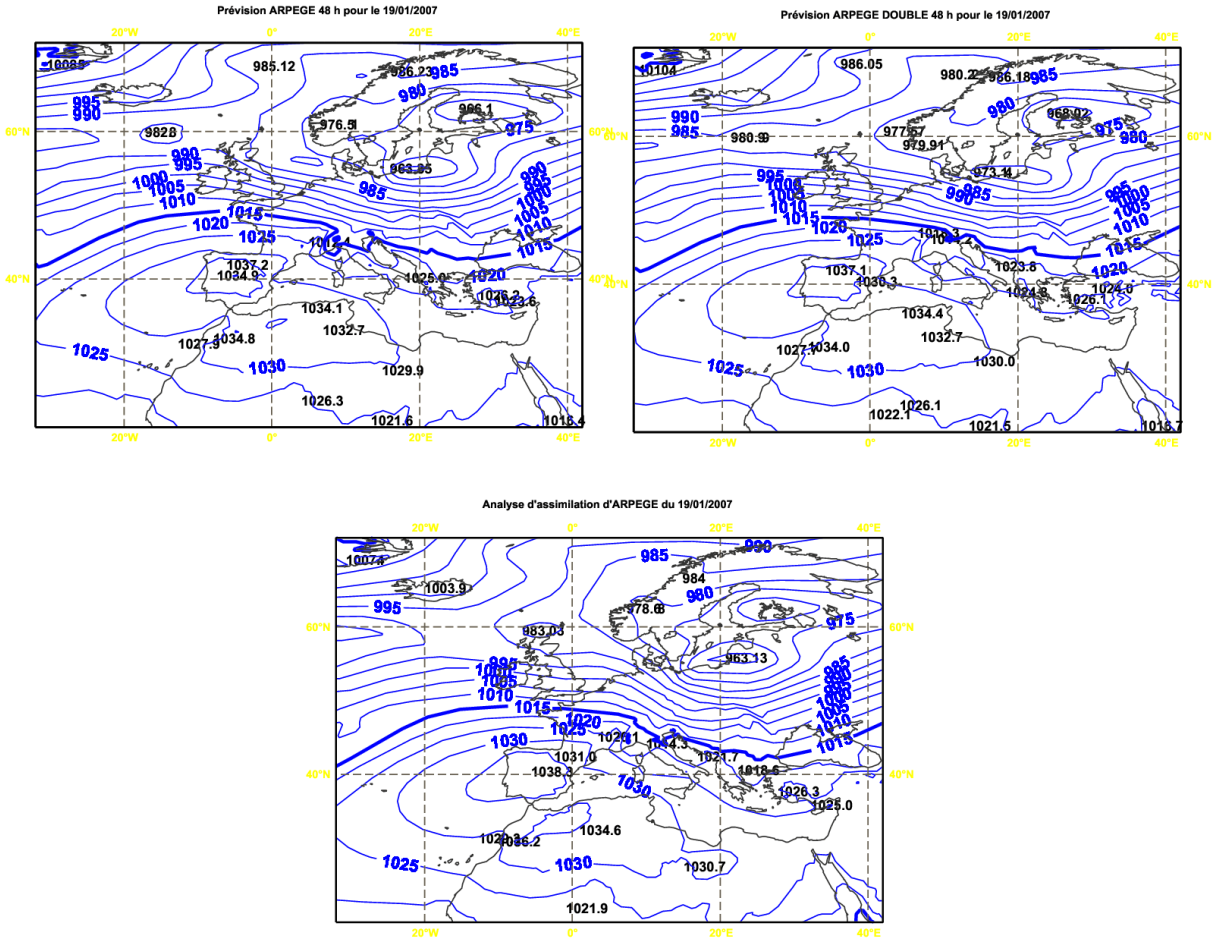

Figure 3 : Forecasts at 48 h for the 19 January 2007 0 h UTC made by: the operational version of ARPEGE model (upper left panel) , the ARPEGE e-suite (upper right panel) and the validating ARPEGE analysis (lower panel). The isolines of reduced pressure are drawn every 5 hPa.

Before these very violent cases, the SLHD diffusion was shown to be a very powerful way to remove the small-scale spurious cyclogenesis. But, its drawbacks for rapid zonal flows were judged too important to allow a switch from the operational version to this e-suite.

Conclusion:

This e-suite shows very interesting properties but its performances are clearly worse than those of the operational version for very rapid zonal flows. In these cases, the speeds of formation and of displacement of the storms are strongly modified and important storms are missed or under-estimated by this e-suite. It is for this reason that only a technical version based on cycle 31T1 without any scientific modification (except the modification of the speed of melting of the deep humidity moisture) became operational the 26 February 2007 after a short period of tests. This is this reduced version which will become the first operational version of ARPEGE-ALADIN running during Spring 2007 on the new NEC supercomputer of Météo-France.

2.5. ALGERIA

2.6. AUSTRIA

2.7. BELGIUM

2.8. BULGARIA

Andrey Bogatchev@meteo.bg

Successful switching to the new coupling and climatology files happened on 30 of January 2006. It should have happened earlier, but there were some problems with climatology files for the integration domain.

AL29T2 was upgraded to AL29T2_OP2 and put to parallel suite. In March it became operational.

A new integration domain of almost the same size, but with a higher resolution was implemented. The characteristics of the domain are as follow:

NDLON = 144; NDGLG = 108; NDLUXG = 122; NDGUXG = 92

Coordinates of the centre: ELONC = 25.5 ; ELATC = 42.75

Horizontal resolution 9 km, time step – 400 s.

At 17 of April this domain became operational.

New parallel suite was constructed for the 72 h forecast. The system again is based on shifted forecast, but the initial condition is the 6h ARPEGE forecast. Thus, initial time for each run became 06 and 18 UTC.

Later on the operational application switched to 46 levels and 3 hours coupling frequency in collaboration with our colleagues from Romania and coordinated by system support team from Toulouse.

In October operations were switched to 72 hours forecast.

Libraries:

Al31T1 were ported to our LINUX PC using gmkpack 6.2 and Intel FORTRAN 9.0.

It is important to outline,

1. that FA routines from XRD should not be compiled with specific Intel optimisations (especially facies.F).
2. During the ee927 Doctor Hook should be switched off.

2.9. CROATIA

Martina Tudor and Stjepan Ivatek-Šahdan

2.9.1. Summary

The operational suite on the old SGI machine (Mrcina) was stopped on 6th October 2006. It is still used for research due to difficulties in porting some research tools on the new SGI Altix. Since it is not maintained it will be switched off permanently.

The new SGI machine (Viking) has been upgraded with 8 processors in July 2006 reaching total 24 CPUs, that caused some disturbance in the operational suite but now it is the only machine used for the operational 72 hour forecast.

The backup for the transfer of the LBC files is changed from RETIM to ecgate. The research on EPS, coupling of physics to dynamics, NH dynamics and SLHD in high resolution has continued. A version of Alaro0 is ported to Viking, it provides the second operational 72 hour forecast since 7th December 2006 on the same domain and resolution (8km) and on the same number of levels in the vertical as the reference (first) Aladin 72 hour forecast. Both are run twice a day, for 00 and 12 UTC starting from ARPEGE analyses with DFI.

2.9.2. Operational suite

Status

ALADIN is operationally run twice a day, at 00 and at 12 UTC, with two versions: the reference "CZ" package and the Alaro0 -3MT (with prognostic TKE, cloud water and ice, rain and snow, but without prognostic convective species). However, both are run with the old Geleyn radiation scheme since the amount of low clouds increases and that is preferred by the forecasters. Coupling files are retrieved from ARPEGE (Meteo-France global model) via Internet and ecgate. Model resolution for both versions of Aladin is 8 km. Alaro is run only on the 8 km resolution Croatian domain and only reference Aladin is run on 2 km resolution for the high-resolution dynamical adaptation domains but with 2 different representations of orography, both without envelope. The execution of the suite is not controlled by the PBS Pro on the new SGI any more since the temporary licence for the 8 new processors expired on 14th November 2006 so the whole operational suite is run from cron. The research became more difficult without the scheduler so it is planned to devote one third of the machine to the long jobs only, and to run the operational suite using only 2/3 of the available CPUs.

Initialisation of ALADIN on Croatian domain is provided by Digital Filter Initialisation (DFI) for both versions of Aladin. Coupling frequency and frequency of output files is 3 hours. The forecast range is 72 hours. The operational versions of Aladin are AL29T2mxl (aem suite in Prague) and AL29T2 plus Alaro0 modset.

Visualisation of numerous meteorological fields from the new SGI is done on the archiving machine while the intranet Aladin pages containing more than numerous operational products remain LINUX PC. The many forecasted fields are plotted for both versions of Aladin, as well as their differences (fig.1).

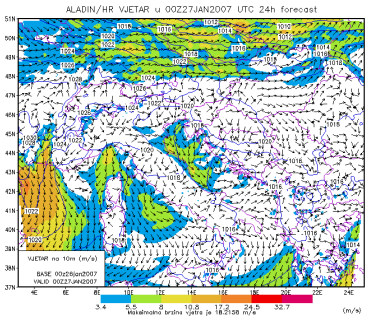

10m wind Aladin

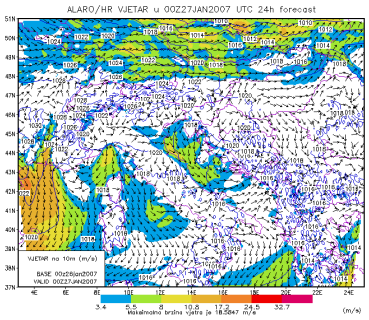

10m wind Alaro0

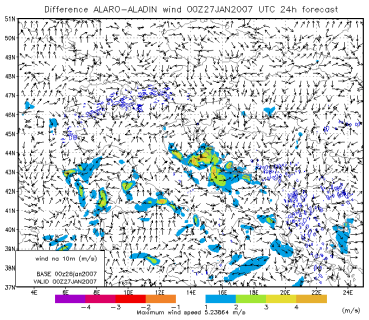

10 m wind difference

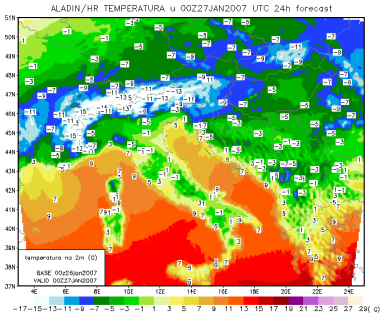

2m temperature Aladin

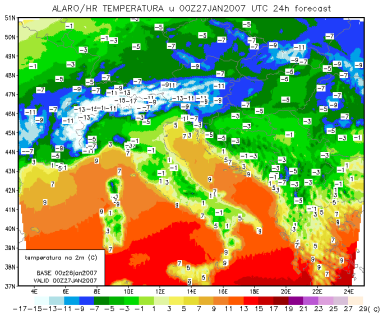

2m temperature Alaro

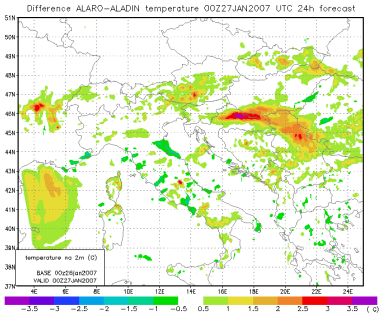

2m temperature difference

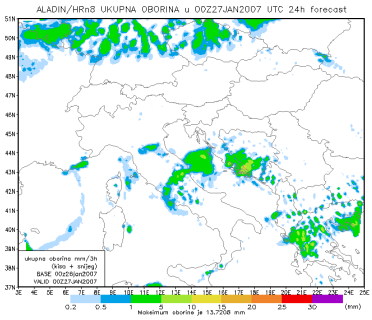

3 hr total prec. Aladin

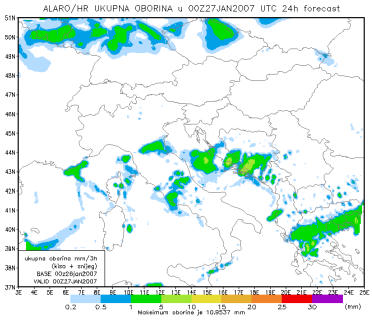

3hr total prec Alaro

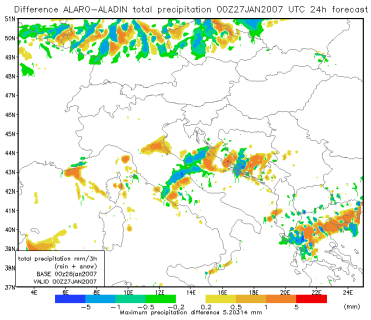

3hr total prec difference

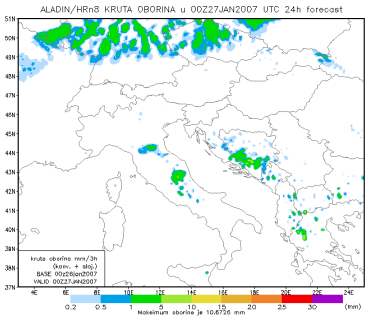

3hr total snow Aladin

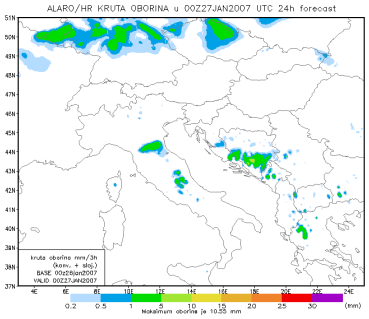

3hr total snow Alaro

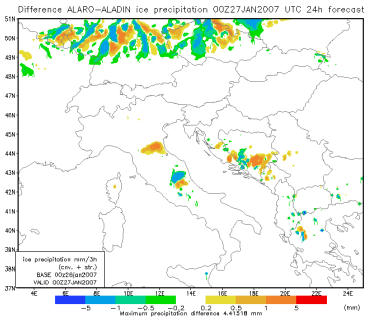

3hr total snow difference

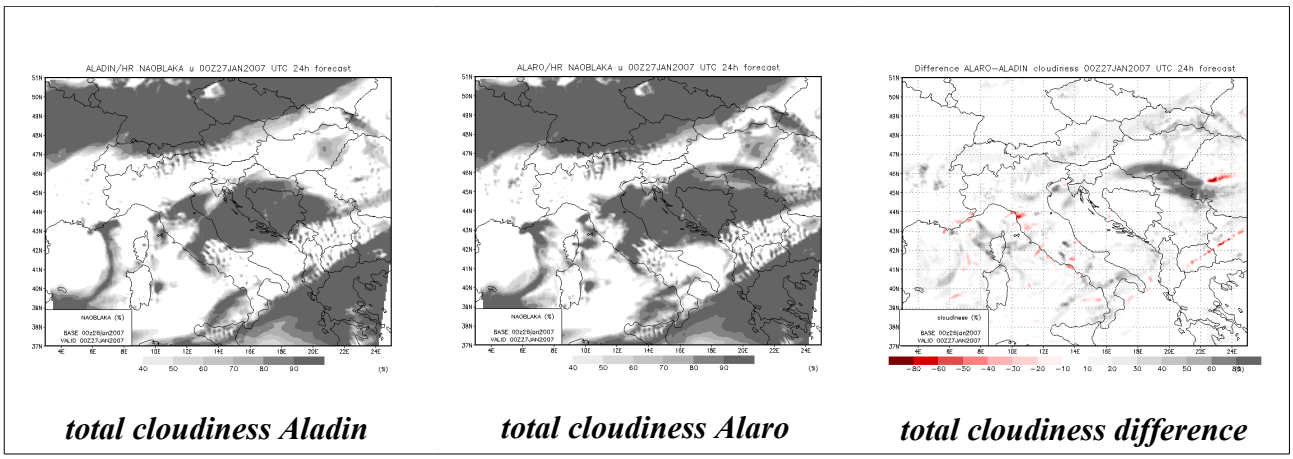

Figure 1. Comparison of forecasts with AL29T2mxl, nicknamed "Aladin" (left), AL29T2 with prognostic TKE, cloud and precipitation species, nicknamed "Alaro" (center) 8-km resolution forecasts and their difference (right).

Comparison of forecasts with data measured on SYNOP and automatic stations, done hourly for the last 5 runs for both versions of Aladin gives an EPS-like picture through 5 days (fig. 2) . Also, comparison of 24 hour precipitation with the measurements from the SYNOP stations provides an insight into effect of prognostic cloud and precipitation species (Figure 3). The products are available on the Intranet & Internet. Internet address with some of the ALADIN products, like total precipitation and 10 m wind: http://prognoza.hr/aladin_prognoza_e.html .

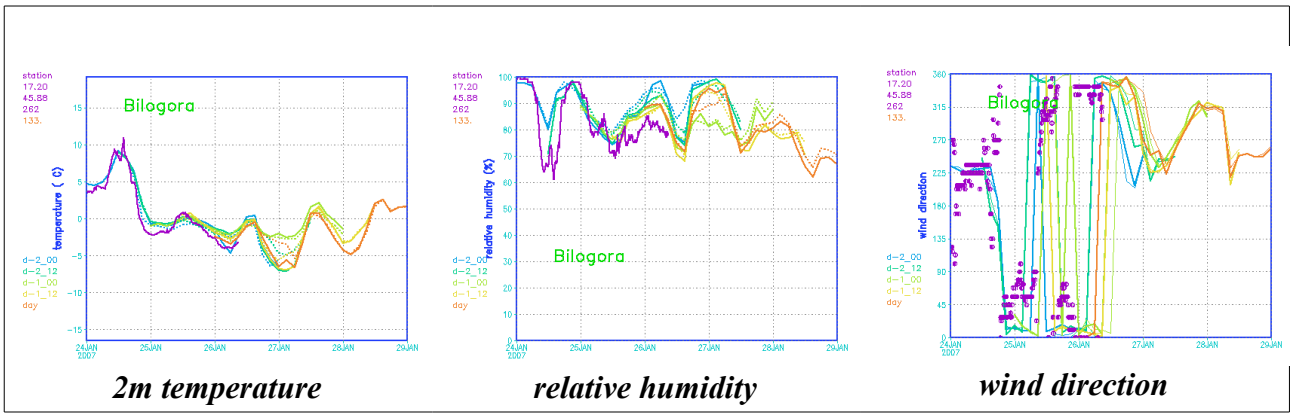

Figure 2. Comparison of forecasts with to the measurements from automatic stations for 2m temperature (left), relative humidity (center) and wind direction (right) on Bilogora station, AL29T2mxl forecasts are in full lines, Alaro is dashed (or thin line for wind direction), measured 10-minute average is purple.

The new computer

SGI Altix LSB-3700 BX2 Server with 24x Intel Itanium2 1.6GHz/6MB, 48 GB standard system memory, 2x146 GB/10Krpm SCSI disk drive, OS SUSE Linux Enterprise Server 9 for IPF with SGI Package, Intel Fortran & C++ compilers, PBS Pro for LINUX (useless since the licence is valid only for 16 processors). gmkpack is ported, but used far less frequently than wished.

Operational model version

The first operational version of Aladin is AL29T2 including the "mxl" modifications introduced in Prague. The semi-Lagrangian horizontal diffusion is on. 72 hour forecast on 18 CPUs takes 32 minutes.

The second operational version (run after the first one) is AL29T2 including "mxl" modifications as well as Alaro0 package with prognostic TKE, cloud water, ice, rain and snow species. 72 hour forecast on 18 CPUs takes 43 minutes.

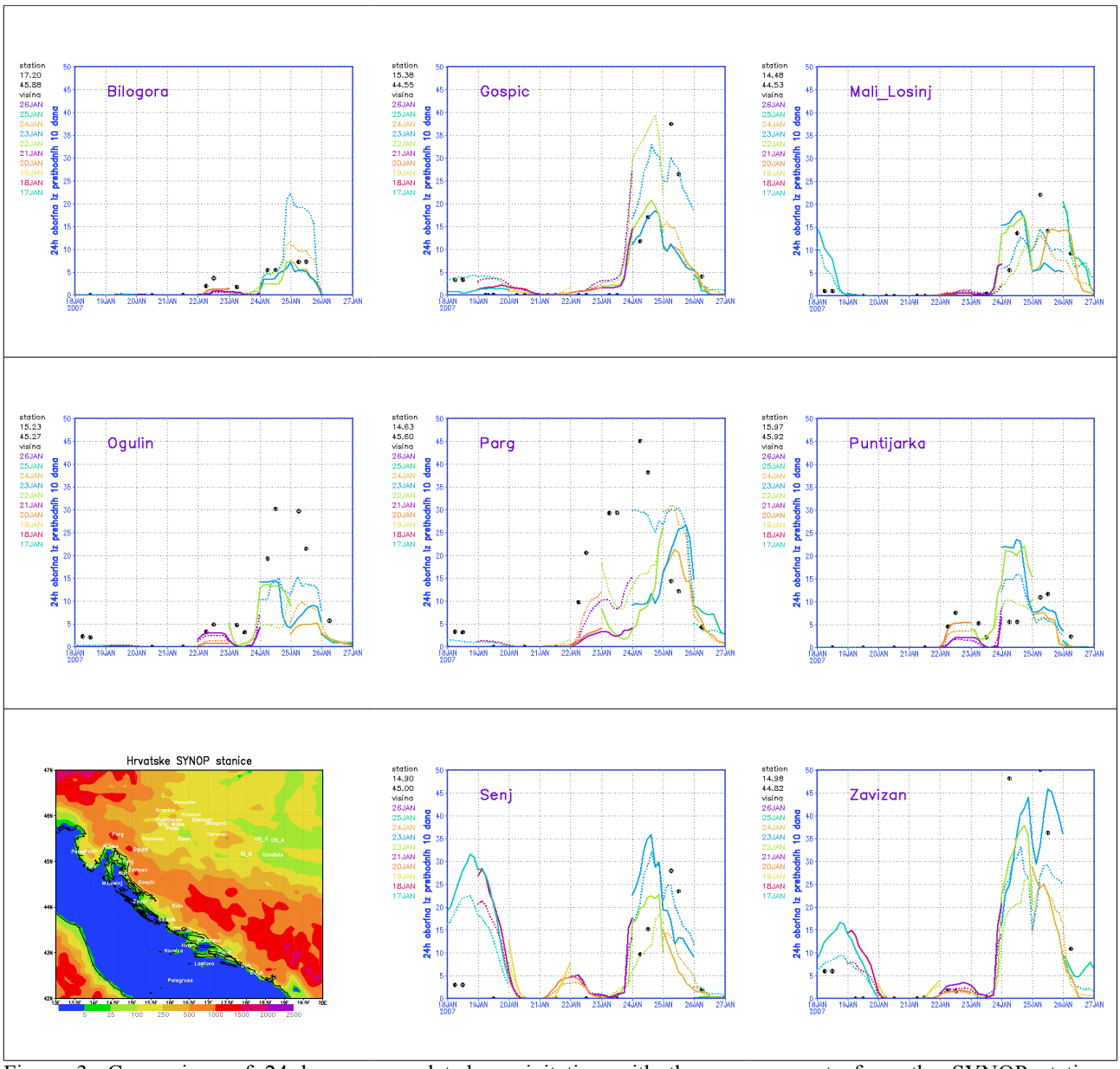

Figure 3. Comparison of 24 hour accumulated precipitation with the measurements from the SYNOP stations, AL29T2mxl forecasts are in full lines, Alaro are dashed, measured 24 hour precipitation is in black dots, the locations of different SYNOP stations in Croatia are show in the lower left panel.

Zavižan and Puntijarka are on tops of mountains, Parg is below a mountain peak and Bilogora is on a peak of a local hill. Gospić and Ogulin are inland from the Velebit mountain while Senj and Mali Lošinj are on the sea side of the Velebit mountain.

Plans

ALARO0 is now run operationally twice a day. The size of domain and forecast range are kept the same as in the reference AL29T2mxl.

We are currently investigating the possibility to use only one large high resolution dynamical adaptation domain which shall not only cover inland Croatia but also most of the Adriatic Sea, since the 10m wind field forecast is most important for the sea, rather than several smaller domains.

2.10. CZECH REPUBLIC

2.11. FRANCE

2.12. HUNGARY

(kullmann.l@met.hu)

There were several changes in the operational version of the ALADIN/HU model during the second half of 2006:

- Forecast and 3d-var assimilation are based on cy30t1.
- Operational suite is running on the new machine of HMS (SGI Altix).
- Production is performed 4 times per day: at 0 UTC 54h, at 6 and 12 UTC 48h and at 18 UTC 36h integration is running.
- Practically the 3d-var assimilation suite is unchanged at 0 and 12 UTC: two 6 hour cycles are made and the production is calculated from a short-cutoff analysis valid at the production time.
- At 6 and 18 UTC there is no update of the guess, the production is running from the short cut-off analysis using the previous 6h production as first guess.

2.12.1. *The main characteristics of the recent operational suite*:

- ALADIN cycle: cy30t1
- Horizontal resolution: 8 km
- Vertical levels: 49
- Grid: linear
- Data assimilation: 3d-var with 6h cycling
- Observations: SYNOP (geopotential), TEMP (temperature, wind components, humidity, geopotential), AMDAR (temperature, wind components), ATOVS:AMSU-A and AMSU-B radiances.

2.12.2. *Parallel suites during the period*:

- BACKUP: We run a backup suite on the IBM (p655) machine. The same 3d-var system is used as for the operational but production is performed only at 0 and 12 UTC. For the backup we use cy28t3.
- Dynamical adaptation as a reference to 3d-var system at same vertical and horizontal resolution (cy28t3 is used).
- ALADIN 3d-var using ensemble B matrix (based on cy28t3).

2.13. MOROCCO

2.14. POLAND

2.15. PORTUGAL

2.16. ROMANIA

2.17. SLOVAKIA

2.18. SLOVENIA

(more details neva.pristov@rzs-hm.si)

Operational suite of ALADIN is still based on cy29t2. There were no major changes in operational setup, only some modifications related to post-processing.

Selected fields (grib format) are made available for www.rclace.eu web page, as well as for PEPS and EURORISK projects. for this some modifications in gribuse program were needed.

New version of PINUTS has been tested and bugs were reported.

The transfer of coupling files from ARPEGE model via Internet from Toulouse was stable. Files were significantly delayed 7 times.

Due to the planned activities related to a tender for a new computer planned for 2007, work on present system has been limited to just the necessary maintenance.

2.19. TUNISIA

2.20. HIRLAM

3. RSEARCH & DEVELOPMENTS

3.1. ALGERIA

3.2. AUSTRIA

3.3. BELGIUM

3.4. BULGARIA

3.5. CROATIA

3.5.1. Alaro0

The research of the impact of different parts of the Alaro0 package continues. Main impact is observed in the precipitation, cloudiness and temperature fields.

3.5.2. Air-Sea interaction

In the framework of the DART project the impact of the air-sea interaction on atmospheric conditions is being studied.

3.5.3. LAM EPS

The research on downscaling of the ECMWF EPS members has continued and resulted in ECMWF Tech. Memo No 507.

3.6. CZECH REPUBLIC

3.7. FRANCE

3.8. HUNGARY

(kullmann.l@met.hu)

The main scientific orientation of the Hungarian Meteorological Service for the ALADIN project is unchanged: data assimilation, short range ensemble prediction and high resolution meso-gamma scale modeling (AROME model).

The main scientific developments for the second half of 2006 can be summarized as follows:

3.8.1. DATA ASSIMILATION:

1. *Computation of ensemble Jb and its inter comparison to NMC*. We computed new B matrix based on ensemble method by downscaling from the ARPEGE model. We ran three experiments, for one month time period, with different sigma B tunings: no tuning, tuning every field with the same amount, using different tuning values for different fields. We compared the experiments to the reference which was calculated with NMC method. The results showed that ensemble Jb improves the forecast especially when tuning every field with the same amount.

2. *Assimilation of SEVIRI data*. We performed experiments assimilating SEVIRI data. To be able to pre-process the data some code changes were needed inside bator. First a two week period run was performed to recalculate the bias correction. After that a two week long experiment was run (using the new bias correction file) and compared to the reference run without using SEVIRI data. (A detailed report is available from Alena Trojakova or Michal Majek)

3. *3D-FGAT experiments*. Experiments were made with 3d-fgat method (see paper in the current

newsletter). The results are promising, showing improvement on several model levels.

4. *Congrad minimization method*. We studied the conjugate gradient minimization method in 131 configuration (see paper in the current newsletter). The results shows that it speeds up the minimization time to some extent.

3.8.2. LAMEPS:

Research with singular vectors computed with the ALADIN model was continued in the second half of 2006. The configuration 601 seems to work well with cy30. Speed of the convergence (during the singular vector computation), as well as CPU time and memory usage were analyzed. First results with the ALADIN singular vectors were presented in the ALADIN- HIRLAM LAMEPS workshop in Vienna in November, 2006. When computing singular vectors with ALADIN it is important to compare the results with singular vectors computed with different models. Comparison with ARPEGE singular vectors is obvious. In addition research has started to compare the ALADIN singular vectors with high resolution IFS singular vectors (see presentation of Martin Leutbecher at the ALADIN-HIRLAM LAMEPS workshop in Vienna in November, 2006). The next step is to use the singular vectors to generate perturbations, which will be used as initial conditions for the ALADIN ensemble system.

3.8.3. AROME:

The first experiments with AROME showed that in many cases it improves the forecast (especially the precipitation and temperature forecast) compared to ALADIN. However the forecast is quite sensitive to the coupling model since the integration domain is small. Some experiments were made to analyse this sensitivity on coupling frequency, domain size and coupling zone size. The results show that the coupling frequency and coupling zone size have little impact. In some cases however one can see little improvement when enlarging the coupling zone size. The size of the integration domain has the most influence, but due to the computational cost it is not recommended to enlarge it very much.

3.9. MOROCCO

3.10. POLAND

3.11. PORTUGAL

3.12. ROMANIA

3.13. SLOVAKIA

3.14. SLOVENIA

(more details neva.pristov@rzs-hm.si)

A new prognostic precipitation scheme in ALARO-0 was available by the end of September. Further validation started in October when Dunja Drvar came for a 2 weeks stay in Ljubljana. Precipitation fields obtained with the new scheme are much smoother with lower extremes and better distribution. Sensitivity tests for the Wegener-Bergeron-Findeisen auto conversion in a case with mixed rain/snow event showed that the scheme is well tuned. Prognostic cloud condensates produced by the micro-physics compared to ones produced by cloudiness scheme are of the same

order of magnitude. Stratiform precipitation fluxes in the new and the old schemes have similar vertical distribution and the values are very similar throughout the entire integration period.

Procedure on how to prepare coupling files from ECMWF model for ALADIN has been tried out (congratulations to Sandor Kertez for very nice documentation). They were used for a case over the Guadeloupe region and results were compared with a high-resolution NH model. The wind field showed to be useful.

Our group supported B. Strajnar, a PhD student working on a comparison between dynamic adaptation and mesoscale analysis methods for initial conditions for ALADIN over Slovenia. His contribution is also included in this Newsletter.

ALADIN verification project

Lovro Kalin (Croatia) was in Ljubljana for 3 weeks. During his stay he prepared the final content of a monthly verification report for one station. Besides graphs and scores for temperature and precipitation, new ones have been added for cloudiness, humidity and wind. At the moment, monthly reports are not yet in operational production (technical procedure has still to be implemented).

Some work has been done on development of code to get data needed for verification from grib fields, so that also other models (ECMWF, DWD) can be included.

3.15. TUNISIA

3.16. HIRLAM

4. PAPERS and ARTICLES

4.1. Z. Juhász[1] and G. Bölöni[2]: Tests with the CONGRAD minimization algorithm within the ALADIN/HU 3D-VAR system.

4.1.1. Introduction

This is a summary about a comparison of the two existing minimization algorithms in ALADIN 3DVAR. Under minimization algorithm we understand the mathematical method for computing the minimum of the cost function in the variational assimilation. These two algorithms are coded in ARPEGE/ALADIN under the M1QN3 and the CONGRAD subroutines. In ALADIN so far the M1QN3 method has been used for both test and operational versions. The purpose of the presented comparison was on one hand to understand the algorithms more in depth and on the other hand to compare their efficiency in practice.

The M1QN3 method belongs to the family of quasi-Newton methods while the CONGRAD method is a conjugate gradient method combined with the Lanczos algorithm. Both methods aim to minimize the variational

$$J(\boldsymbol{x})=(\boldsymbol{x}-\boldsymbol{x}_b)^T B^{-1}(\boldsymbol{x}-\boldsymbol{x}_b)+(\boldsymbol{y}-H[\boldsymbol{x}])^T R^{-1}(\boldsymbol{y}-H[\boldsymbol{x}])$$

cost function with respect to the $\boldsymbol{x}$ control vector through an iterative algorithm. In the formula of the cost function $\boldsymbol{x}_b$ and $\boldsymbol{y}$ denote respectively the background and the observations, B and R stand for their error covariance matrices and H is the observation operator. The iterative minimization process can be written as follows:

where n is $\boldsymbol{x}_{k+1}=\boldsymbol{x}_k+a_k\boldsymbol{d}_k$ number $k=0,1,\ldots,n$ of iterations, $\boldsymbol{d}_k$ is the vector pointing to a descent direction and a_k is the factor determining the length of the step to be taken in this direction. The two methods differ in generating of the $\boldsymbol{d}_k$ sequence. While M1QN3 uses the first derivative of the cost function and the limited storage required approximation of its second derivative, CONGRAD operates with the conjugate directions and the $\boldsymbol{d}_1,\ldots,\boldsymbol{d}_{k-1}$ vectors are taken from the so called Lanczos method using favorable eigenvalue properties to find the best directions in the first few iterations. For the reason of simplicity this paper will not include more detailed comparison and analysis of the minimization algorithms but will concentrate on some tests done with ALADIN 3DVAR at HMS. For those interested more in depth the following papers are proposed for reading: *Bertsekas (1999), Golub and Van Loan (1989), Eijkhout (1995), Meurant and Strakos (2006)*

4.1.2. Tests and results

The tests consisted of running 3DVAR analyses with both methods described above within the ALADIN/HU system. All the tests were done on one single date using the same background and observations (SYNOP and TEMP). The model geometry used is the presently operational Central European domain with ~8 km resolution (360 x 320 points) and 49 vertical levels. All the results were obtained with 4 processor runs (1.3 GHz each) on the IBM p690 machine of HMS. The efficiency of the two methods can be measured by comparing their total CPU costs until reaching a certain J_{min} value. We choose the required J_{min} to be the value corresponding to our operational setting (M1QN3 with 70 iterations).

1 University of Eötvös Loránd

2 Hungarian Meteorological Service (HMS)

	No. of iterations	*Total CPU*	*Average CPU / iteration*	*Costfunction (J)*
M1QN3	70	1506 sec	21.51 sec	'0.2752845E+04'
CONGRAD	45	975 sec	21.66 sec	'0.2751173E+04'

Table 1. Comparison of the M1QN3 and CONGRAD methods

Looking at the summary of the comparisons (Table 1.) one can see that the CONGRAD method uses less CPU than M1QN3 in order to reach the same costfunction value. The difference is around 10 minutes within the 4 processor runs. In percentage CONGRAD uses 65% of the CPU used by M1QN3. Taking into account this percentage, in an operational environment where the minimization last for 10 minutes (using 24 CPUs) the expected gain with the CONGRAD method is about 3.5 minutes. Following Table 1. it turns out as well that one single iteration step is more efficient in case of the CONGRAD method as it reaches the required J_{min} within less iterations (45) than M1QN3 (70). One iteration step costs approximately the same in both methods in terms of CPU. Some of our statements above can be seen also on Fig1. Note that at the beginning of the minimization there are about 10 iterations with an almost constant costfunction value. With CONGRAD even a large oscillation in the costfunction value is present before the decrease starts. Unfortunately we did not find an explanation or any reference yet to this behavior in the literature. We mention also that these first 10 iterations are not counted in the minimization. For instance if one maximizes the number of iterations as 60 through the namelist of conf. 131 in the reality 70 iterations will be performed including the extra 10 before the decrease of the costfunction value starts.

4.1.3. Concluding remarks

The tests shown prove that the CONGRAD algorithm is more efficient than M1QN3 considering the speed of the minimization. The gain in the CPU with CONGRAD is more pronounced in case of low number of processors (10 min. gain on 4 procs.) but it is remarkable even in an operational environment (3.5 min. gain on 24 procs.). However one should remember that the tests were done on one single case and that the qualities of the analyses were not compared or validated from meteorological point of view. In order to go to real practical conclusions test cases or score comparisons are needed as well.

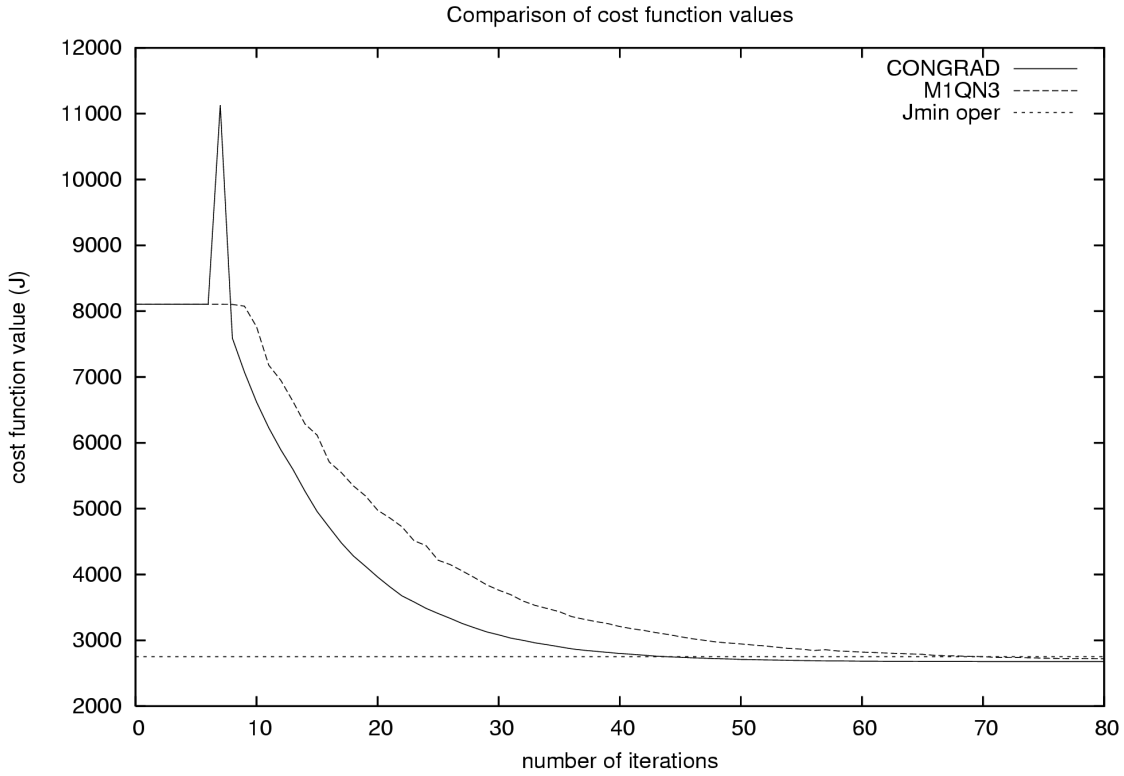

Fig 1. Evolution of the costfunction during the minimization with M1QN3 and CONGRAD. 'Jmin oper' stands for the cost function value provided by the present ALADIN/HU 3DVAR minimization settings (M1QN3 with 70 iterations).

References

Bertsekas D. P., 1999: Nonlinear Programming. *Athena Scientific, Belmont, Massachusetts*

Golub G. H. and C. F. Van Loan, 1989: Matrix Computations. *The John Hopkins University Press, Baltimore, Maryland*

Eijkhout V., 1995: LAPACK working note No. 51: Qualitative Properties of the Conjugate Gradient and Lanczos Methods in a Matrix Framework, *Univ. of Tennessee, Department of Computer Science, 33 pp*

Meurant G. and Z. Strakos, 2006: The Lanczos and conjugate gradient algorithms in finite precision arithmetic, Acta Numerica vol. 15, pp 471-542, Cambridge University Press

4.2. T. Haiden: Predicting snowfall line and precipitation type from ALADIN forecasts.

ZAMG, Vienna, Austria

4.2.1. Introduction

The ALADIN model provides forecasts of liquid and solid precipitation at the height of the model topography. This information is however of limited use in orographically structured terrain, where the model topography may differ greatly from the actual topography. For the city of Innsbruck, for example, which is located at about 600 m above msl, the current ALADIN-AUSTRIA model topography has a height of 1500 m, giving a difference in elevation of 900 m. In several alpine valleys these differences reach values of up to 1500 m. Using a semi-envelope or mean orography instead of the full envelope reduces these differences but does not eliminate the problem of predicting the actual snowfall line in terrain that is only partially resolved by a model. This is an issue in flood forecasting, where the amount of precipitation stored as snow on the ground (thus not immediately contributing to runoff) needs to be estimated. It is also crucial in road weather forecasts for the planning of road maintenance measures like plowing and salting.

Furthermore, for such applications the distinction between rain and snow may not be sufficient. In cases where the atmosphere is well-mixed, and the temperature continuously decreases with height, the boundary between snowfall and rainfall will be relatively narrow. However, in more stable cases, or when the snowfall line works its way downwards due to latent heat effects, there may be a broader height range with temperatures close to 0°C and associated snow/rain mix (‘Schneeregen’). If rain falls into a near-surface layer of cold air, or on a surface with sub-freezing temperature, freezing rain will occur. This precipitation type is the most critical of all since it has enormous effects on transportation and may cause widespread structural damage in severe cases (Rauber et al., 1994).

4.2.2. Extrapolation of the ALADIN forecast into valleys

Since most of the alpine valleys are not represented in the ALADIN model, it is necessary to find a method of extrapolating the temperature forecast to elevations below model topography. Because of the large annual, diurnal, and synoptic variations in lower-tropospheric stability a constant standard-atmosphere correction does not give satisfactory results.

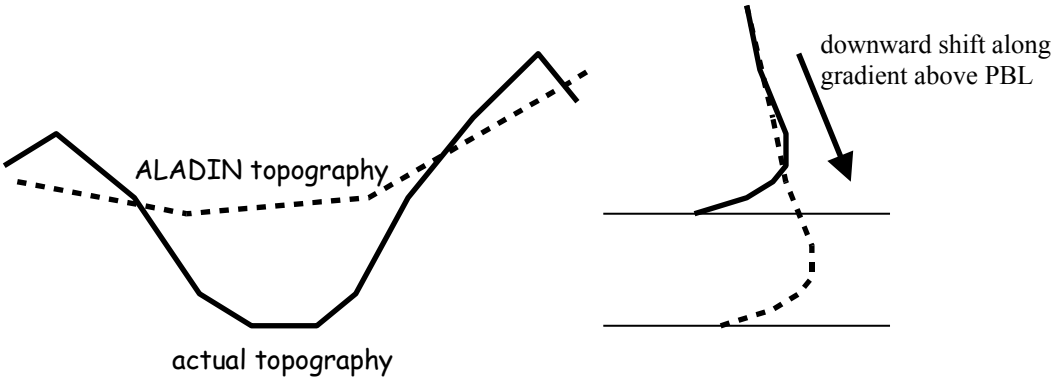

Figure 1: In valley atmospheres not represented in the ALADIN forecast, the PBL temperature profile is shifted down to the valley floor surface, along the gradient above the PBL.

A better extrapolation is obtained if the actual temperature gradient as forecasted by ALADIN is taken into account. In this case a question arises concerning the height interval from which to determine the gradient. The basic idea is to keep the profile of the near-surface layer as predicted by

ALADIN, and perform the shift based on the stratification above (Figure 1). In practice, the gradient for the profile shift is determined from the layer between 500 and 1000 m above the model surface, while the shape of the profile below 500 m is retained. For specific humidity, a similar shift is performed but with zero gradient because the actual gradients predicted by ALADIN were found to be too variable.

The amount of downward shift is computed from the difference between ALADIN model surface and valley floor surface. The valley floor surface represents the local level of lowest terrain and is computed from high-resolution elevation data.

4.2.3. Computation of snowfall line

One of the derived fields from ALADIN-AUSTRIA we operationally compute outside the model is the snowfall line. The distinction between rain and snow should be based on wet-bulb temperature T_w rather than temperature T because ventilation effects keep the temperature of falling precipitation close to T_w. It is well known that snowfall may occur at several degrees above 0°C if the atmosphere is sufficiently dry. Steinacker (1983) has shown empirically that the threshold value of T_w for the rain/snow distinction is close to $(T_w)_{crit}$ = +1.5°C. This is the value we use in the computation of ALADIN snowfall line.

The ALADIN forecast of temperature T and specific humidity q on pressure levels is interpolated to the INCA grid with a uniform grid-spacing of 200 m in the vertical, as described in Section 2. Next, starting from the top, T_w is computed at each level, marching downward. When the first $T_w > (T_w)_{crit}$ is found, the height of the snowfall line is computed from linear interpolation between this level and the one above. Since there is no closed analytical expression for $T_w = f(T,q,p)$ the computation is iterative, using a bisection algorithm. In cases where the snowfall line is below the lowest terrain elevations, it is set to a default value.

4.2.4. Computation of precipitation type

The determination of precipitation type is also based on the wet-bulb temperature. According to the observational study of Steinacker (1983) a snow/rain mix is most likely to occur in the range 0°C$\leq T_w \leq$ +1.5°C. Below 0°C precipitation predominantly falls as pure snow, and above +1.5°C it is most likely pure rain. [Thus the snowfall line as described above actually represents the boundary between a snow/rain mix and pure rain.] Because of the potentially complicated vertical temperature and humidity structure in the lower atmosphere, it is not sufficient to just rely on near-surface values. For example, even if $T_w <$ 0°C, theoretically allowing pure snowfall, there may be a warm layer aloft where the precipitation has already completely melted and it actually rains. The algorithm which determines precipitation type therefore uses both near-surface information (2m temperature, 2m wet-bulb temperature, ground temperature) and upper-air information (snowfall line as determined above).

1) $T_w <$ 0°C. If this is the case, the relation between snowfall line z_s and surface elevation z is tested. If $z_s - z < -(\Delta z)_{melt}$, snowfall is diagnosed, if $-(\Delta z)_{melt} < z_s - z < 0$, snow/rain mix, and if $z_s - z \geq 0$ rainfall.

5) 0°C $\leq T_w <$ +1.5°C. If $z_s - z < -(\Delta z)_{melt}$, snow/rain mix is diagnosed, otherwise rainfall.

6) $T_w \geq$ +1.5°C. Rainfall is diagnosed.

The value of $(\Delta z)_{melt}$ which represents the width of the melting layer, is currently set to 100 m. This somewhat arbitrary assumption will soon be replaced by the actual width computed from

the thresholds T_w = 0°C and T_w = +1.5°C.

In cases where the above diagnosis gives rainfall, an additional test for freezing rain is performed. Freezing rain is assumed to occur when either the air temperature or the ground temperature is below 0°C. In the latter case, however, the air temperature must not exceed a critical value which is currently set to +2°C. In order to clarify whether this additional 'safety precaution' is really necessary, future freezing rain events will have to be analyzed.

The analysis of ground temperature in INCA is based on surface observations of –10cm soil temperature and 2m air temperature. In its current version it is only used for the determination of freezing rain potential. Outside the nowcasting range, the ALADIN forecast of ground surface temperature is used (adapted to actual terrain height).

4.2.5. Operational application

The computations described above have been operationally implemented in INCA, which performs a precipitation analysis every 15 minutes. Since temperature, humidity, and ground temperature are updated only every 1 hour, a linear interpolation in time is used to provide an update on precipitation type every 15 minutes. The example in Figure 2 shows an analysis where all four precipitation types are present.

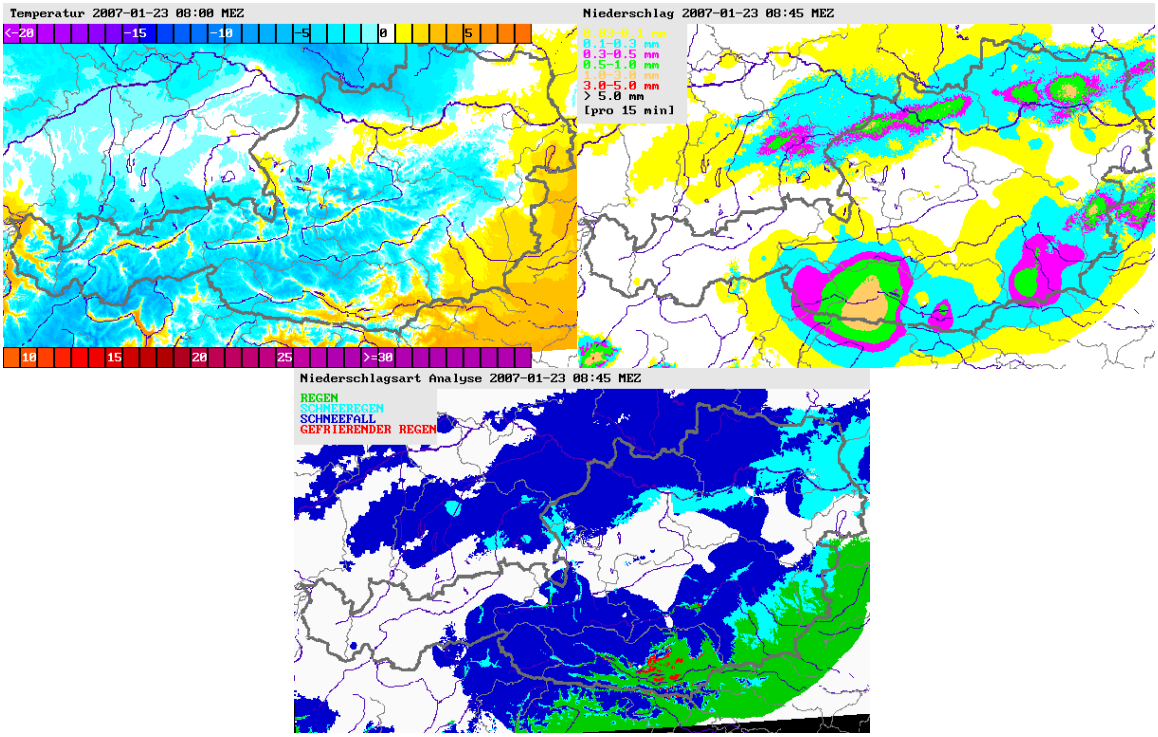

Figure 2: Example of an INCA analysis of temperature (upper left), precipitation (upper right), and resulting precipitation type (bottom). Snowfall indicated blue, snow/rain mix is light blue, rain is green, freezing rain is red. In this case freezing rain is diagnosed in some cold air pools which are present in inner-alpine basins. The temperature analysis is based on ALADIN as a first guess.

4.2.6. Conclusions

The current algorithm gives satisfactory results with regard to the distinction between snow, snow/rain mix, and rain, and there are indications that it gives useful guidance with regard to the occurrence of freezing rain. However, since the full operational implementation no major freezing

rain event occurred in Austria, so this still needs to be verified. Operationally, the field 'precipitation type' is used quite intensively both by forecasters and for automatically generated products like maps in internet portals.

The analysis of ground temperature in its current version is strongly based on –10 cm soil temperature (for lack of actual surface measurements). If there is a prolonged cold episode, and a warm rain event afterwards where not all cold surface air is mixed out, it would correctly indicate freezing rain. However, since the –10 cm temperature reacts more slowly than the actual surface temperature the current method would most likely overestimate the duration and extent of the freezing rain event. We plan to test if the 5 cm air temperature, and the difference between 2 m and 5 cm air temperature will give additional useful information regarding the actual surface ground temperature.

References

Haiden, T., A. Kann, K. Stadlbacher, M. Steinheimer, and C. Wittmann, 2006: Integrated Nowcasting through Comprehensive Analysis (INCA) - System overview. ZAMG report, 40p.
http://www.zamg.ac.at/fix/INCA_system.doc

Rauber, R. M., M. K. Ramamurthy, and A. Tokay, 1994: Synoptic and mesoscale structure of a severe freezing rain event: the St. Valentine's day ice storm. *Wea. Forecasting,* **9,** 183-208.

Steinacker, R., 1983: Diagnose und Prognose der Schneefallgrenze. [Diagnosis and forecast of snowfall-line.] *Wetter und Leben*, **35,** 81-90.

4.3. A. Kann and Y. Wang: ALADIN Limited Area Ensemble Forecasting (LAEF) experiments: Dealing with Uncertainties in the LBC.

ZAMG, Vienna, Austria

4.3.1. Introduction

Since 2006, an experimental ALADIN regional EPS system LAEF (Limited Area Ensemble Forecasting, Wang and Kann, 2006) is implemented at ZAMG. Up to now, work has been focused on the initial condition perturbation (comparing Breeding, *E*nsemble *T*ransform, *E*nsemble *T*ransform *K*alman *F*ilter) and on the impact of different physical parameterizations using dynamical downscaling technique (Kann and Wang, 2006). A further problem of LAM-EPS concerns the use of adequate boundary conditions which is investigated in the following abstract in order to study the performance during a winter episode from 26.01.2006 to 26.02.2006.

4.3.2. The ALADIN LAEF configuration

The ALADIN model used for the ensemble forecasting is run in hydrostatic mode, with 18 km horizontal resolution, and 31 levels in the vertical. The model domain covers the area 25°W – 51°E, 26°N – 57°N, which includes Europe and a large part of the North Atlantic.

4.3.3. Experiments and Results

The main goal of this study is to investigate the impact of the inconsistency in the generation of the ensemble lateral boundary conditions from global EPS system with the generation of the ensemble initial conditions from the LAM-EPS itself.

Impact of perturbation on LBC

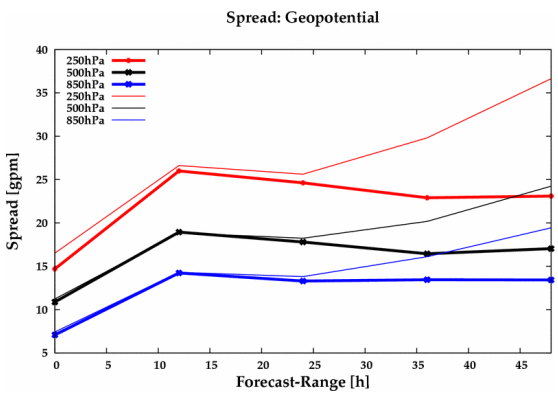

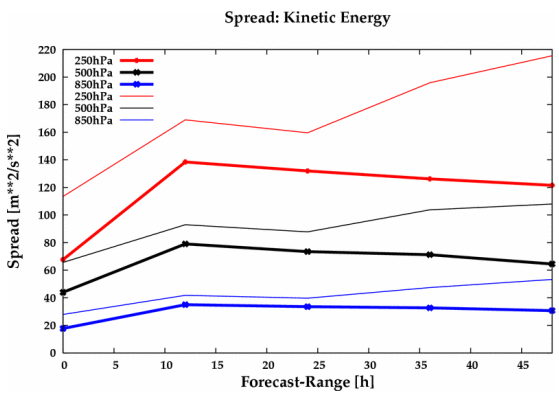

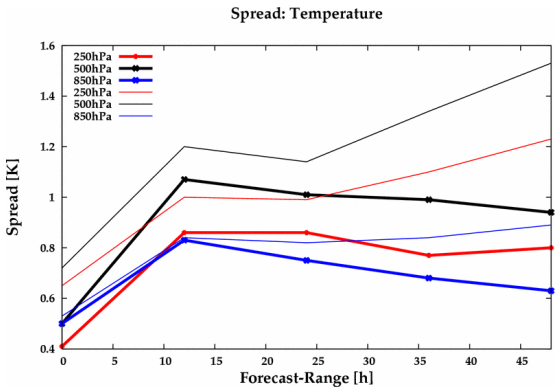

Spread of *Geopotential*, *Kinetic Energy* and *Temperature* on 3 levels (red: 250hPa, black: 500hPa, blue: 850hPa) as a function of forecast range. Thick lines: coupling with control LBC, thin lines: coupling with PEARP (Arpege EPS) members. Without coupling with perturbed LBC, the ensemble members converge and their spread decreases.

Impact of differently perturbed LBC on the performance of LAEF

EXP-1: Breeding method coupled with perturbed LBC from PEARP (Singular Vectors)
EXP-2: Breeding method coupled with perturbed LBC from NCEP-ENS (Breeding Vectors)

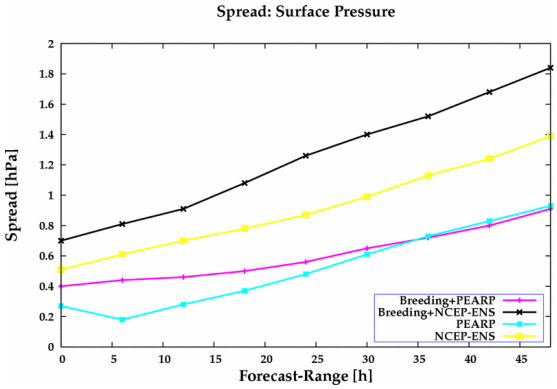

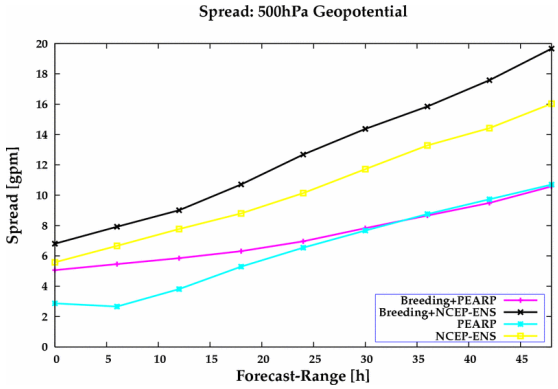

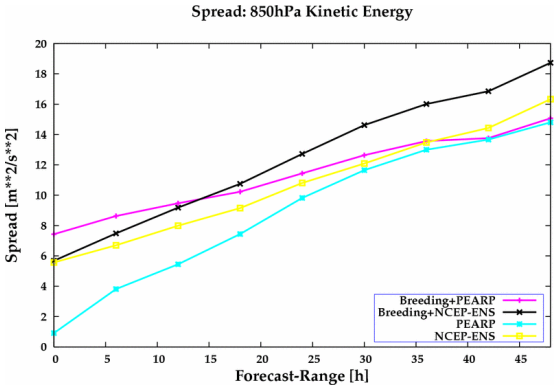

Spread of *Surface Pressure* (top left), *Geopotential* (top right) and *Kinetic Energy* (bottom left) as a function of forecast range. Experiments: Breeding coupled with PEARP (purple), Breeding coupled with NCEP-ENS (black), PEARP members (light blue), NCEP-ENS (yellow). Breeding coupled with NCEP-ENS perturbed LBC shows much larger spread, partly due to the spread of the coupling model itself, partly due to a combination with Breeding within LAEF.

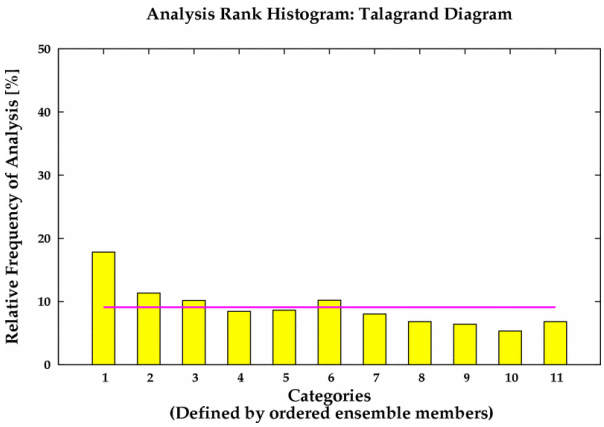

Talagrand Diagram: *Geopotential* 500hPa + 24h, Breeding experiment coupled with ***PEARP*** members. Almost flat distribution with only weak ensemble high bias.

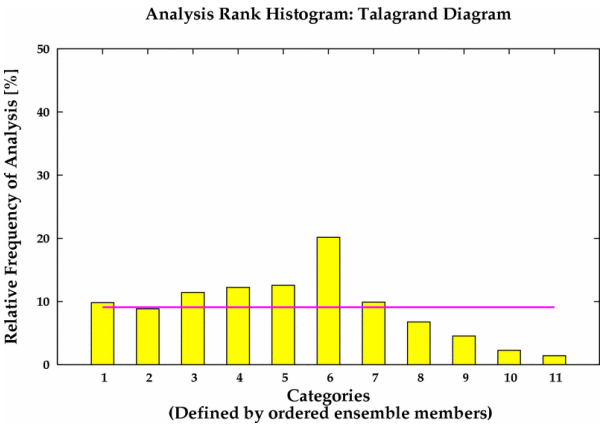

Talagrand Diagram: *Geopotential* 500hPa + 24h, Breeding experiment coupled with ***NCEP*** members. The ensemble spread is slightly too large.

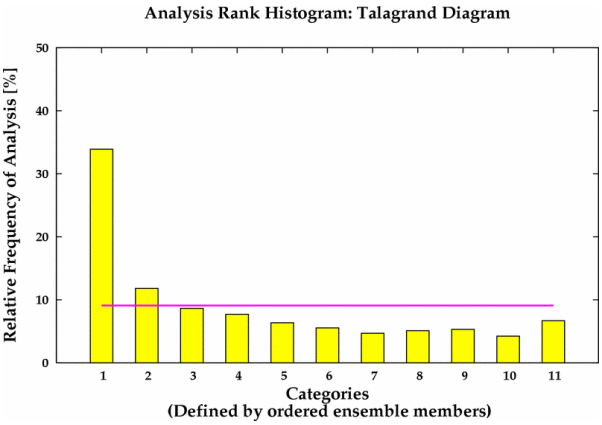

Talagrand Diagram: *Geopotential* 500hPa + 48h, Breeding experiment coupled with ***PEARP*** members. It shows a large ensemble high bias (higher than expected frequency for low observations).

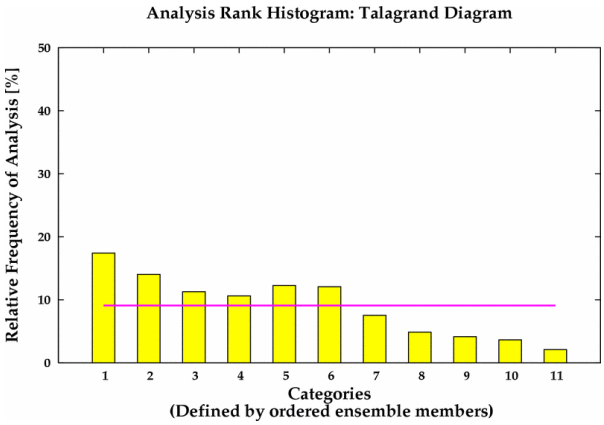

Talagrand Diagram: *Geopotential* 500hPa + 48h, Breeding experiment coupled with ***NCEP*** members. Again, an ensemble high bias is shown, but less pronounced.

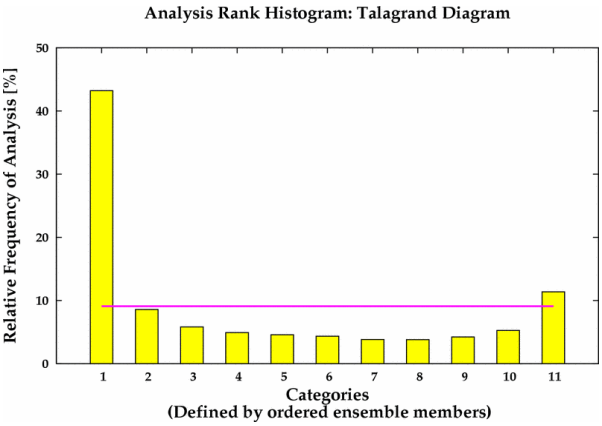

Talagrand Diagram: *Temperature* 850hPa + 48h, Breeding experiment coupled with ***PEARP*** members. Again, a large ensemble high bias is shown.

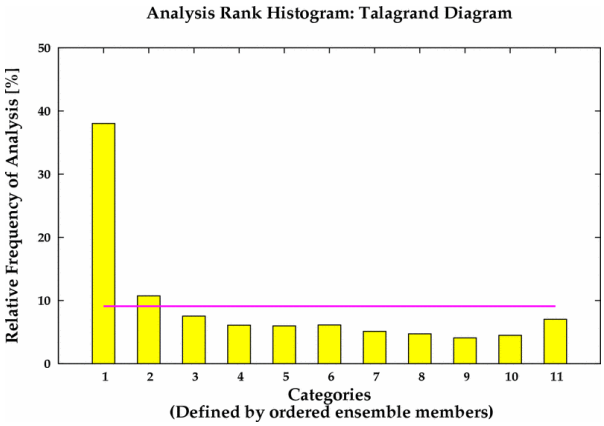

Talagrand Diagram: *Temperature* 850hPa + 48h, Breeding experiment coupled with ***NCEP*** members. Large ensemble high bias.

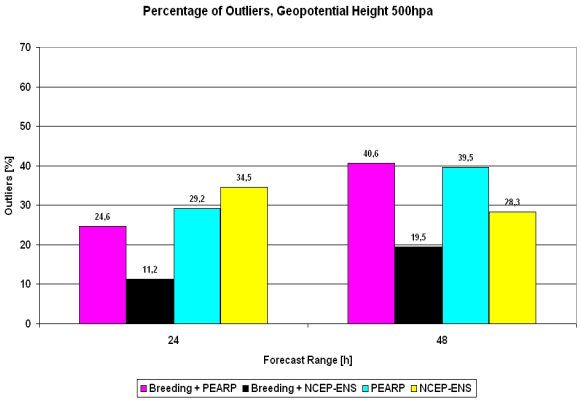

Outliers: *Geopotential* 500hPa +24h and +48h, Breeding experiment coupled with ***PEARP*** members (purple) vs. coupled with ***NCEP*** members (black). The frequency of outliers is halvened for Breeding + NCEP-ENS.

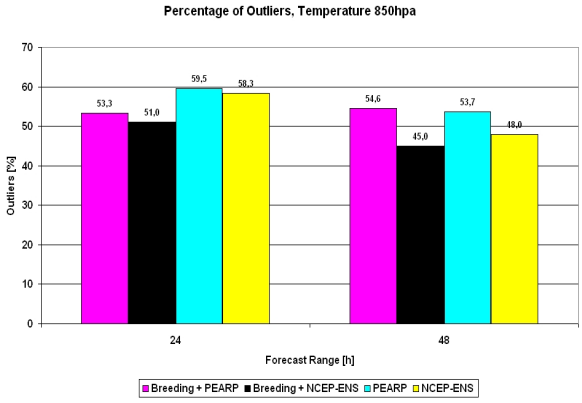

Outliers: *Temperature* 850hPa +24h and +48h, Breeding experiment coupled with ***PEARP*** members (purple) vs. coupled with ***NCEP*** members (black). The percentage of outliers is reduced, but not that pronounced than regarding Geopotential.

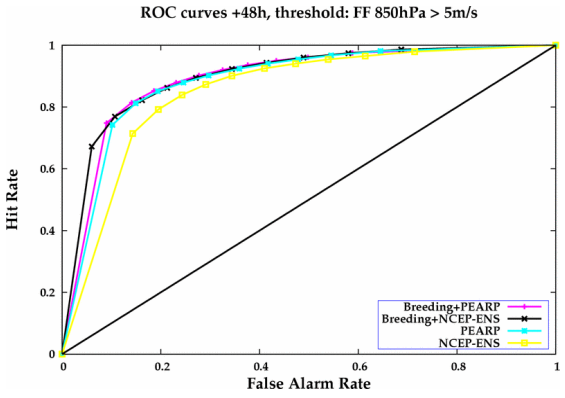

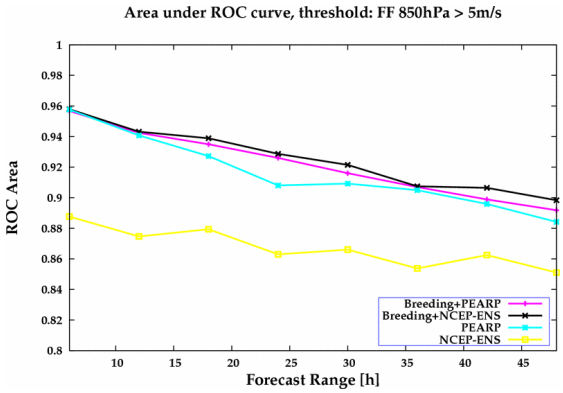

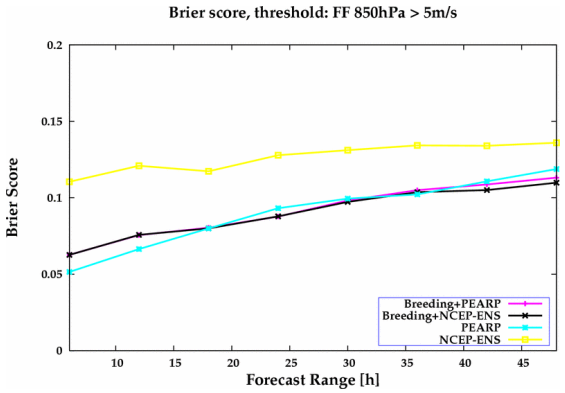

ROC curves (top left), **Areas under ROC curves** (top right) and **Brier score** (bottom left) for threshold FF in 850hPa greater 5m/s. Breeding coupled with PEARP (purple), Breeding coupled with NCEP-ENS (black), PEARP (light blue) and NCEP-ENS (yellow). All experiments show similar results, but NECP-ENS performs worst.

4.3.4. Conclusion

A comparison of LAEF experiments using Breeding method for constructing initial perturbation coupled with boundary conditions gained by Singular Vector technique and by Breeding technique gives an impression of the general impact of the LBC on LAEF. From the winter episode it turned out that perturbed lateral boundary conditions are necessary for growing diversity of EPS members for forecast ranges greater than 12 hours in order to avoid convergence. LAEF using Breeding method coupled with LBC from NCEP-ENS (Breeding) slightly outperforms LAEF coupled with LBC from PEARP (SV), especially regarding spread.

Additional experiments concerning the coupling problem will be carried out, e.g. using lateral boundary conditions from ECMWF EPS, in order to improve performance of LAEF considerably.

References

Wang Y., Kann A.: ALADIN Limited Area Ensemble Forecasting. *Aladin Newsletter* **29**, 2006.

Kann A., Wang Y.: ALADIN Limited Area Ensemble Forecasting (LAEF) experiments: Multiphysics downscaling of PEARP. *Aladin Newsletter* **30**, 2006.

4.4. S. Kertész: Forecast experiments with the ALADIN 3D-FGAT analysis system.

Hungarian Meteorological Service

4.4.1. Introduction

The FGAT (First Guess at Appropriate Time) technique was first implemented in the ECMWF optimal interpolation analysis system (*ECMWF*, 1992). Its extension to variational data assimilation, the so-called 3D-FGAT system, is regarded as an intermediate step between 3D-VAR and 4D-VAR. In contrast to 3D-VAR, which cannot handle temporal information and is restricted to the analysis time, 3D-FGAT is even able to take into account the temporal distribution of the observations (though only in a limited way). The 3D-FGAT scheme was operationally used at different forecast centres (e.g. at the ECMWF) and it is still an operational option for HIRLAM (*Huang et al.,* 2002). The work with the ALADIN 3D-FGAT system started only a couple of years ago (*Soci*, 2004) and up to now only a few experiments have been carried out (*Dziedzic*, 2005, *Vasiliu*, 2006).

In this paper the recent research studies devoted to the ALADIN 3D-FGAT system at the Hungarian Meteorological Service (HMS) are presented. These studies focused on three main topics. At first, the choice of the temporal position of the 3D-FGAT analysis increment was investigated. It was followed by a comparison of the 3D-VAR and 3D-FGAT systems. Finally the possible usage of all the available SYNOP reports in the observation window was tested.

4.4.2. Theoretical background

The 3D-FGAT system can be best described as a simplification of 4D-VAR. In 4D-VAR the analysis is performed for a time interval (observation window) and the result is the trajectory that lies closest to both the $\mathbf{x}_b$ background state (specified at the beginning of the observation window) and the $\mathbf{y}$ observations. In practice the observation window is divided into *n* time-slots and all the observations within a given time-slot are supposed to be valid at the middle of the time-slot. In the incremental formalism of 4D-VAR the analysis is yielded by the minimization of a *J* cost function with respect to the $\delta\mathbf{x}=\mathbf{x}-\mathbf{x}_b$ analysis increment. The cost function takes the following form:

$$J(\delta\mathbf{x})=\delta\mathbf{x}^T\mathbf{B}^{-1}\delta\mathbf{x}+\sum_{i=1}^{n}(\mathbf{d}_i-\mathbf{H}\,\delta\mathbf{x}_i)^T\mathbf{R}^{-1}(\mathbf{d}_i-\mathbf{H}\,\delta\mathbf{x}_i)$$

where

- $\mathbf{B}$ is the background error covariance matrix,
- $\mathbf{R}$ is the observation error covariance matrix,
- $\mathbf{H}$ is the tangent linear operator of the *H* observation operator,
- $M_i(\mathbf{x}_b)$ is the background trajectory computed by the *M* forecast model,
- $\mathbf{d}_i=\mathbf{y}_i-H(M_i(\mathbf{x}_b))$ is the innovation vector that gives the departure between the observations and the background trajectory,
- $\delta\mathbf{x}_i=\mathbf{M}_i\delta\mathbf{x}$ is the increment propagated forward in time with the $\mathbf{M}$ tangent linear operator of the forecast model. Both *H* and *M* are linearised along the background trajectory.

This minimization problem is solved by an iterative process that in each step requires the evaluation of the *J* cost function and its ∇J gradient. Throughout the iterations the **d** innovation vector is constant (it has to be computed only once) but in each iteration step the integration of the $\mathbf{M}$ tangent linear model and its $\mathbf{M}^T$ adjoint is required making 4D-VAR computationally expensive.

The computational costs and the scientific complexity of the problem can be greatly reduced

by using the 3D-FGAT algorithm that we get from 4D-VAR by setting the tangent linear model operator and its adjoint to the identity $\mathbf{M}=\mathbf{M}^T=\mathbf{I}$. This means that $\delta\mathbf{x}_i=\delta\mathbf{x}$ so in 3D-FGAT the following cost function has to be minimized:

$$J(\delta\mathbf{x})=\delta\mathbf{x}^T\mathbf{B}^{-1}\delta\mathbf{x}+\sum_{i=1}^{n}(\mathbf{d}_i-\mathbf{H}\delta\mathbf{x})^T\mathbf{R}^{-1}(\mathbf{d}_i-\mathbf{H}\delta\mathbf{x})$$

It can be seen that in 3D-FGAT we still have the background trajectory and the innovation vector is computed correctly (the name FGAT comes from this fact) but the temporal information in the increment is completely lost. As a consequence the incremental 3D-FGAT analysis is ambiguous since the resulting analysis increment is not fixed in time and theoretically it can be added at any time position to the background trajectory.

Further simplification of the minimization problem, by removing all the temporal information from the system, results in the 3D-VAR algorithm with the following cost function:

$$J(\delta\mathbf{x})=\delta\mathbf{x}^{\boldsymbol{T}}\mathbf{B}^{-1}\delta\mathbf{x}+(\mathbf{d}-\mathbf{H}\delta\mathbf{x})^T\mathbf{R}^{-1}(\mathbf{d}-\mathbf{H}\delta\mathbf{x})$$

In 3D-VAR everything refers to the analysis time that is usually the middle of the observation window. All the observations in the observation window are supposed to be valid at this time and there is no background trajectory, instead the background is also specified at the middle of the observation window.

4.4.3. Theoretical aspects of observation handling in 3D-FGAT

The 3D-FGAT system is thought to be more advanced than 3D-VAR due to its more precise observation handling. However, this takes effect only if there are observations at different times than the analysis time, otherwise the two systems give identical results. Concerning the temporal-spatial distribution of these observations two major cases can be distinguished:

1. The observing platform is moving. There can be cases when there is only one observation for a given location in the observation window. An example for it is a sensor on a quasi-polar satellite. With other moving platforms it can happen that in the vicinity of certain locations there are a plenty of observations at different times. This is the case of the aircraft-based observations (AIREP reports).
2. The observation platform is fixed and there are more measurements within the observation window like for the land SYNOP observations. In this case there can be more observations at exactly the same location but with different observation times.

The theoretical investigation of these cases is quite easy if there is only one observation location for the whole analysis. Let us suppose at first that we have only one y observation for a model variable and it is located at a given model grid point. With these assumptions the observation operator directly assigns some *k*-th element of the model space to the observation, so the innovation can be written as $d=y-(\boldsymbol{x}_b)_k$ and the resulting 3D-FGAT analysis increment takes the following form:

$$(\delta\mathbf{x})_k=\frac{\sigma_{bk}^2}{\sigma_o^2+\sigma_{bk}^2}\ d$$

where

- σ_{bk} is the background error variance for point *k* in the model space,
- σ_o is the observation error for the given observation.

Obviously, the 3D-VAR analysis would yield the same increment but with a less accurately computed *d* innovation if the observation is far from the analysis time. This may indicate the clear

advantage of 3D-FGAT over 3D-VAR for example for a sensor of a polar satellite (as it was described above).

Let us suppose now that we have one observation with the conditions mentioned above in each of the *n* timeslots. Then the *k*-th element of the 3D-FGAT analysis increment can be written as:

$$(\delta \mathbf{x})_k = \frac{\sigma_{bk}^2}{\frac{\sigma_o^2}{n} + \sigma_{bk}^2} \; \frac{1}{n} \sum_{i=1}^{n} d_i$$

If these observations would be assimilated with 3D-VAR then the increment would have the same form again (supposing that **R** is diagonal) but it would be based on completely wrong d_i innovation values. This formula means that the increment is yielded as if the average background departure were taken into account with a decreased observation error. As we mentioned this can be the case of the land SYNOP reports and also to a certain extent of the AIREP reports. Concerning these observation types it is not clear from the formulae presented above which solution produces better result in 3D-FGAT: using only one observation at (or around) a certain location at the analysis time or using a kind of averaging by taking more observations at different times.

4.4.4. Implementation of 3D-FGAT in ALADIN

The implementation of the incremental 3D-FGAT system in ALADIN/ARPEGE/IFS follows the scheme described in Chapter 2, i.e. 3D-FGAT is equivalent with an outer loop of 4D-VAR where the tangent linear model and its adjoint is set to the identity operator. From the practical point of view an ALADIN 3D-FGAT run is rather similar to a 3D-VAR one. Both systems require the same steps such as observation pre-processing, observation screening (configuration 002) and minimization (configuration 131), but there are some relevant differences:

- In the observation pre-processing the main difference is that in 3D-FGAT the observation window is divided into time-slots. Time-slots must be defined during the observation pre-processing and an ODB (Observational DataBase) with timeslots has to be created.
- The screening in 3D-FGAT works with the background trajectory and the innovation vectors (i.e. background departures) are computed using the appropriate observation times. So the quality control using these departures is more accurate than in 3D-VAR. The background trajectory is computed by the screening itself. This model integration is started from the $\mathbf{x}_b$ background state. This means that the background state is always specified at the beginning of the observation window in contrast to 3D-VAR where it is valid at the middle of the window. Practically 3D-FGAT runs the same screening as 4D-VAR.
- The minimization in 3D-FGAT also performs one model integration and computes the background trajectory again. In the end of the minimization the resulting analysis increment is added to the background trajectory at the beginning of the observation window, this is the hard-coded setting.

Concerning the computational costs a 3D-FGAT run requires an extra CPU time only for the computation of the background trajectory. The minimization itself in 3D-FGAT is only slightly slower than in 3D-VAR.

4.4.5. Description of the experiments

The experiments were carried out for the period of 4-21 May, 2005 with the ALADIN CY28T3 model version using a 12 km horizontal resolution with 37 vertical levels (up to 5 hPa). The integration domain is shown on Figure 1. In each experiment a 6 hour assimilation cycle with a ±3 hour observation window was used and two 48 hour model integrations were performed at 00

and 12 UTC. The first 4 days of the investigated period was regarded as a warm-up time and forecasts were run only for the remaining two weeks of the period (8-21 May). The same B-matrix (standard NMC) and statistics (e.g. bias correction coefficients) were used both in 3D-VAR and 3D-FGAT. Instead of having a surface analysis the surface fields from the ARPEGE analyses (or forecasts) were copied into the ALADIN background. In the 3D-FGAT experiments the 6 hour observation window was divided into 7 one hour time-slots starting at -3:30 h and ending at +3:30 h relating to the middle of the window.

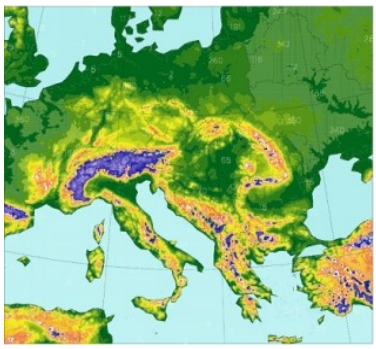

Figure 1: The integration domain and orography of the ALADIN model

In the experiments all observation types available at HMS were used: land SYNOP, AIREP, AMV winds (from MSG), TEMP, Wind profiler observations and NOAA AMSU-A and AMSU-B sensors. The characteristics of the reference set of observations are shown in Table 1. Beside these observations additional parameters and observation times were used in some of the experiments.

Observations	***Parameters***	***Temporal usage***
SYNOP (land)	Z	one report per station (closest to the analysis time)
AIREP	U, V ,T (thinning: 25 km)	all the reports in the observation window
AMV	U, V (thinning: 25 km)	observations 15 minutes before the analysis time
TEMP	T, U, V, Q, Z	one report per station (closest to the analysis time)
Wind profiler	U, V	one report per station (closest to the analysis time)
AMSU A,B	T_b (thinning: 80 km)	all the reports in the observation window

Table 1: The reference set of observations used in the experiments

4.4.6. The timing of the analysis increment in 3D-FGAT

In the first set of experiments the timing of the analysis increment was investigated. As we described above, the ALADIN model adds the increment to the background trajectory at the beginning of the observation window. It means that with a 6 hour analysis scheme 3D-FGAT analyses are available at 03, 09, 15 and 21 UTC and in order to have a 48 hour forecast from e.g. 00 UTC we have to run a 54 hour forecast from 21 UTC. This scheme (illustrated on Figure 2a) was tested and proved to be insufficient comparing to 3D-VAR (*Vasiliu*, 2006). One of the reason of this feature could be the extra 3 hours of integration that can spoil the information in the analysis. Another idea was that TEMP observations, which have huge impact on analysis quality, are located at the middle of the observation window but with this scheme their effect is taken into account 3 hours before. Therefore it was thought that the increment should be added to the background trajectory at the middle of the assimilation window. This modified cycling scheme (that was implemented by adding the increment to the trajectory by an external program) can be seen on Figure 2b.

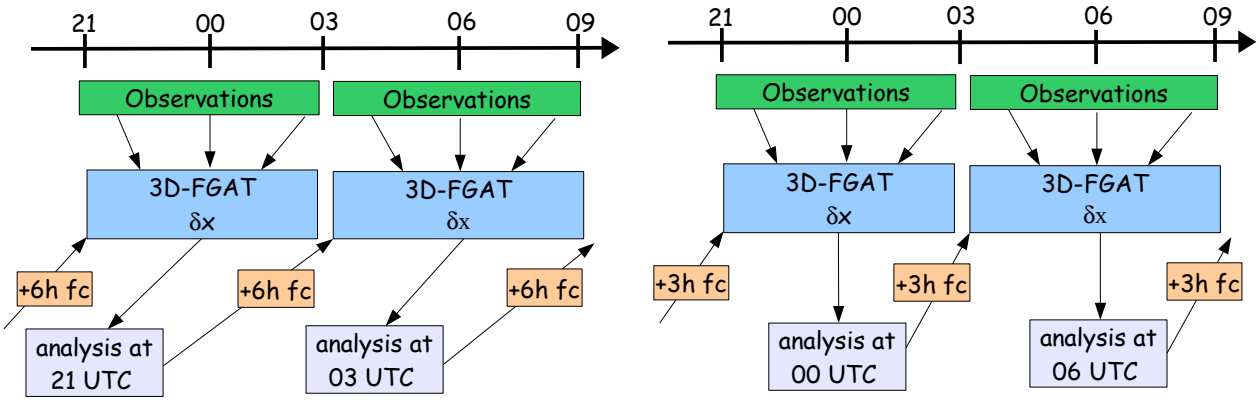

a) increment positioned to the beginning of the window

b) increment positioned to the middle of the window

Figure 2: The two cycling schemes of 3D-FGAT that were tested: using the default increment position at the beginning of the observation window (Figure a, on the left), and adding the increment to the background trajectory at the middle of the observation window (Figure b, on the right).

In order to test these schemes two 3D-FGAT experiments were performed using the reference set of observations (see Table 1). The comparison of the forecasts clearly showed that the increment should be added to the background trajectory at the middle of the observation window: in this case the verification scores are significantly better for both the surface and upper air parameters (Figure 3). Thus, all the 3D-FGAT experiments presented in the rest of this report were performed using this scheme.

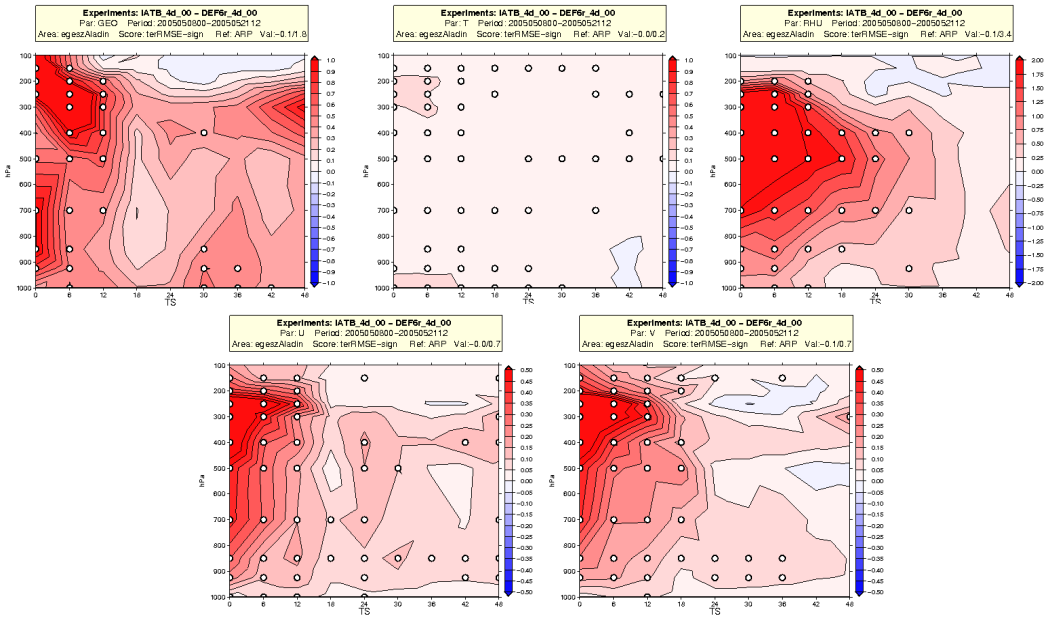

Figure 3.: Difference of RMSE scores of the 00 UTC forecasts based on the original (increment at the beginning of the window) and the modified (increment in the middle of the window) 3D-FGAT cycling schemes. Red shades indicate that the new scheme is better, while blue shades indicate the opposite. White circles show that the difference is significant on a 90% confidence level. The verification was performed against ARPEGE analyses. The figure order is the following (from left to right): Z, T, RHU, U and V.

4.4.7. Comparing 3D-FGAT with 3D-VAR

For the sake of the correct comparison of 3D-FGAT with 3D-VAR the 6 hour analysis cycling in 3D-VAR started (at 00 UTC, 4 May) from the 3 hour forecast made by the 3D-FGAT screening. So for the first analysis the background state of 3D-VAR and the middle point of the background

trajectory of 3D-FGAT (where the increment is positioned to) were the same. These experiments consisted of two parts: at first the reference set of observations were used, then the usage of a shorter (±1 hour) observation window for AIREP both in 3D-VAR an 3D-FGAT was investigated.

Reference experiments

In these experiments the reference set of observations (see Table 1) was used with a 6h observation window. It means that with the exception of AIREP reports and satellite radiances all the observations were available at the analysis time. As a consequence, the difference between 3D-VAR and 3D-FGAT must be the result of the different handling of these two observation types.

Comparison of observation handling

The comparison of the observation handling was carried out by the investigation of the background departures. The analysis departures could have been also investigated, however due to the timing problems with the 3D-FGAT analysis increment this comparison was rather ignored. The screening quality control (observations finally get active or rejected status) was also studied because some of the screening tests are based on the background departures. Therefore it was expected that for observations far from the analysis time 3D-FGAT (due to its more precise background departure computation) would reject less observations than 3D-VAR. The results are presented in Table 2.

		Total	*Rejected*		*Obs-Guess Mean*		*Obs-Guess STD*	
			3D-VAR	*3D-FGAT**	*3D-VAR*	*3D-FGAT*	*3D-VAR*	*3D-FGAT*
SYNOP	Z	87432	1412	+0.5%	5.5	1.49	75.88	74.04
AIREP	T	647906	192578	-5.1%	0.08	0.1	1.13	1.02
	U	641724	188572	-5.3%	0.16	0.16	3.05	2.76
	V	641724	188572	-5.3%	0.09	0.06	3.05	2.75
SATOB	U	163692	147380	-0.02%	-0.44	-0.46	2.78	2.79
	V	163692	147380	-0.02%	0.32	0.78	2.67	2.74
TEMP	Z	51028	4020	+0.1%	-1.5	-1.6	14.4	14.4
	T	131094	3974	+0.2%	0.01	0.02	1.26	1.25
	U	116986	2282	+1.1%	0.2	0.2	3.05	3.05
	V	116986	2282	+1.1%	-0.04	-0.05	3.04	3.04
	Q	119632	37886	+0.4%	-0.03	-0.03	0.82	0.82
Windprofiler	U	69644	66250	0%	0.08	0.1	3.01	2.84
	V	62838	59678	+0.2%	-0.11	-0.11	2.42	2.56
NOAA15 AMSU-A	T_b	918174	712434	-1.3%	-0.05	-0.12	0.37	0.34
NOAA16 AMSU-A	T_b	2461824	2102952	-0.3%	-0.13	0.22	0.35	0.36
NOAA16 AMSU-B	T_b	10365349	10192964	-0.9%	0.04	0.01	2.95	2.89
NOAA17 AMSU-B	T_b	5565294	5509780	+0.02%	-0.49	-0.7	2.96	2.81

* :relative difference with respect to 3D-VAR

Table 2: Number of the rejected observations and background departure statistics in the screening of the default 3D-VAR and 3D-FGAT experiments for the whole 18-day period

It can be seen in Table 2 that the figures for 3D-VAR and 3D-FGAT are quite similar for most of the observations. As it was expected, the largest difference was found in AIREP and satellite radiances. Apart from these observations, the differences can be attributed to the different backgrounds (at the analysis time) produced by the two analysis cycles. The quality of these backgrounds can be easily estimated with the background departures from TEMP observations (indeed it is a verification against TEMP). These values indicate that the two backgrounds at the analysis time have nearly the same quality in both systems.

It is obvious from Table 2 that AIREP reports are handled much better in 3D-FGAT than in

3D-VAR. The investigation of the vertical profiles for AIREP departures also verifies it. In Figure 4 it can be clearly seen that for temperature the 3D-FGAT background is much closer to the observations in the lower part of the troposphere. This feature corresponds to the fact that temperature near the surface can change rapidly throughout the 6 hour observation window and it can result in large errors in the computation of innovation vectors in 3D-VAR (large differences can occur between the edges and the centre of the observation window where the background state is specified). On the other hand 3D-FGAT can improve this feature a lot by computing the departures accurately. The improvement is most significant at 12 UTC (not shown) but it emerges even in the average analysis statistics (taking 00, 06, 12 and 18 UTC all together). The two wind components show similar features but the main difference can be found around the flight level (near 250 hPa). The advanced computation of innovation vector is also reflected in the screening rejection statistics because 3D-FGAT rejects a slightly less (6%) number of AIREP observations than 3D-VAR.

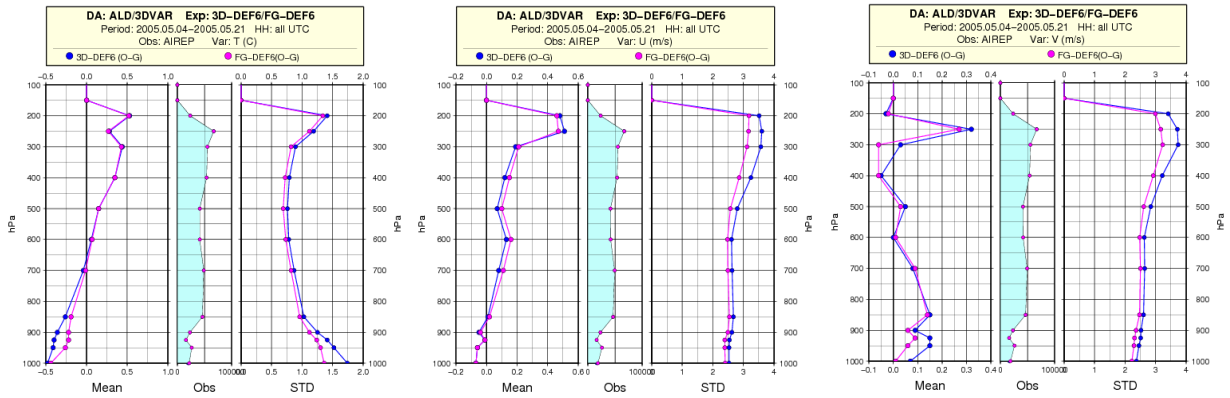

Figure 4: Background departure statistics for AIREP temperature in the 3D-VAR (blue) and 3D-FGAT (magenta) analyses (from left to right: T, U and V)

Unlike the AIREP observations, the background departure statistics for satellite radiances are not clearly better in 3D-FGAT. Regarding the mean values the background in 3D-VAR is closer to the observations than in 3D-FGAT while for the RMSE values the situation is just the opposite. Besides, the number of the rejected observations in screening shows a rather small difference.

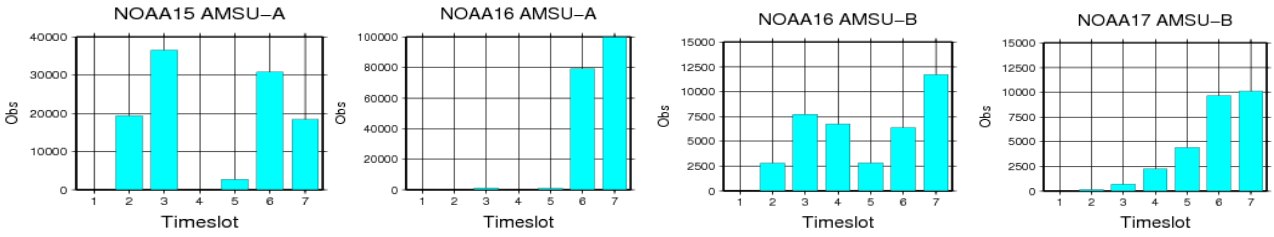

Figure 5: Temporal distribution of the active satellite radiance data for the different satellite sensors

In order to see how much the background departures in 3D-VAR and 3D-FGAT could differ at all, the temporal distribution of the satellite radiance data was investigated. It can be seen on Figure 5 that for all the sensors there are quite a large number of observations far from the analysis time (time-slot 4), so 3D-FGAT departures are expected to be smaller than the 3D-VAR ones (both in terms of mean and standard deviation). It is interesting that in the case of NOAA16 AMSU-A albeit almost all the data are available by 2 or 3 hours later than the analysis time and yet the difference can be only seen in the mean departures.

The reason for the larger mean background departures in 3D-FGAT might be the fact that the bias correction coefficients were computed by 3D-VAR for both systems (*Randrimampianina,* 2005 and 2006). Thus, bias correction coefficients were determined from an inaccurate background departure computation and then they were applied in 3D-FGAT. However, if it is the case it is still

unclear why 3D-FGAT is better in terms of standard deviation.

Comparison of forecast results

The verification for the surface parameters against SYNOP observations indicates a very small difference between 3D-VAR and 3D-FGAT (not shown). This feature is also reflected in the subjective forecast evaluation: the evolution of weather systems with regards to precipitation and cloud patterns are rather similar and the small scale differences are not systematically better or worse in either case.

The situation is different for the upper air parameters where the verification was performed against ARPEGE analyses (Figure 6). The RMSE scores of the 00 UTC 3D-FGAT forecasts are slightly better for the first 12 hours for geopotential in the upper troposphere and for U and V wind components near the 250 hPa level. This difference proved to be significant on a 90% confidence level. However, the geopotential in the lower troposphere in the 6-24 h forecast range is significantly worse in 3D-FGAT. For the relative humidity there is little difference between the two systems and the temperature forecasts are almost identical (not shown). For the 12 UTC runs the RMSE scores indicates smaller differences of the same sign as for 00 UTC except the geopotential. This parameter is worse (but not significantly) in 3D-FGAT for the first 12 hours around 250 hPa than in 3D-VAR but slightly better after 24 hours.

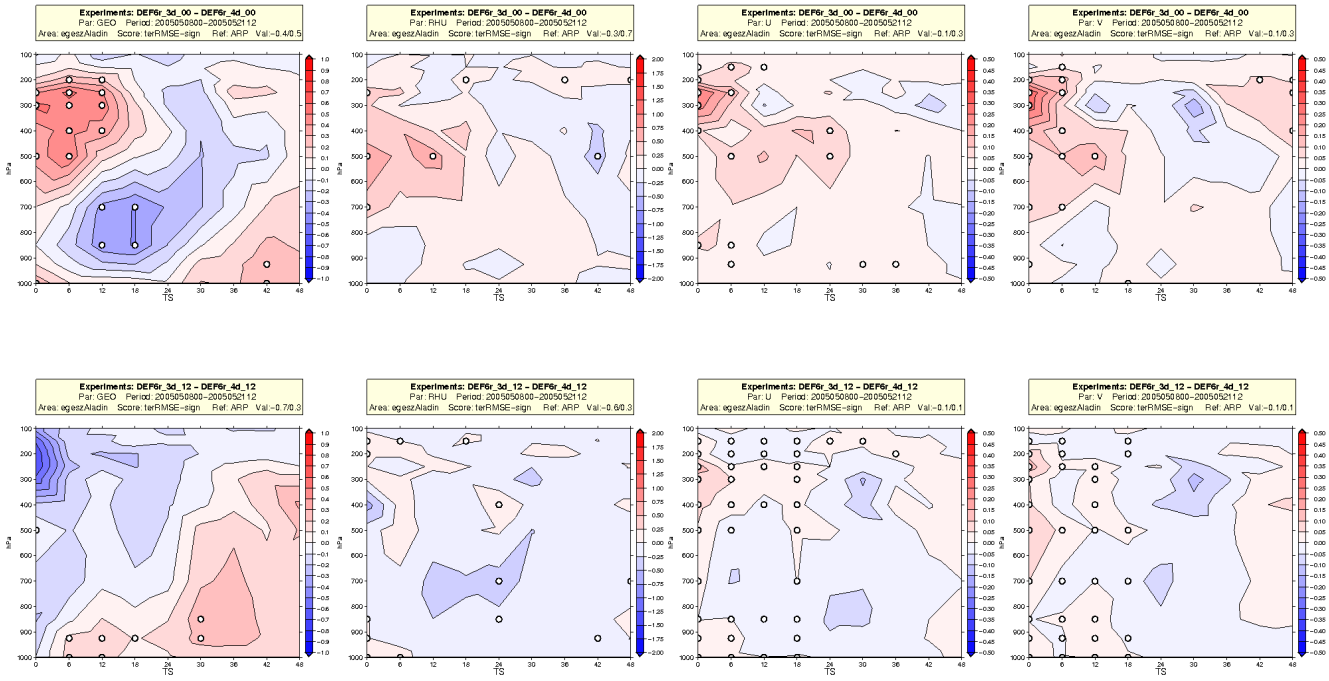

Figure 6: Difference of RMSE scores of the 00 (upper row) and 12 (lower row) UTC forecasts based on 3D-VAR and 3D-FGAT. Red shades indicate that 3D-FGAT is better, while blue shades indicate the opposite. White circles show that the difference is significant on a 90% confidence level. The verification was based on ARPEGE analyses. The figure order is the following (from left to right): Z, RHU, U and V.

The bias scores of the upper air parameters show only small differences in temperature, U and V, but a larger difference can be seen for geopotential and relative humidity (Figure 7). An interesting feature is that for both these latter parameters the bias scores indicate just the opposite as the RMSE scores: where 3D-FGAT is better in terms of RMSE there 3D-VAR is better in terms of bias and vice versa. It has to be mentioned that there is a noisy pattern for geopotential in Figure 7 around 200 hPa. It was verified that this is the consequence of visualizing the difference of the absolute values of the bias scores (the bias difference itself resulted in rather smooth fields - not shown).

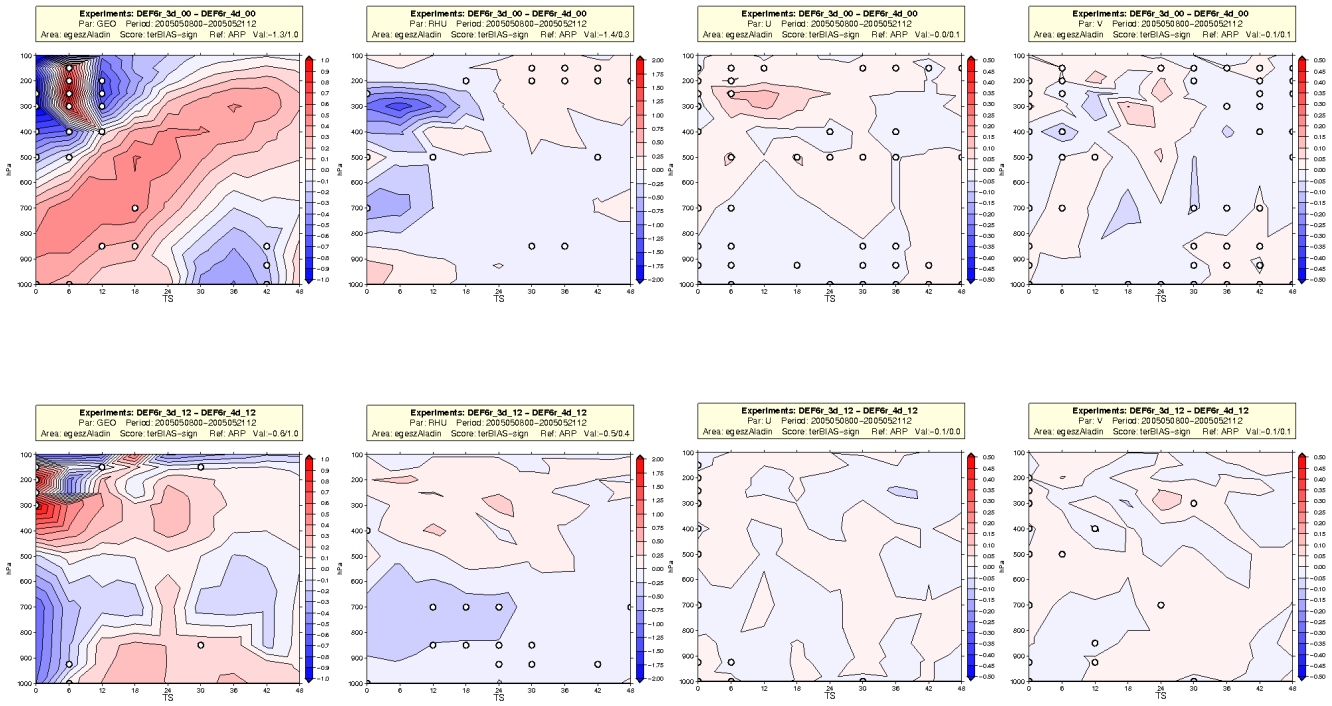

Figure 7: Difference of absolute value of bias scores of the 00 (upper row) and 12 (lower row) UTC forecasts based on 3D-VAR and 3D-FGAT. Red shades indicate that 3D-FGAT is better, while blue shades indicate the opposite. White circles show that the difference is significant on a 90% confidence level. The verification was based on ARPEGE analyses. The figure order is the following (from left to right): Z, RHU, U and V.

The results for U and V can for the 00 UTC runs be directly attributed to the effect of AIREP data but the case of geopotential is not straightforward. Although it can be explained as a consequence of the improved temperature usage for AIREP in 3D-FGAT (since geopotential is strongly linked to temperature), but then the small differences in the temperature forecasts still remain unclear. The other problem with this assumption is related to the wrong geopotential RMSE scores in 3D-FGAT near the flight level at 12 UTC. This is inconsistent with the fact that 3D-FGAT turned to be the most advanced in AIREP temperature handling at the 12 UTC analyses.

Another interesting feature is that although significantly more AIREP reports are used at 12 UTC than at 00 UTC but the difference between 3D-FGAT and 3D-VAR is smaller for the 12 UTC runs (at least for U and V). It may indicate that the usage of more wind AIREP measurements lessens the difference between 3D-FGAT and 3D-VAR in terms of forecast scores.

Using a shorter AIREP window

The evaluation of the reference experiments exhibited that the usage of AIREP reports in 3D-FGAT is more advanced than in 3D-VAR. However, the usage of all the AIREP reports in the 6 hour observation window is not the optimal configuration for 3D-VAR since it is optimal if only observations near the analysis time are used. Thus, another set of experiments was run with the same settings as in the reference experiments but in this case the observation window for AIREP was shrunk to ±1 h in both 3D-FGAT and 3D-VAR. Please note that the results presented below are only preliminary ones and the detailed evaluation of these experiments has not been finished yet.

The comparison of the 3D-FGAT and 3D-VAR forecast experiments using a ±1 h AIREP window is shown in Figure 8. It can be clearly seen that 3D-FGAT still performs better than 3D-VAR for the 00 UTC forecasts while 3D-VAR is slightly better at the 12 UTC runs in geopotential scores. If we compare the RMSE difference patterns in Figure 8 with the reference (±3h AIREP window) case (see Figure 6) we can conclude that the shortening of the AIREP window lessens the difference between 3D-FGAT and 3D-VAR. It can be also concluded that the better performance of

3D-FGAT over 3D-VAR in the reference case around 250 hPa in the first 6h is the clear consequence of the larger AIREP window

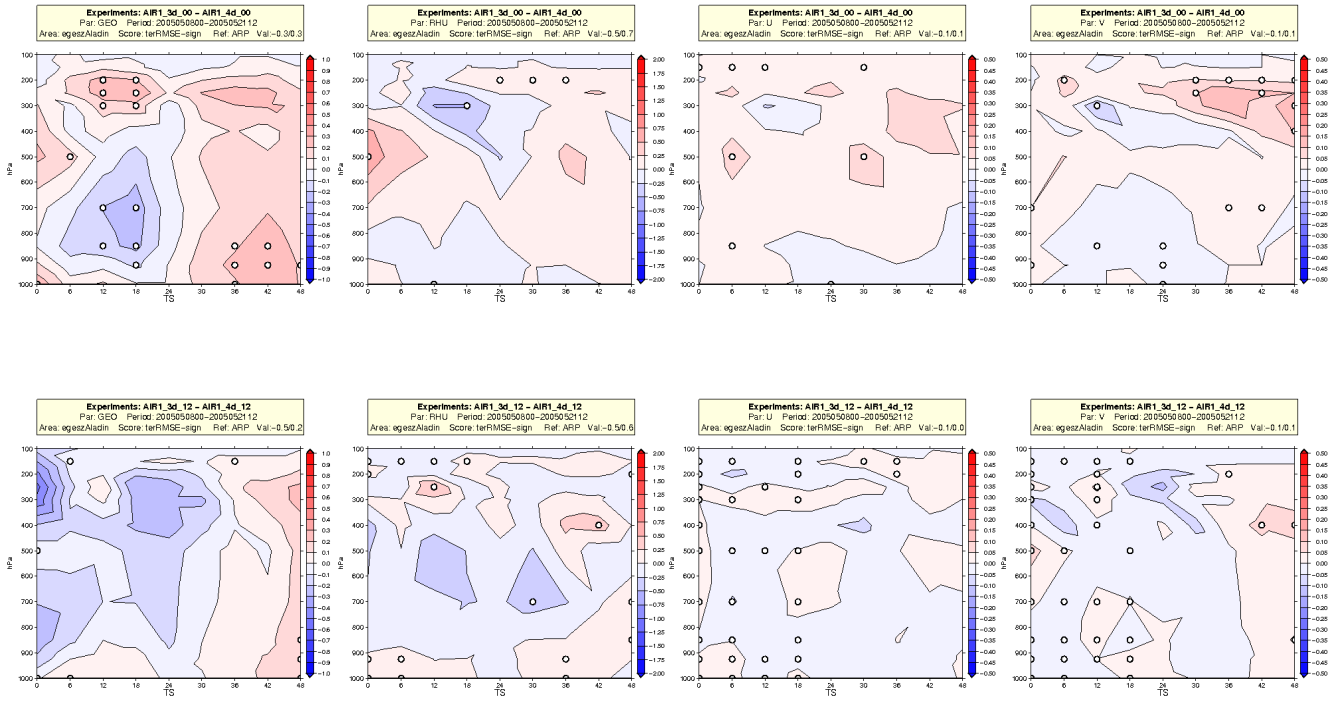

Figure 8: Difference of RMSE scores of the 00 (upper row) and 12 (lower row) UTC forecasts based on 3D-VAR and 3D-FGAT experiments with ±1h of AIREP window. Red shades indicate that 3D-FGAT is better, while blue shades indicate the opposite. White circles show that the difference is significant on a 90% confidence level. The verification was performed against ARPEGE analyses. The figure order is as follows (from left to right): Z, RHU, U and V.

The differences observed in Figure 8 may indicate that the AIREP window is still large enough to result in some differences between the two systems (AIREP is still distributed over 3 time-slots for 3D-FGAT in this case). Another explanation could be that this difference is caused directly by the more precise departure computation for the satellite radiance data (coming from polar orbit satellites) in 3D-FGAT. This idea could be easily verified by using no AIREP data in the experiments.

It was also investigated that how much the shortening of the AIREP window affects the performance of 3D-FGAT itself. In order to test it the 3D-FGAT experiment with the ±1 h AIREP window was compared with the reference one. It can be seen in Figure 9 that the shortening of the AIREP window degraded the forecast results both for the 00 and 12 UTC runs. The only case where an improvement can be seen is the first 6 h of 12 UTC forecasts in around 200 hPa. An implicit consequence of these results (and it was also exhibited by upper air verification - not shown) that the reference 3D-FGAT configuration (with ±3h AIREP window) is even better in terms of RMSE scores than 3D-VAR with the shorter AIREP window. The only exception is the geopotential around 250 hPa in the first 6h of the 12 UTC runs.

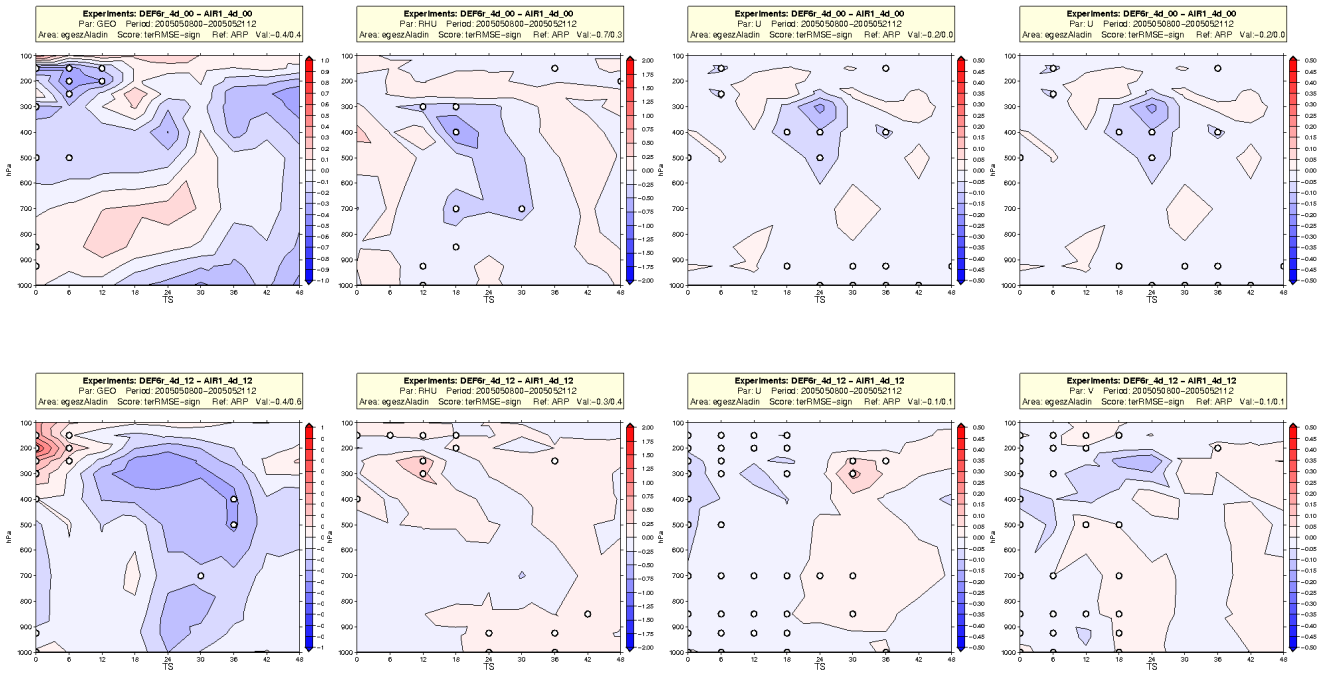

Figure 9: Difference of RMSE scores of the 00 (upper row) and 12 (lower row) UTC forecasts based on 3D-FGAT with ±1h and ±3h of AIREP window. Red shades indicate that the ±1h AIREP window size is better, while blue shades indicate the opposite. White circles show that the difference is significant on a 90% confidence level. The verification was performed against ARPEGE analyses. The figure order is as follows (from left to right): Z, RHU, U and V.

4.4.8. Using all the SYNOP reports in 3D-FGAT

In the reference experiments only one SYNOP report (the closest one to the analysis time) for a given station was used. However, the ALADIN 3D-FGAT system makes possible the usage of all the (even hourly) SYNOP reports within the observation window and in each time-slot there can be one report from a given station. As it was described in Chapter 3 it is a different case than for the fast moving platforms such as AIREP because the location of the observations is fixed now.

In the first experiment the reference set of observations was complemented by all the available SYNOP reports. It means that only geopotential was taken from SYNOP but it was used in all the possible time-slots. Thus, for a given station even 7 observed geopotential values could be used by 3D-FGAT (one per each time-slot). The forecast results based on these 3D-FGAT analyses were compared with the reference 3D-FGAT experiment (see Chapter 6.1). Both the surface (not shown) and the upper air verification scores (Figure 10) indicate that there is an extremely small difference between the two experiments with the exception of the geopotential for which the reference configuration performs significantly better for the 00 UTC runs in the 24-48 h forecast period.

In the next step the observations used in the previous experiment were complemented with all the possible 2m temperature and relative humidity observations from SYNOP reports. The forecast results now were compared with the modified reference 3D-FGAT experiment using also 2m temperature and relative humidity. The comparison of the upper air scores exhibited only a small difference between the experiments again (Figure 11). However, this time at least the scores for geopotential are more similar and there is some improvement in wind in the upper troposphere.

All things considered we can conclude that regardless of the assimilated SYNOP parameters the usage of SYNOP reports with all the possible times cannot improve the reference ALADIN 3D-FGAT configuration. According to Chapter 3 the possible reason can be that the average of the innovations for a given station does not differ too much from the innovation at the analysis time. However, this hypothesis was not checked.

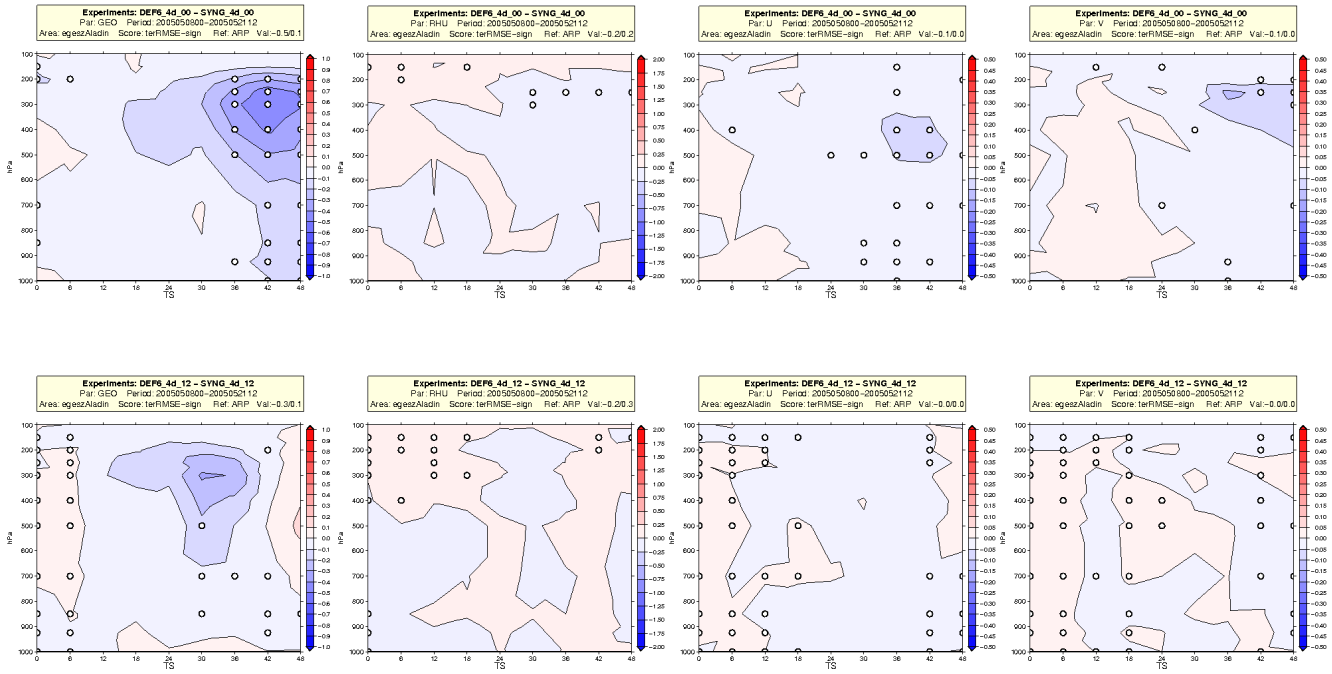

Figure 10: Difference of RMSE scores of the 00 (upper row) and 12 (lower row) UTC forecasts based on the reference system and the system using all the available SYNOP geopotential observations. Blue shades indicate that the reference system is better, while red shades indicate the opposite. White circles show that the difference is significant on a 90% confidence level. The verification was performed against ARPEGE analyses. The figure order is the following (from left to right): Z, RHU, U and V.

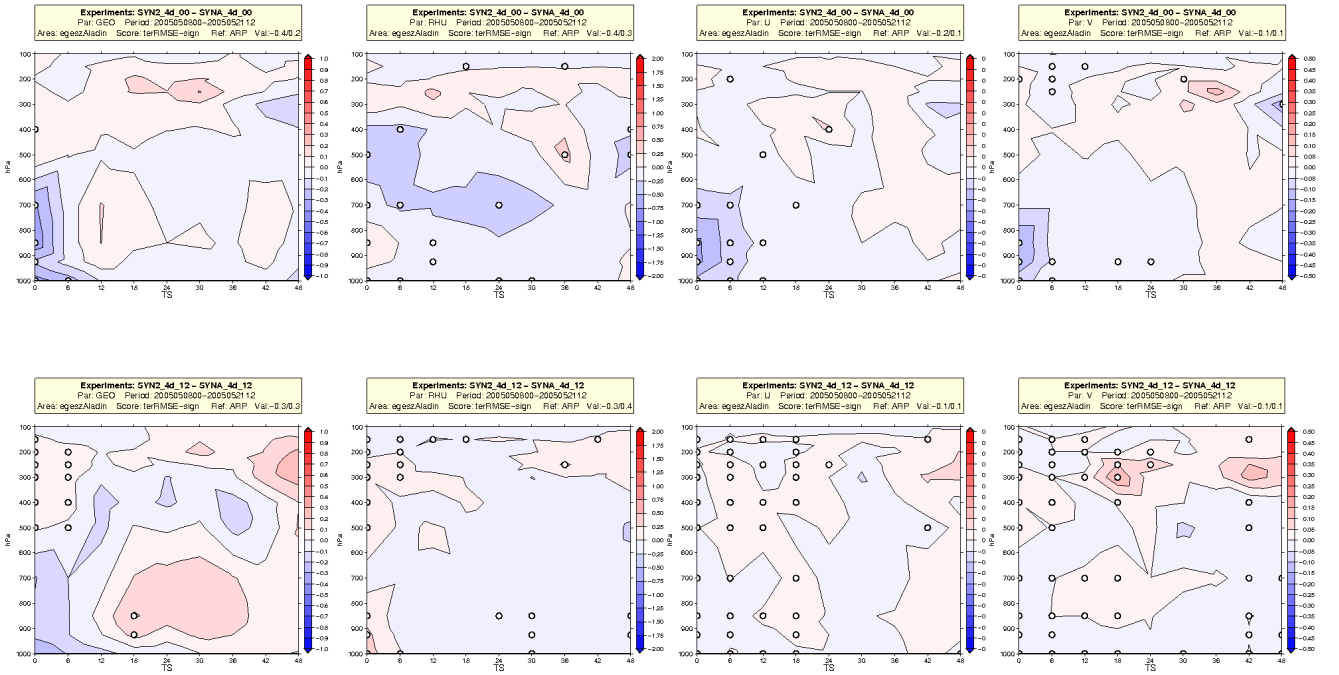

Figure 11: Difference of RMSE scores of the 00 (upper row) and 12 (lower row) UTC forecasts based on the reference system complemented with T2 and RHU2 and the system using all the available SYNOP observations. Blue shades indicate that the reference system is better, while red shades indicate the opposite. White circles show that the difference is significant on a 90% confidence level. The verification was performed against ARPEGE analyses. The figure order is the following (from left to right): Z, RHU, U and V.

4.4.9. Concluding remarks

In this paper the ALADIN 3D-FGAT system was tested using all the observation types available at HMS. As a first result it was verified that according to the expectations the 3D-FGAT analysis increment should be added to the trajectory at the middle of the observation window.

In the second step 3D-FGAT and 3D-VAR were compared using the same set of observations in both systems with a ±3h observation window. Concerning the temporal distribution of the observations the two systems could differ only in the different usage of AIREP and satellite radiance data. The experiments revealed that the 3D-FGAT analysis is more advanced in AIREP report handling and to a less extent for satellite radiances, too. None the less the forecast results are rather similar though 3D-FGAT is a slightly better for the 00 UTC runs for some upper air parameters. A shorter (±1h) AIREP observation windows was also tested and it turned out that in this case 3D-FGAT is still better than 3D-VAR at 00 UTC. It was also verified that the usage of a shorter AIREP window deteriorate the performance of 3D-FGAT in terms of forecast scores.

Finally the possible usage of all the land SYNOP reports (one in each time-slot for a station) in 3D-FGAT was also investigated. These experiments revealed that this approach cannot improve the forecast quality.

The recent research work is related to the determination of the optimal size of the observation window for SYNOP, AIREP and AMV reports in 3D-FGAT. Further tests with the use of satellite radiance bias correction coefficients computed with 3D-FGAT are also planned. The possible usage of a 3h assimilation cycle and new observation types such as SEVIRI radiances will be also considered.

Acknowledgements – The fruitful discussions and the strong support I received from my colleagues at the Numerical Weather Prediction Division of HMS is highly acknowledged.

References

Dziedzic, A., 2005: Test de l'assimilation 3D-VAR FGAT sous OLIVE dans le modele ALADIN. *Internal MF report.*

(available at:http://www.cnrm.meteo.fr/aladin/publications/Report2005/DZIEDZIC.pdf)

ECMWF, 1992: ECMWF Data Assimilation – Scientific Documentation. ECMWF Research Manual 1, 3rd Edition

Huang, X-Y., K. S. Morgensen and X. Yang, 2002: First-guess at the appropriate time: the HIRLAM implementation and experiments, Proceedings for HIRLAM workshop on variational data assimilation and remote sensing, Helsinki 22-23 January, 2002, pp 28-43.

Randriamampianina, R., 2005: Radiance-bias correction for a limited area model, *Időjárás*, Vol. 109/3, pp. 143-155.

Randriamampianina, R., 2006: Use and impact of the full grid AMSU-B data in the ALADIN/HU model model. *ALADIN Newsletter no. 29.*

Soci C., 2004: 3D-FGAT in ALADIN analysis. *Internal MF report.*

(available at: http://www.cnrm.meteo.fr/aladin/publications/Report/Cornel2004.ps)

Soci C., 2004: Further tests with 3D-FGAT in ALADIN analysis. *Internal MF report.* (available at: http://www.cnrm.meteo.fr/aladin/publications/Report/Cornel2004nov.ps)

Vasiliu S., 2006: An evaluation of the 3D-FGAT scheme for the ALADIN/Hungary model. *ALADIN Newsletter no. 29.*

4.5. Y. Seity[1], E. Bazile[1], S Malardel[2] and M. Tardy[3]: AROME prototype validations

[1]Météo-France CNRM/GMAP, [2]Météo-France, CNRM/GMME, [3]DPREVI/COMPAS.

4.5.1. Introduction :

A first version of the AROME prototype has been built in 2004. Daily experimentations have started in May 2005 over the South-West of France. This paper will present some validation studies performed with this prototype :

- An inter-comparison exercice over Austria concerning rainfalls evaluation during a 3 months period.

- A subjective day-to-day evaluation of the behaviour of the model.

4.5.2. Description of AROME Prototype:

AROME numerical simulations presented in this paper were performed without data assimilation, which is still under developments (Brousseau et al., 2006). AROME prototype ran in dynamical adaptation mode from ALADIN-France. It used a 2,5 km horizontal grid, with 41 vertical levels and a time step of 60 seconds. The following physical parameterizations are switched on (on cycle 31T2) : externalized surface scheme SURFEX1.3, ICE3 microphysical scheme, 1D mesoNH turbulence scheme with Bougeault-Lacarrère closure condition and turbulence cloud scheme (MASDEV4_6_Bug4), ECMWF radiation scheme with 6 spectral bands in short-wave, and Kain-Fritch Bechtold shallow convection scheme without convective cloud scheme.

4.5.3. Inter-comparison study over Austria :

The INCA analysis (Integrated Nowcasting through Comprehensive Analysis) developed by the Central Institute for Meteorology and Geodynamics in Vienna is a good reference to verify forecast precipitation. This analysis is a synthesis of rain-gauge stations interpolation and radar data (T. Haiden et al.,2005).

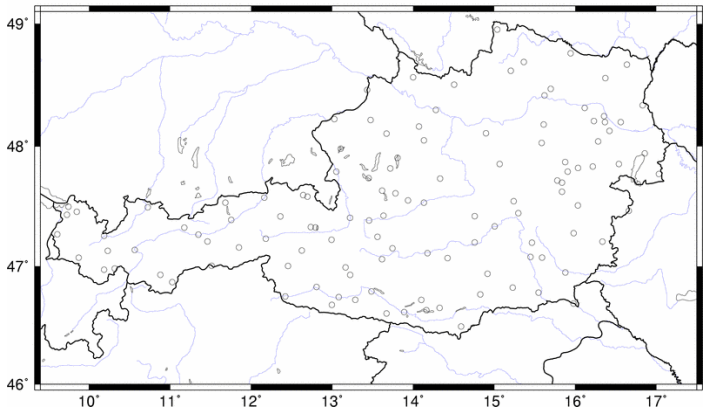

Figure 1 : INCA Analysis domain inside AUSTRIA.

AROME took part of the AMADEUS project (in collaboration with ZAMG, in particular Y. Wang and F. Wimmer). Several Numerical Weather Prediction (NWP) models starting at 0TU are compared over Austrian country (Figure 1) : ARPEGE (25km), ALADIN-France(10km), AROME (2.5km) during August 2005, October 2005, and April 2006. Daily cumulative rainfalls (0-24TU) are compared with the analysis on a 20km horizontal grid. During August, deep convective events

are frequent, with an extreme heavy rain event in the middle of the month. During October and April, cumulated amounts of precipitation are lower, and mainly due to stratiforme precipitations.

Equitable Threat Score (ETS) has been calculated by the following formula :

$$ETS = \frac{\text{Correct Detection} - \text{Correct detection in reference}}{\text{Correct Detection} + \text{lack of detection} + \text{false alarms} - \text{Correct detection in reference}}$$

This score gives the estimation of the amelioration of the model compared with the reference. False alarms and lack of detection are equally treated. Perfect model will have ETS=1.

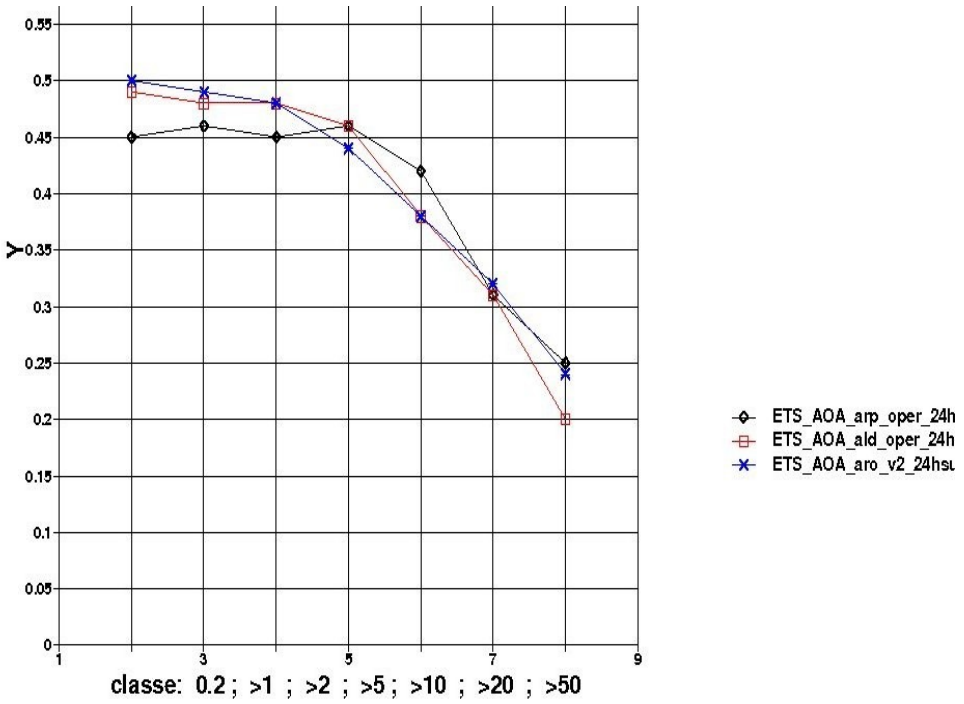

Figure2 : ETS scores for August 2005, October 2005 and April 2006 (20km, 24h rainfall) ARPEGE in black, ALADIN-France in red and AROME in blue.

Figure 2 gives the results of the ETS computed over the whole 3 months. For each model, the ETS decreases when rainfall amounts increases. The model quality is about the same, with a small benefit for AROME in light and heavy rain classes. Heavy rains, which mostly occurred over the Alps are over-estimated by the models.

4.5.4. Daily evaluation of the AROME prototype :

From a daily subjective evaluation of the prototype since May 2006, a good behaviour of the AROME prototype in North West cloudy sky situations has been noticed. An example is shown on Figure 3. The organisation and the structure of rainfalls is more correct than in ALADIN-France.

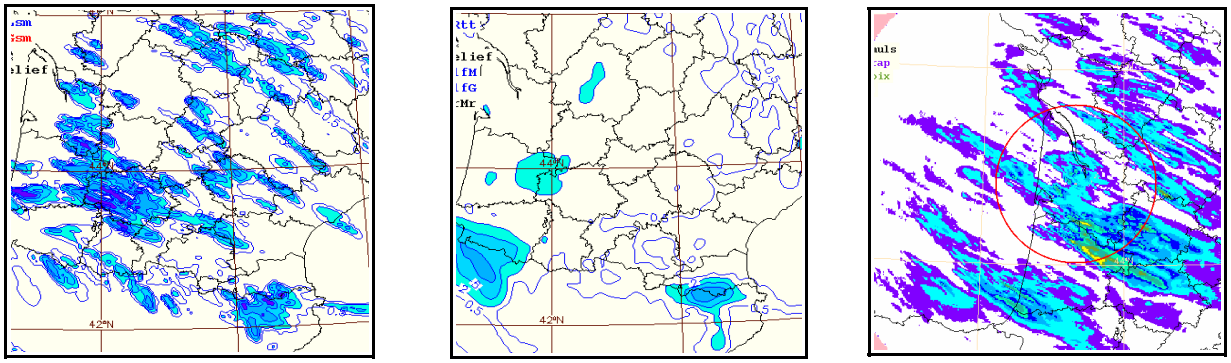

a)AROME Prototype, b) ALADIN-France c) radar observation.

Figure 3 : Cumulative surface rainfall between 12-15TU on October 4th 2006 :

We have also observed a better representation of urban effects, probably due to the use of a specific urban scheme in AROME (Town Energy Budget from SURFEX) :

a) hot spots : Figure 4 shows an example around Montpellier in the north-western part, with a hot spot over the city with a maximum temperature around 21 °C, well simulated by AROME and not seen by ALADIN.

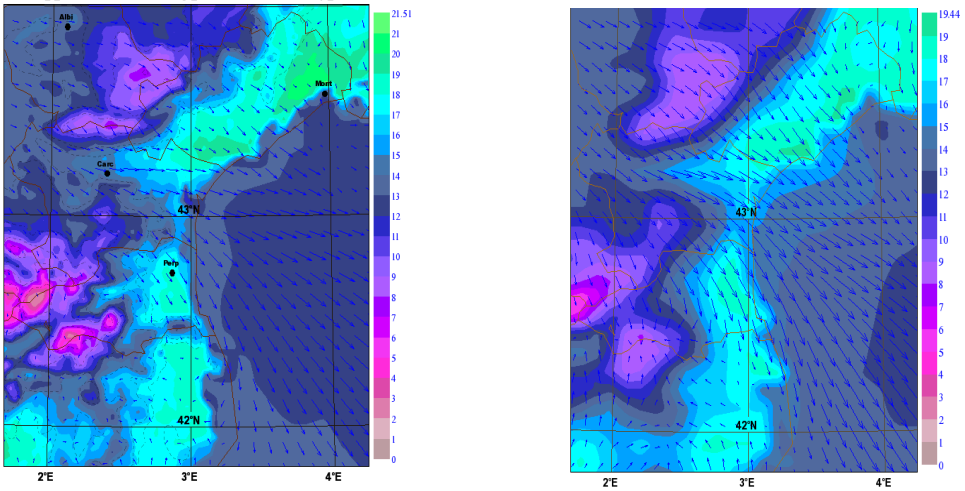

a) AROME Prototype, b) ALADIN-France

Figure 4 : 2m Temperature and 10m wind at April 13rd 2006 at 13TU :

b) In case of strong winds, the stress imposed by the city reduces the wind speed in AROME. It was particularly observed over Paris in January 18th 2007 during an event of strong winds (Figure 5), in which ALADIN has a trend to over-estimate the wind over Paris.

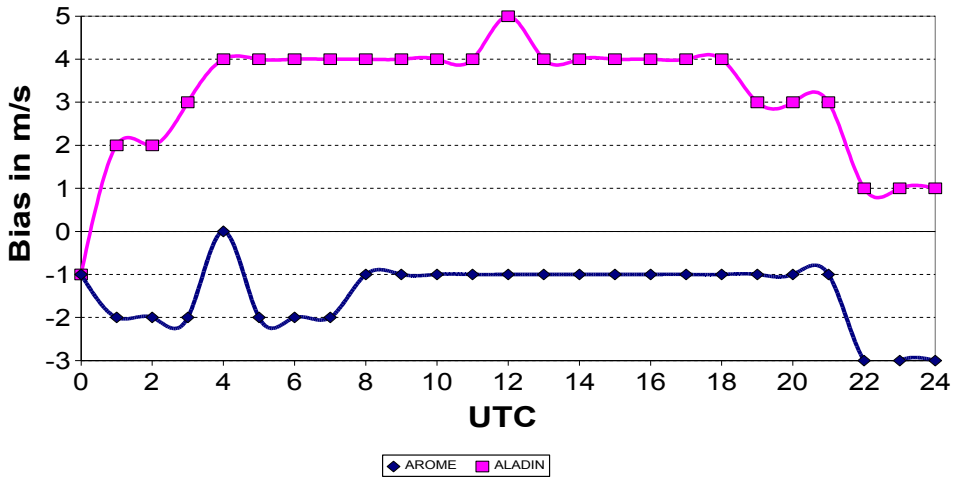

Fig. 5: 10m wind biais in PARIS-Monsouris, January 18th 2007.

On the other hand, some problems were reported concerning 2 meters temperatures and in areas near the domain borders. They are still under investigations. For 2 meters temperature for example, different diagnostics have been developed and are still under tests.

4.5.5. Conclusion and outlook

The AROME prototype forecast quality has started to be evaluated by different ways:

A systematic and statistical objective evaluation, like the one presented here concerning three months of precipitation over Austria, and by a daily subjective evaluation. These studies show a correct behaviour of the model, even if we still have known and not yet known problems.

The AROME prototype is running daily on our new NEC supercomputer since the end of January 2007 on a domain covering the whole French territory. The evaluation will continue on this bigger domain, with collaborations with forecasters. The assimilation part is planned to complete the prototype in spring 2007, with a new step of evaluation of the model quality.

References :

Brousseau, P. and Seity Y., 2006, A first prototype for the AROME Data assimilation system *ALADIN Newsletter 29.*

Haiden T., 2005, Integrated Nowcasting through Comprehensive Analysis (INCA) : System overview, Internal note, C*entral Institute for Meteorology and Geodynamics*, Vienna, Austria.

4.6. M. Amodei and J. Stein: Comparison of precipitation forecasts by two operational NWP models: The global model ARPEGE and the smaller mesh LAM ALADIN.

Météo-France/DPrevi/COMPAS

4.6.1. Objective:

The 24 hours accumulated precipitation forecasted by ARPEGE and ALADIN is verified and compared over France according to the methodology recommended by the WGNE (Working Group on Numerical Experiment) in order to :

- Define a set of relevant scores to verify the precipitation forecasted by the French operational high-resolution LAM, ALADIN today, AROME in the future.
- Evaluate differences between **2** models and determine if they are statistically significant.

4.6.2. Observations and models used:

The temporal period contains 9 trimesters from December 2004 until February 2006.

The climatological state network (Figure 1) contains almost 4000 observations per day. These observations, spaced by around 10 km, are averaged on the 0.2° verification grid to provide the reference data.

The spatial resolution of the uniform verification grid is 0.2° x 0.2°.

The persistence of the precipitation of the previous day provides the trivial forecast used to compute skill scores.

The ALADIN forecasts, available over a 0.1°, are averaged over 4 points and the ARPEGE ones are interpolated from a 0.25° grid.

The global ARPEGE model provides lateral boundary condition to ALADIN. The physical packages are similar for the 2 models. Since the 25th of July 2005, the ALADIN model has its own 3DVAR assimilation and assimilates the high-resolution SEVIRI radiances from Meteosat 8.

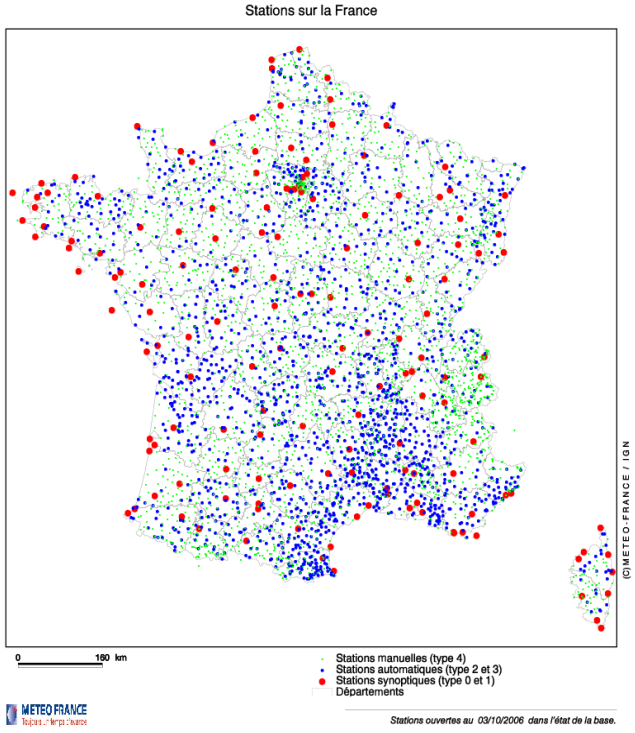

Figure 1: Climatological state network: manual stations (green), automatic stations (blue) and synoptic stations (red)

4.6.3. Deterministic approach:

Verification is performed in a deterministic framework. Scores are computed over every trimester from the contingency tables for the different thresholds 0.2, 1, 2, 5, 10, 20 mm/day over France. A bootstrap re sampling technique is used to compute a box plot for the different scores but also to test the significance of the difference between both models according to *Hamill* (1999).

Autumn 2004 and 2005 are comparable according to the rainfall histogram and surround the 3DVAR beginning (Figure 2). During Autumn 2005, (cross on Figure 3) ALADIN exhibits significantly higher HSS than ARPEGE for all thresholds excepted the 20 mm/day. During Autumn 2004 (closed circle on Figure 3), the differences were smaller and in favour of ARPEGE. This evolution can be explained by the assimilation benefit for the ALADIN forecasts.

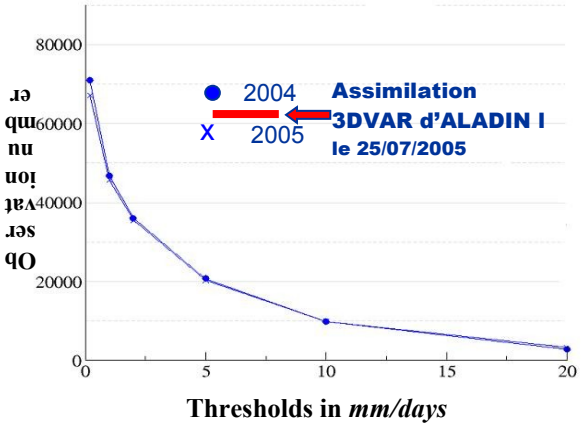

Figure 2: Number of the precipitation observations for Autumn 2004 (closed circle) and 2005 (cross)

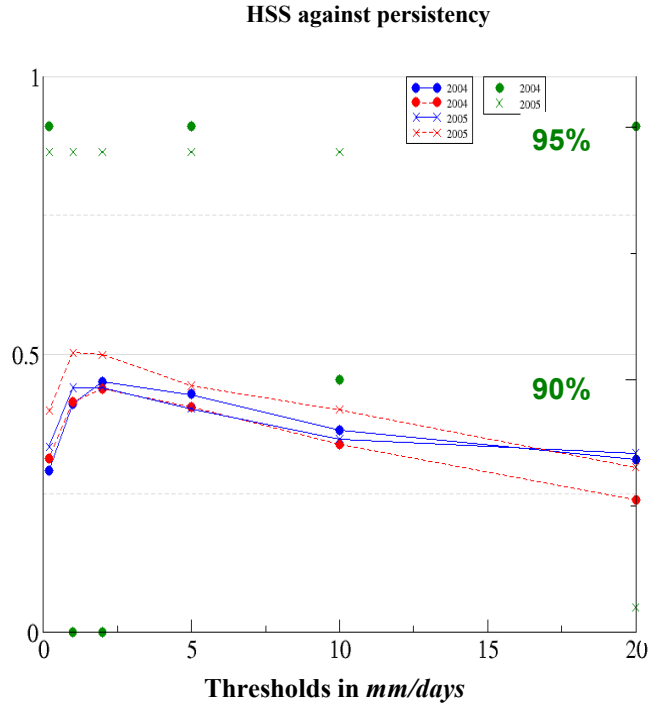

Figure 3: HSS for the Autumn 2004 (closed circle) and 2005 (cross). Green symbols indicate when the model difference is significant at 90%, 95% or not

The temporal evolution of the HSS (Figure 4) shows the significant superiority of ALADIN for the rain detection (threshold 0.2 mm/day). For stronger precipitation (20 mm/day), this is the contrary. The improvement occurring after JJA_2005 for the ALADIN model is permanent for both thresholds and is due to 3DVAR assimilation introduced in ALADIN on the 25/07/2005. Nevertheless, it only leads to a reduction of the gap between both models for strong precipitation.

4.6.4. Fuzzy approach:

In order to avoid the "double penalty" which affects the high-resolution models, a statistical post-processing is performed to allow a probabilistic treatment of the forecasts *(Robert 2004, Theis et al. 2005).* A probability to exceed a given threshold is computed in a square of nxn grid points for the forecasts and the persistence. The verification is performed by computing the Brier Skill Score (BSS) and Rank Probability Skill Score (RPSS). Both are estimated according to the persistence. 2 BSS are computed:

- **BSS-SO** single observation – neighbourhood forecast gives us a local verification
- **BSS-NO** neighbourhood observations- neighbourhood forecast gives us a regional verification.

The neighbourhood characteristic size (NCS) vary from 60 km to 242 km. Both BSS are plotted for two seasons (DJF 2006 and JJA 2004) (Figure 5). By comparing both figures, we conclude that winter precipitation is better forecasted than summer one because of the more convective nature of the summer rainfalls.

BSS-NO outperforms BSS-LO for all thresholds and NCS. BSS-NO grows continuously with NCS to reach a maximum of 0.9 in winter while BSS-LO is quasi-constant. However in winter the BSS-LO slowly decreases for the largest neighbourhood. BSS-LO peaks for NCS= 130-140 km,

indicating that information at greater distances is not pertinent for the local forecast.

Strong BSS-NO values in winter show the ability of the ALADIN model to predict regional precipitations. Note that the relative bad performances for the 0.2 mm/d are probably due to measurement threshold of certain rain gauges. During summer, the probabilistic scores reduce the double penalty influence for the convective cases more frequent in this season for the strong threshold 20 mm/d. Therefore, BSS-NO increases the most quickly for the 20 mm/d among all these thresholds. For these reasons, BSS-NO is more relevant in the framework of precipitation verification for operational model.

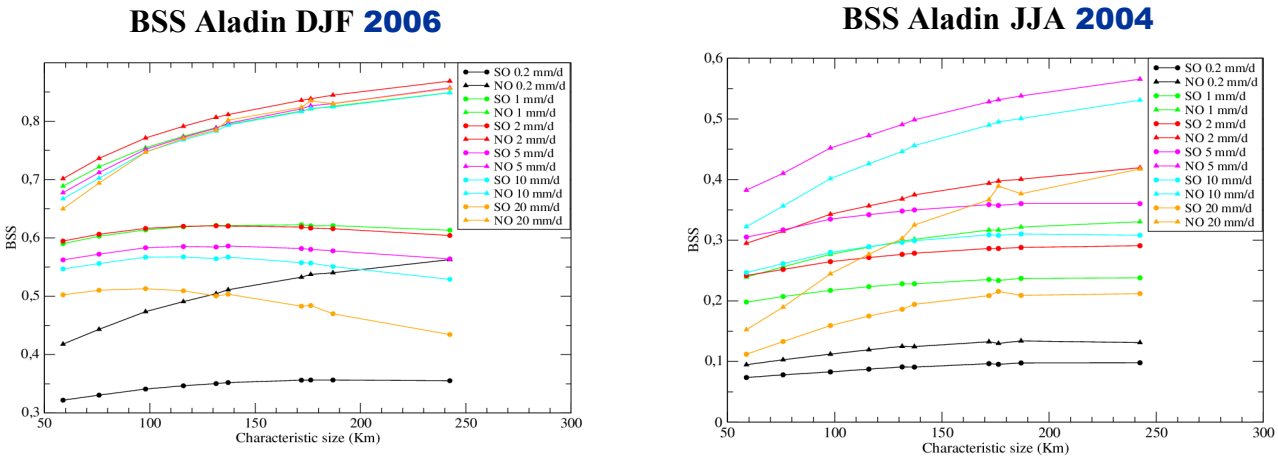

Figure 5: BSS_SO (closed circle) and BSS_NO (triangle) for several NCS, Winter 2006 (left) and summer 2004 (right). The thresholds (0.2 to 20 mm/d) are differentiated by colours.

The comparison between the two models is shown for the BSS-NO along the whole period, for extreme thresholds values (0.2 mm/d, 20 mm/d) and 2 NCS (60 km, 242 km)(Figure 6).

The largest neighbourhood always achieves the largest forecast improvement whatever the trimester. The BSS-NO_242km is 10% larger than the BSS-NO_60km.

The fuzzy approach shows an improvement of the ALADIN model for the rain detection (0.2 mm/d) during the two last trimesters after the ALADIN assimilation introduction. This is coherent with the classical HSS scores. But for the 20 mm threshold, the ALADIN improvement after JJA 2005 is greater for BSS than for HSS. This is related to a reduction of the double penalty importance allowed by the fuzzy method. Nevertheless, the impact is not as important as for very high-resolution models because the resolution ratio between ARPEGE and ALADIN is only 2.3 and they share the same physical package.

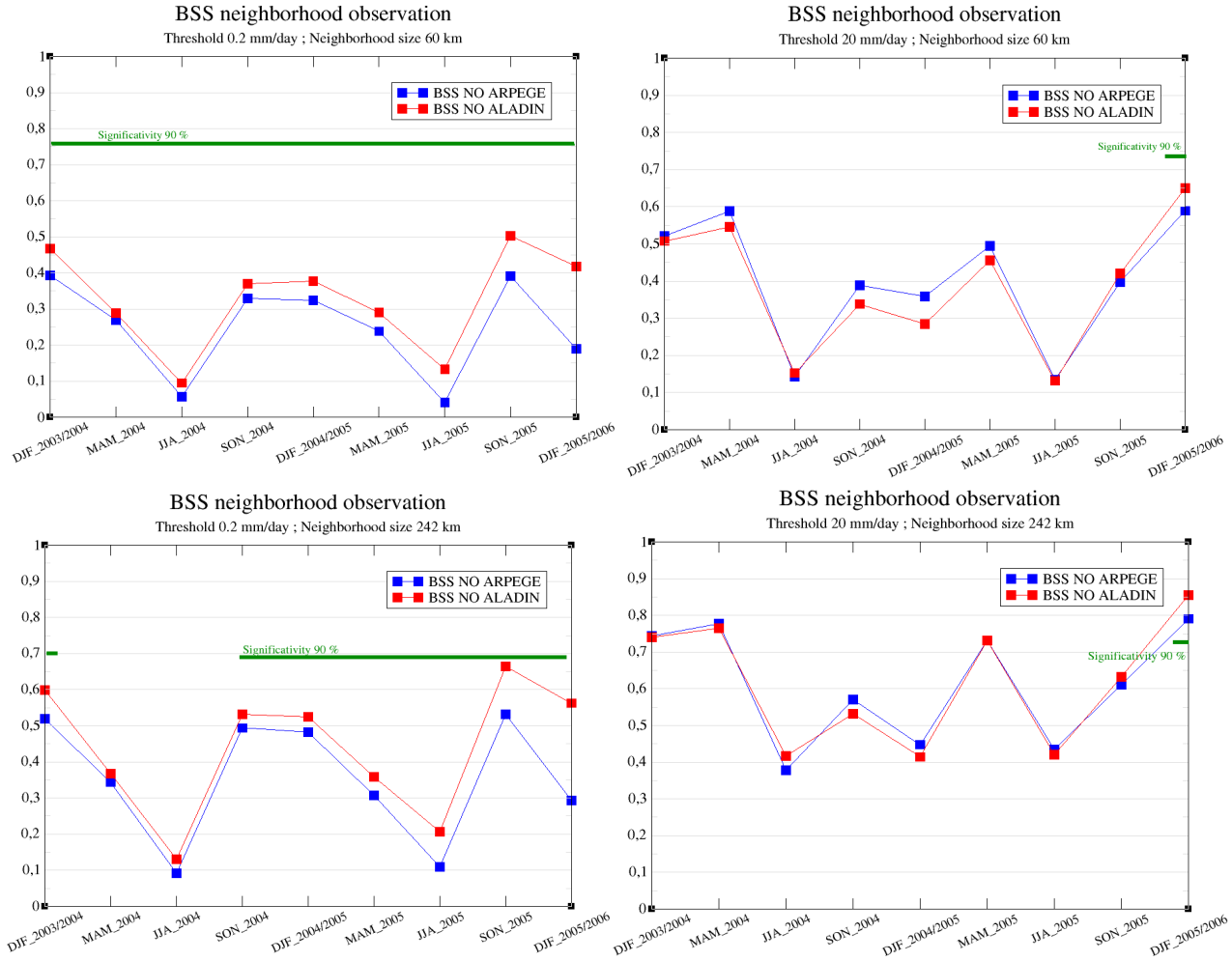

Figure 6: BSS_NO evolution along the whole period for extreme thresholds values 0.2 mm/days (left), 20 mm/day (right) and for 2 NCS 60 km (top) and 242 km (bottom). Green line indicates when the model difference is significant at 90%.

A more synthetic information is given by the Rank Probability Skill Score (RPSS). RPSS-SO and RPSS-NO are computed in the same way as the BSS. Reference is provided by the persistence. RPS of the two models and of the persistence have been multiplied by a factor 15 and plotted together with the RPSS. These curves confirm, that the RPSS variations are mainly due to the RPS variations and the ALADIN improvement is clear after the introduction of its proper assimilation. We also notice the improvement in term of skill scores when a larger verification box is used (fig.7).

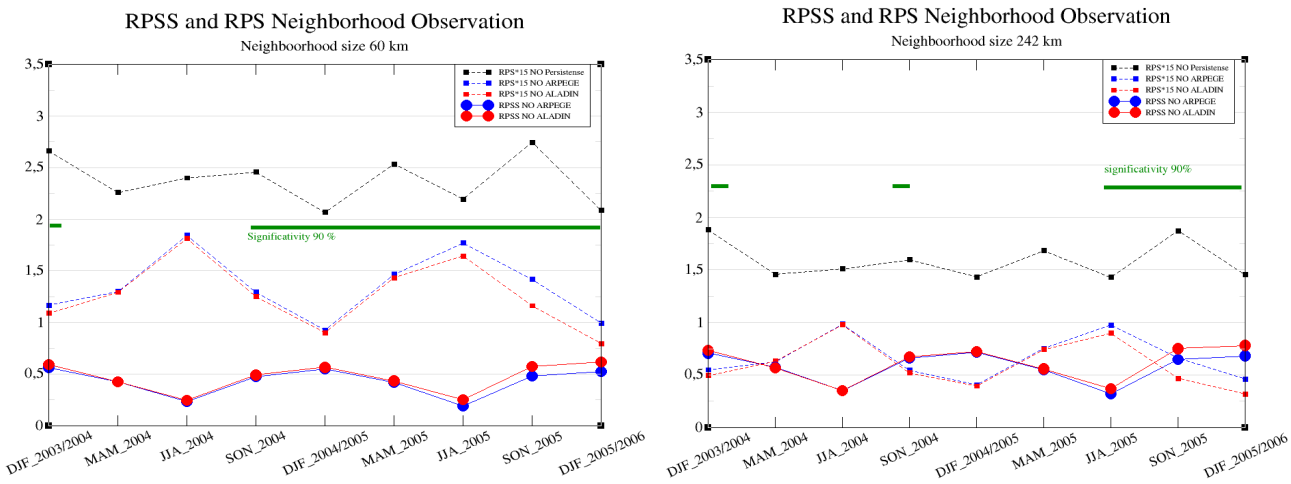

Figure 7: RPSS_NO (full line) and RPS_NO (dot line) evolution along the whole period for 2 NCS 60 km (left) and 242 km (right). Green line indicates when the model difference is significant at 90%.

4.6.5. Conclusion

- The probabilistic approach has been used to evaluate the differences between the global ARPEGE model and the LAM ALADIN. BSS-NO against persistency is a good candidate to measure the impact of higher resolution forecasts. It partly reduces the influence of the double penalty. Statistical significance can be added to this treatment.
- This method allowed us to show the ALADIN improvement for the precipitation forecast brought by the inclusion of a proper assimilation scheme using higher resolution data.

Future

• The daily rain-gauges will be replaced by the ANTILOPE hourly analysis mixing rain gauges with radar data.

• The AROME prototype of the future high-resolution model will be verified according to this methodology.

References

Hamill, T.M, 1999: Hypothesis test for evaluating numerical precipitation forecasts. *Weather and Forecasting.*, **14,** 155-167.

Roberts,N., 2004: The evaluation of storm-scale NWP precipitation forecasts. *Met Office JCMM*.

Theis,S. ,A. Hense and U. Damrath, 2005: Probabilistic precipitation forecasts from a deterministic model: a pragmatic approach. *Meteorol. Appl.*, 12, 257-268

4.7. B. Strajnar: A comparison between dynamic adaptation and mesoscale analysis methods for initial conditions for ALADIN over Slovenia.

University in Ljubljana

4.7.1. Introduction

There are two common strategies of initial conditions for limited area models. In dynamic adaptation, the analysis is taken from a global model and interpolated to a denser grid of a regional model. Another strategy is a mesoscale analysis, where observations are assimilated directly to a regional model at highest resolution possible. The global model provides only boundary conditions, needed for integration. The high resolution picture of the atmospheric state is already present in the analysis.

This paper presents a comparison between operational applications of those two strategies to ALADIN limited area model. The dynamic adaptation using ARPEGE analysis is performed in Slovenian meteorological service and the mesoscale analysis is performed in Hungarian meteorological service (*Bölöni*, 2005). While the ARPEGE analysis uses four dimensional variational assimilation (4D-Var) and a great variety of observations, the mesoscale analysis uses three-dimensional variational assimilation (3D-Var) upper-air analysis and optimal interpolation (OI) surface pressure analysis (soil analysis is taken from ARPEGE). In the mesoscale analysis, fewer types of observations are used (surface pressure, radiosonde data, AMDAR aircraft measurements and ATOVS AMSU-A microwave radiances), but are assimilated in higher resolution. The background error covariance matrix for variational assimilation is computed using NMC method (*Berre, 2000*; *Široka et al.*, 2003).

4.7.2. Data set and differences statistics

The data set consists of analyses (ARPEGE and mesoscale) at 00 UTC and subsequent operational 24 h forecasts (the two analysis-forecast pairs are denoted by ALADIN/SI and ALADIN/HU) in the period of June 2006. To compare the meteorological fields defined on different gridpoints, the analyses and forecasts were first interpolated to a grid named ALPS, which covered the Alps and also the complete area of Slovenia with resolution of 10 km. The fields were also interpolated to pressure levels.

The first results were the greater variability of differences near the surface than on the upper-air levels. On average, Hungarian operational analyses and forecasts predicted higher values of temperature (0.25 K analyses, 1 K forecasts at 950 hPa) and lower values of relative humidity (5% analyses, 7% forecasts at 950 hPa). There were no significant differences in geopotential. The average wind gridpoint differences were small, their variability did not change much with height.

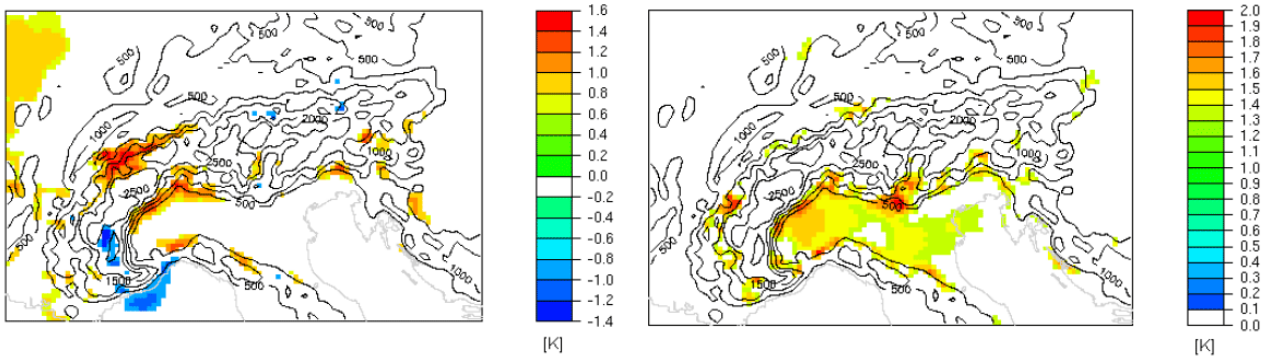

Fig. 1: One tenth (n = 800) maximal average gridpoint temperature differences (ALADIN/HU – ALADIN/SI) on ALPS domain: analyses of 925 hPa (left) and forecasts 925 hPa (right). Isolines of orography are overlaid.

The spatial distribution of average differences was also investigated. A significant part of differences in geopotential, temperature, wind and humidity were connected with differences in the orography representation in both analyses and forecasts (Fig. 1). Some other significant temperature differences were found particularly in the Po basin – they could appear due to different vertical resolution in Slovenian and Hungarian configurations (37 and 49 vertical levels). The second can therefore describe the inversion layers in the basin more realistically.

4.7.3. Verification

The forecasts as well as analyses were verified against the measurements of 11 Slovenian automatic meteorological stations, which were selected in different relief types (mountain, valley and seaside stations), following *Žagar et al.*, 2006. The verified parameters were 2 m temperature, 10 m wind and daily precipitation. As a model prediction in the observing station, the nearest model point was taken.

Classical verification scores for temperature were very similar for both analyses, but were different in the forecasts, where a positive bias in Hungarian forecasts was detected (not shown). The bias was also reported by Hungarian meteorological service and was corrected on 28th June, when the ARPEGE analysis was taken as a first guess of the mesoscale analysis.

The success of both strategies in predicting wind is approximately equal, the scores depend on station position (Fig. 2). This illustrates the problem of assimilation of 10 m wind, since the measurements on some stations strongly depend on local wind properties and are not widely representative. The scores are somewhat better in forecasts than analyses (no assimilation of surface wind) and the differences between two strategies are smaller in forecasts. The same model dynamics and approximately equal horizontal resolution decreases those differences during time integration.

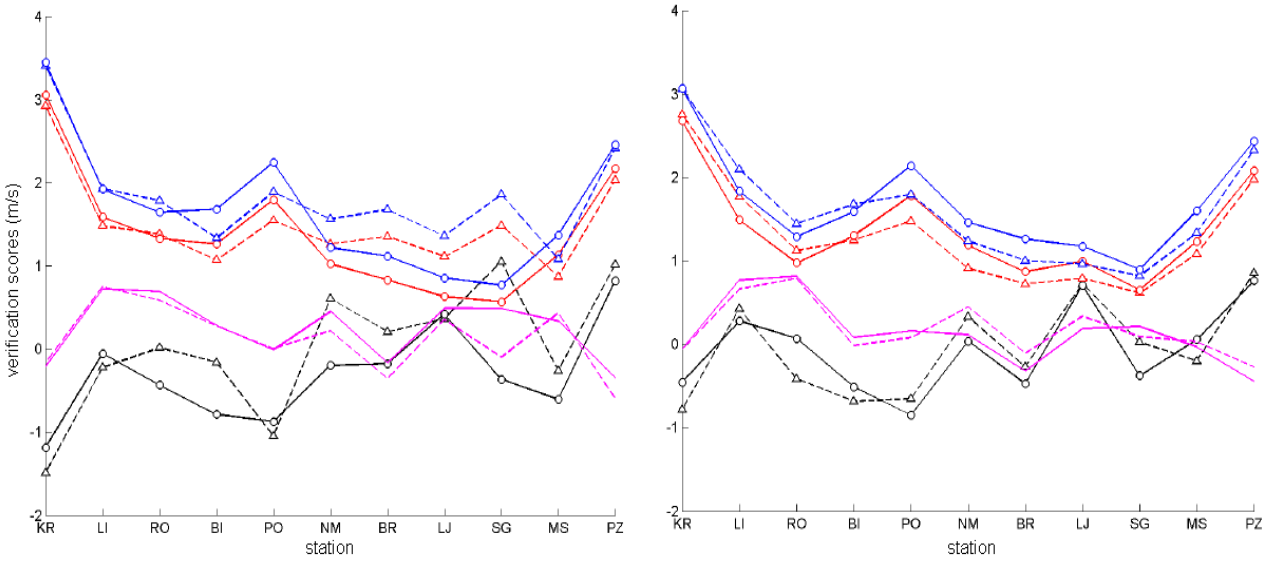

Fig. 2: Verification scores of 10 m wind (meridional component) for analyses (left) and forecasts (right) on different Slovenian stations: ALADIN/HU (dashed lines with triangles), ARPEGE-ALADIN/SI (solid with circles). Mean absolute error (blue), root mean square error (red), anomaly correlation (magenta) and bias (black).

The last verification parameter was daily rainfall. Since the classical continuous verification methods are unsuccessful for precipitation, the multi-category and binary verification methods were used (*Jolliffe* and *Stephenson*, 2003). The performance of ALADIN/HU was better in cases when smaller amounts of daily precipitation, but slightly worse in cases with precipitation over 10 mm (only few in the period of June 2006, fig.3). Both forecasting systems underestimated the number of

events with no measurable precipitation. While ALADIN/SI forecasted one half such cases, ALADIN/HU predicted one forth more cases. The models predicted to many precipitation cases with precipitation amount up to 10 mm. Binary verification scores and relative operating characteristics (Fig. 3, right) also indicate a slightly better performance of ALADIN/HU.

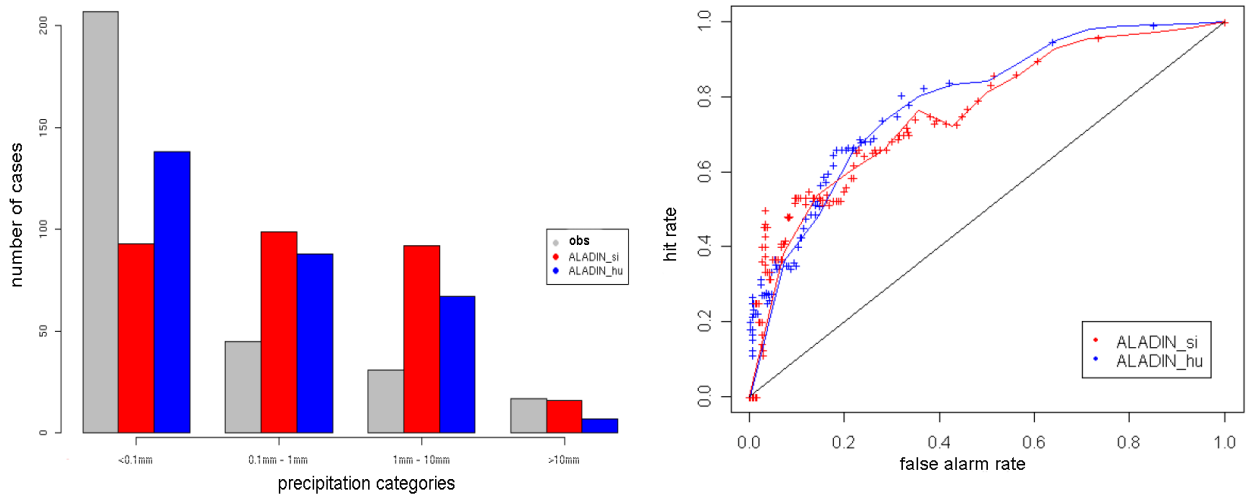

Figure 3: Multi-category precipitation verification (left): observed events (grey), ALADIN/SI (red) and ALADIN/HU (blue) forecasts. Right: relative operating characteristics (same colours).

4.7.4. Case study

Significant differences in precipitation forecasts were found on 30th June 2006. In the early morning there were a few thunderstorms, moving in NE direction. While the convective part of forecasted precipitation were similar, the difference occurred in stratiform precipitation, where ALADIN/SI predicted a band with over 60 mm, while ALADIN/HU predicted only about 10 mm.

The verification of this event was only possible using radar measurements and reports of few automatic meteorological stations. Conventional rainfall measurements were not useful, because the previous day was also rainy. Radar daily rainfall cumulation values were up to 15 mm, while the maximum reported value from automatic station was 25 mm (Murska Sobota, which was on the line of most intense thunderstorms), other stations reported much less or no precipitation.

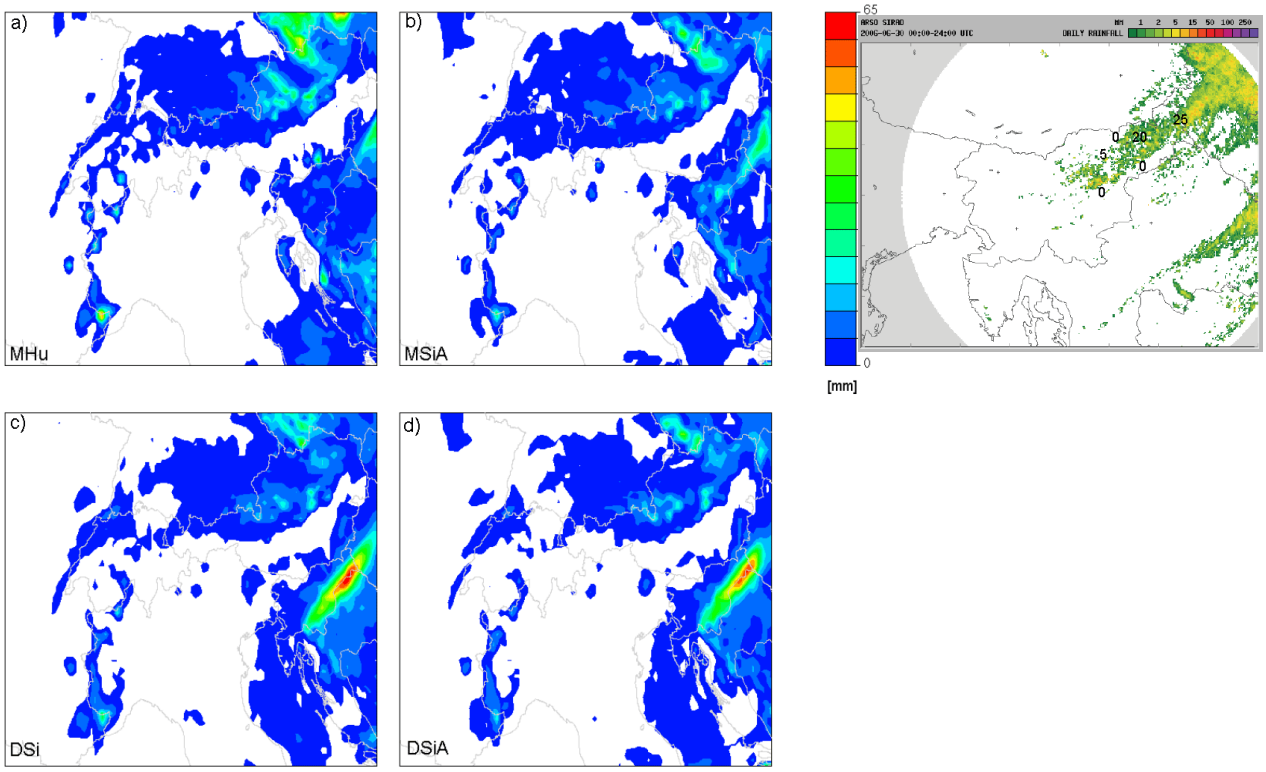

Fig. 4: Daily precipitation forecasts on 00 UTC 30th June 2006 (left): a – operational forecast ALADIN/HU, b – simulation using mesoscale analysis and ALADIN/SI, c – operational Slovenian forecast, d - control forecast with ARPEGE analysis on ALPS domain, and daily radar cumulation with some reports of automatic stations (right).

The differences could occur due to model differences (horizontal and vertical resolution, configurations, parameters) or due to different initial conditions. To investigate that, simulations with both types of analyses were repeated using Slovenian configuration ALADIN/SI on ALPS domain (Fig. 4). The simulation with initial conditions obtained by mesoscale analysis using configuration ALADIN/SI seems to best describe observed event. These simulations clearly show that the main reason for detected differences in forecasts over Slovenia is to be found in initial conditions.

Further investigations showed that a weak front was passing over Slovenia. The frontal wind convergence was more pronounced in ARPEGE analysis and resulted in a precipitation band. The wind field in this analysis was too smooth and overestimated the intensity of the event. This suggests the importance of having high resolution fields already in the analysis.

Other interesting thing to check is the importance of observations, used in the analysis at 30th June 2006 00 UTC. Simulations were repeated using the first guesses for both mesoscale and ARPEGE analysis (i.e. short-range forecast started at 29th June 2006 18 UTC, Fig. 5).

The over forecasted precipitation band over Slovenia is present also in the forecast using ARPEGE first guess, maximum values are even somewhat higher. There is also a precipitation area on the northern side of the Alps (in north-east Austria). Using the recent observations, ARPEGE analysis reduces the amount of precipitation. The forecasts using mesoscale analysis and its first guess does not differ a lot. The area of forecasted precipitation just moves slightly in the west direction. The relative impact of new observations is generally small. This illustrates the general lack of local observations. Since the observations can not change the model state enough at single analysis time, the precise first guess is very important. In our case it was provided by a mesoscale model.

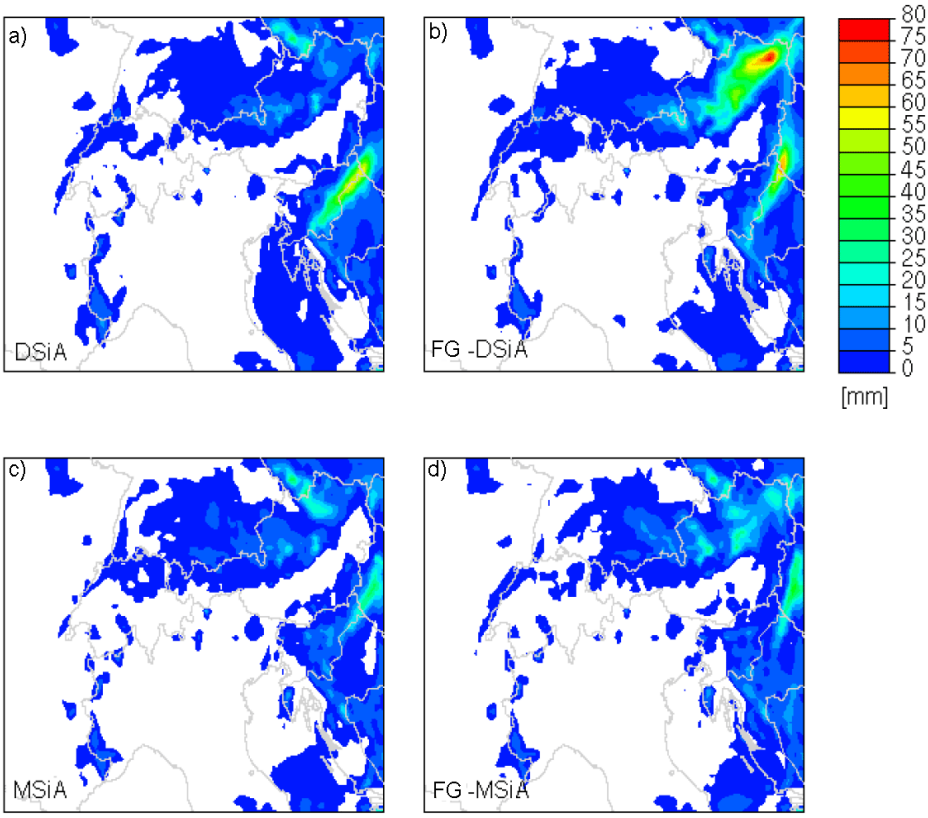

Fig. 5: Daily precipitation ALADIN/SI forecasts initiated at 00 UTC 30th June 2006 using: a a - mesoscale analysis, b - mesoscale analysis first guess, c - ARPEGE analysis, d - ARPEGE first guess.

4.7.5. Conclusions

The differences between dynamic adaptation and mesoscale analysis in the period of June 2006 were generally small. Biases were found in temperature and moisture fields, mesoscale analysis was hotter and drier near the surface. The performance of 3D-Var in three times better resolution is nearly equal to 4D-Var. No differences in wind illustrate the lack of wind observations on domain. The rare (radiosonde) data is similarly represented in global and mesoscale model resolution. The precipitation amounts were better forecasted by the forecasts with initial conditions obtained by mesoscale analysis, but this can also be due to differences in other model parameters. The case study presented the advantage of high-resolution analysis.

Acknowledgements

This work was done for my diploma thesis at University of Ljubljana. I would like to thank my supervisor Nedjeljka Žagar for advice and guidance. I am also grateful to Jure Cedilnik, Mark Žagar and other colleagues from Slovenian meteorological service for technical help and discussion. I acknowledge Hungarian meteorological service for the data needed.

References

Berre L., 2000. Estimation of synoptic and mesoscale forecast error covariances in a limited area model. *Mon. Wea. Rev.* 128, 644-667.

Bölöni G., 2005. ALADIN 3DVAR at the Hungarian Meteorological Service, 27th EWGLAM meeting presentation, 3-5 October, 2005, Ljubljana.

Jolliffe I.T., Stephenson D.B., 2003. *Forecast verification. A Practioneer's Guide in Atmospheric Science.* Wiley and Sons Ltd, Chichester.

Široka M. et al., 2003. The definition of mesoscale selective forecast error covariances for limited area analysis. *Meteorol. Atmos. Phys.*, 82, 227-244.

Žagar N. et al., 2006. Validation of mesoscale low-level winds obtained by dynamical downscaling of ERA40 over complex terrain. *Tellus A*, 58, 4, 445-455.

5. ALADIN PhD Studies

Vasiliu Steluta: Scientific strategy for the implementation of a 3d-var assimilation scheme for a double-nested limited area model. University of Bucarest – Romania.

Radu Raluca: Extensive study of the coupling problem for a high resolution limited area model.

Simon André: Study of the relationship between turbulent fluxes in deeply stable PBL situations and cyclogenetic activity.

Szczech-Gajewska Małgorzata: Use of IASI/AIRS data over land.

Vivoda Jozef: Application of the predictor-corrector method to non-hydrostatic dynamics Slovakian thesis. SLovak Academy of Sciences.

6. PUBLICATIONS

Berre L., S. E. Stefanescu and M. Belo Pereira, 2006: The representation of the analysis in three error simulation techniques. *Tellus* **58A,** pp.196-209.

Chapnik, B., G. Desroziers, F. Rabier and O. Talagrand, 2006: Diagnosis and tuning of observational error in a quasi-operational data assimilation setting. *Quart. Jour. Roy. Meteor. Soc.*, **132,** pp.543-565.

Fischer C., T. Montmerle, L. Auger et B. Lacroix: 2006: L'assimilation opérationnelle de données régionales à Météo-France. *La Météorologie* **54**

Montmerle, T., J.-P. Lafore, L. Berre and C. Fischer, 2006 : Limited area model error statistics over Western Africa : comparisons with mid-latitude results. *Quart. Jour. Roy. Meteor. Soc.*, **132,** pp.213-231.

Müeller, M., P. Poli, J. Joiner, 2006: The impact of ozone field horizontal inhomogeneities on nadir-viewing orbital backscatter UV measurements. *J. Geophys. Res.*, 2005JD006769, 2006.

Poli, P., 2006: Assimilation of GNSS Radio Occultation Data into Numerical Weather Prediction, in *Atmosphere and Climate: Studies by Occultation Methods*, Springer-Verlag, Eds. Kirchengast, G. Foelsche, U., Steiner, A.K., 196-204, ISBN-10-3-540-34116.

Rivière, G. and A. Joly, 2006: Role of the low-frequency deformation field on the explosive growth of extratropical cyclones at the jet exit Part I: barotropic critical region. *J. Atmos. Sci.,* **63.**.

Rivière, G. and A. Joly, 2006: Role of the low-frequency deformation field on the explosive growth of extratropical cyclones at the jet exit Part II: baroclinic critical region. *J. Atmos. Sci.*, **63**.

Stefanescu, S. E., L. Berre and M. Belo Pereira, 2006: The evolution of dispersion spectra and the evaluation of model differences in an ensemble estimation of error statistics for a limited area analysis. *Mon. Wea. Rev.*, **134**, pp.3456-3478.

Stoffelen, A., G.-J. Marseille, F. Bouttier, D. Vasiljevic, S. de Haan and C. Cardinali, 2006: ADM-Aeolus Doppler wind lidar Observing System Simulation Experiment. *Quart. Jour. Roy. Meteor. Soc.*, **132**, pp.1927-1948.

Horanyi A., S. Kertesz, L. Kullmann, and G. Radnoti, 2006: The ARPEGE/ALADIN mesoscale numerical modeling system and its application at the Hungarian Meteorological Service, *Idojaras*, **110**, pp. 203-227.

Hagel, E. and A. Horanyi,, 2006:The development of a limited area ensemble prediction system at the Hungarian Meteorological Service: sensitivity experiments using global singular vectors, preliminary results, *Idojaras*, **110**, pp. 229-252

Szintai, B. and I. Ihasz,: 2006:The dynamical downscaling of ECMWF EPS products with the ALADIN mesoscale limited area model: preliminary evaluation., *Idojaras*, **110**, pp. 253-277.

Boloni, G., Development of a variational data assimilation system for a limited area model at the Hungarian Meteorological Service, *Idojaras*, **110**, pp. 309-327.

Randriamampianina, R., 2006: Impact of high resolution satellite observations in the ALADIN/HU model, *Idojaras,* **110**, pp. 329-347.